CHALMERS
UNIVERSITY OF TECHNOLOGY

Towards Qualification of Female Human Body Model for Virtual Testing

Setup for 50th percentile female human body model and parametric study of the boundary conditions.

Master's thesis in Product Development

Pushkar Mahesh Dhamane

Department of Mechanics and Maritime Sciences
CHALMERS UNIVERSITY OF TECHNOLOGY
Göteborg, Sweden 2026
www.chalmers.se

MASTER'S THESIS IN PRODUCT DEVELOPMENT

Towards Qualification of Female Human Body Model for Virtual Testing

Setup for 50th percentile female human body model and parametric study of the boundary conditions.

PUSHKAR MAHESH DHAMANE

CHALMERS
UNIVERSITY OF TECHNOLOGY

Department of Mechanics and Maritime Sciences
Division of Vehicle Safety
CHALMERS UNIVERSITY OF TECHNOLOGY
Göteborg, Sweden 2026

Towards Qualification of Female Human Body Model for Virtual Testing
Setup for 50th percentile female human body model and parametric study of the boundary conditions.
PUSHKAR MAHESH DHAMANE

Supervisor: Jobin John, Mechanical Engineering, Chalmers
Yash Niranjan Poojary, Mechanical Engineering, Chalmers

Examiner: Johan Iraeus, Mechanical Engineering, Chalmers

Master’s Thesis 2026
Department of Mechanics and Maritime Sciences
Division of Vehicle Safety
Chalmers University of Technology
SE-412 96 Göteborg
Sweden
Telephone: + 46 (0)31-772 1000

Printed by Chalmers Reproservice
Gothenburg, Sweden 2026

Towards Qualification of Female Human Body Model for Virtual Testing
Setup for 50th percentile female human body model and parametric study of the boundary conditions.
PUSHKAR MAHESH DHAMANE
Department of Mechanics and Maritime Sciences
Division of Vehicle Safety
Chalmers University of Technology

Abstract

Road traffic injuries pose a major global safety challenge for vehicle occupants and vulnerable road users, such as pedestrians and cyclists. To prevent injuries, crash testing plays a vital role in automotive safety assessment. While early biomechanical evaluations relied on post-mortem human surrogates (PMHS), standard physical crash testing today is primarily conducted using Anthropomorphic Test Devices (ATDs). However, ATDs possess structural limitations: their rigid responses cannot fully replicate complex human soft-tissue and skeletal injury mechanisms. Additionally, physical testing using ATDs is constrained by high financial costs and testing complexity.

To address this limitation, virtual testing is being proposed as a complement to physical testing for vehicle safety assessment, for example the HBM4VT framework under Euro NCAP has established qualification protocols for the 50th percentile male HBM (50M) through the Crash Protection 550 (CP550) protocols. This thesis evaluates the biofidelity scoring of a 50th percentile female HBM (50F) across key hub impact scenarios: Kroell (frontal thoracic), Viano (thoracic, abdominal, and pelvic), Compigne (shoulder), and Agnew (angled thoracic) and performs a parametric study on uncertainties that can influence the biofidelity scores. Simulation results were compared against experimental post-mortem human subject (PMHS) reference corridors generated using the ARCGen, with objective metric scores calculated using the Ellipse and Dynamic arc-length warping (DALW) scoring method and, ISO 18571. Evaluated parameters included physical setup variables (seating angle, HBM posture, and arm orientation) and ARCGen algorithmic parameters (cut_simulation with boolean values and number of warping points (nWarpCtrlPts) ranging from 0 to 5. Results demonstrate that scores exhibit higher sensitivity to physical setup variations than corridor algorithm configurations.

Keywords : Post-Mortem Human Subjects (PMHS), Anthropomorphic Test Devices (ATDs), Human body model (HBM), 50th percentile female HBM (50F), ARCGen, Ellipse, Dynamic arc-length warping (DALW), ISO 18571, Parametric study.

Acknowledgement

I would like to express my sincere gratitude to my supervisors and examiner for their guidance and support throughout this thesis work.

My deepest thanks go to my supervisor, Jobin John at Chalmers University of Technology, for sharing his extensive knowledge and expertise. His insightful perspectives continuously enriched this project and helped shape its direction. I am also exceptionally grateful to Yash Niranjan Poojary for his hands-on support in resolving technical challenges and for his steadfast encouragement throughout this period. Their joint guidance was instrumental in helping me master the methods, procedures, and rigorous standards required for this work.

Finally, I wish to extend my profound appreciation to my examiner, Johan Iraeus for his valuable feedback, critical evaluation, and constructive review of this thesis, which greatly elevated the quality and rigor of the final manuscript.

- Pushkar Mahesh Dhamane, Gothenburg, September 2026

List of Acronyms and Abbreviations

ATD	Anthropomorphic Test Devices
FE	Finite Element
FEA	Finite Element Analysis
HBM	Human Body Model
HBM4VT	Human Body Model for Virtual Testing
VRU	Vulnerable Road Users
THUMS	Total Human Model for Safety
GHBMC	Global Human Body Models Consortium
CP550	Crash Protection 550
50M	50^{th} percentile male Human Body Model
50F	50^{th} percentile female Human Body Model
GCS	Global Coordinate System
CoG	Center of Gravity
DALW	Dynamic Arc-Length Warping
DTW	Dynamic Time Warping
ACT	Angle between Acetabulum Centre and mid T1 vertebrae
nWarpCtrlPts	Number of Warping Control Points

List of Figures

List of Tables

Table of Contents

1. Introduction

Road traffic crashes resulted in approximately 1.19 million deaths worldwide in 2021, while millions more sustained non-fatal injuries, many of which led to long-term disabilities (Global Status Report on Road Safety 2023). Road traffic injuries remain the leading cause of death among children and young adults aged 5 to 29 years. Most fatalities occur among the working-age population, with 69% of deaths involving individuals aged 18 to 59 years and 23% involving individuals aged 60 years or older. In addition, males account for approximately three times as many fatalities as females (Global Status Report on Road Safety 2023).

Enhancing road safety for all user groups relies on the design of safe vehicles that reduce occupant and pedestrian injury severity during crashes. Regulatory requirements for front and side impact protection, together with restraint systems such as seatbelts and airbags, help reduce the risk of serious injuries for both vehicle occupants and vulnerable road users. Compliance with these requirements has traditionally relied on physical crash testing using Anthropomorphic Test Devices (ATDs), which are simplified mechanical representations of the human body designed to provide repeatable measurements of occupant response during vehicle collisions.

As crash testing increasingly moved towards virtual environments, finite element (FE) representations of ATDs were developed for numerical crash simulations (Klug et al. 2023). These virtual ATDs enable efficient evaluation of multiple impact scenarios and vehicle designs. However, because they replicate the mechanical characteristics of physical dummies, their relatively high stiffness limits their biofidelity and their ability to represent complex injury mechanisms.

While virtual ATDs remain valuable tools for safety assessment, finite element Human Body Models (HBMs) have been developed to provide a more detailed representation of human anatomy. Several HBMs are currently used in vehicle safety research, including THUMS (Total Human Model for Safety), GHBMC (Global Human Body Models Consortium) (Gayzik et al. 2005), VIVA+, SAFER HBM (Iraeus et al. 2024).

To standardise the use of HBMs in vehicle safety assessments, Euro NCAP introduced the Human Body Models for Virtual Testing (HBM4VT) framework. The framework defines a standardized procedure for the simulation and evaluation of HBMs across a series of defined load cases, including component-level and sled tests. Technical Bulletin CP 550 and CP 551 (Technical Bulletin CP 550 Qualification Procedure for HBM 2025) further provide qualification procedures and acceptance criteria and based on comparisons with Post Mortem Human Subject (PMHS) test data. Together, these guidelines help ensure that HBMs can be used reliably in virtual safety assessments. However, the current qualification procedures have primarily been developed for male HBMs. As virtual testing moves towards representing a population of vehicle occupants, the applicability of these procedures to female HBMs requires further investigation (John et al. 2022).

1.1 Aim

The aim of this thesis is to evaluate the applicability of the HBM4VT qualification framework to a 50th percentile female Human Body Model. To achieve this, HBM4VT load cases are implemented for the VIVA+ female HBM, and the effects of boundary-condition uncertainties and objective rating methodologies on qualification results are investigated.

1. Setup and implement the HBM4VT loadcases for a 50th percentile female VIVA+ Human Body Model.
2. Evaluate the influence of uncertainties in the boundary conditions and scoring methodology parameters on the qualification outcome.
3. Specifically, assess the effect of ARCGen parameter variations on PMHS average responses and corridors, and evaluate their influence on objective metric scores obtained using the Ellipse, Dynamic Arc-Length Warping (DALW), and ISO 18571 scoring methods.

1.2 Delimitations

1. Due to the limited timeframe of this study, only a selected set of load cases were considered, primarily those involving hub impactor-based loading conditions.
2. The Agnew loadcase was partially evaluated as it is currently not part of the HBM4VT loadcases, incorporating Condition I (with circular hub impactor) while Condition II (rectangular hub impactor) was not performed along with parametric sensitivity studies were not performed due to time constraints.
3. Only VIVA+ HBM was selected as the model for this study.

2. Theory

This section presents the theoretical background for the Euro NCAP HBM4VT qualification framework and the core technical concepts utilized throughout this thesis. Specifically, it introduces the working principles of the ARCGen corridor generating tool, followed by the formulation of the Ellipse, DALW, and ISO 18571 objective scoring methodologies.

2.1 Framework of HBM4VT

The HBM4VT qualification process follows a framework as shown in Figure 1. The process begins with the definition of simulation input files, consisting of HBM and the load-case-specific test environment. Depending on the selected qualification load case, the environment includes component-level impactors, tabletop setups, or full sled-test conditions. The model setup is done in ANSA (version 24.1.2, BETA CAE Systems) and the simulation is performed in LS-DYNA (version R12.0, Ansys Inc.) to generate the HBM response under a given loading condition. The simulation results are stored in output files, binout and d3plot files, containing kinematic and kinetic data. The simulation outputs are processed in Jupyter notebooks using python and dynasaur library (Technical Bulletin CP 550 Qualification Procedure for HBM 2025). Further the extracted outputs are compared against PMHS data using objective scores.

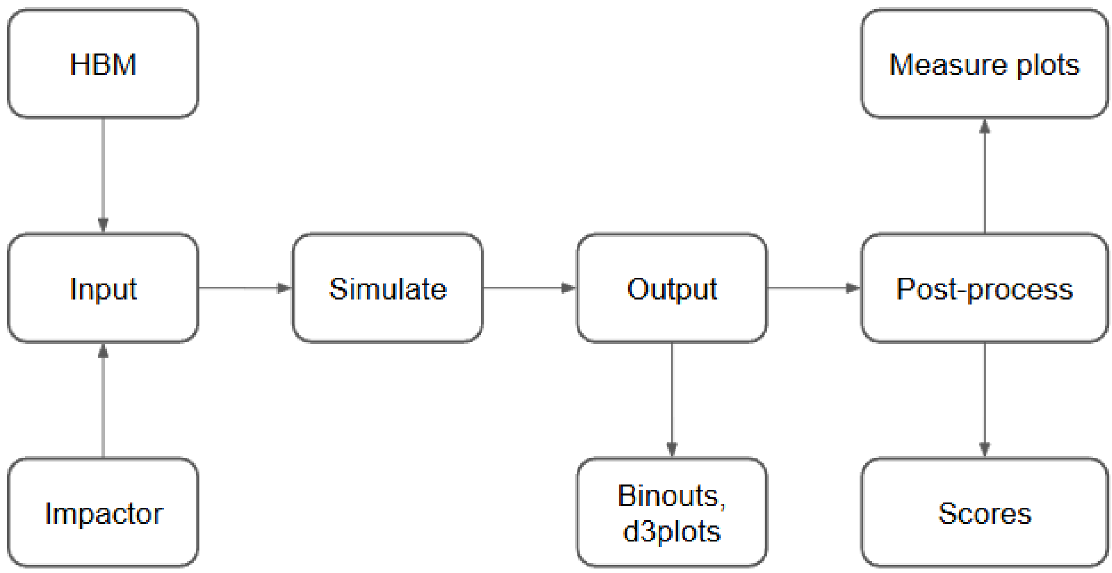

Figure 1 - Overall simulation and validation workflow of HBM4VT, depicting the setup from HBM and impactor input models, binary output generation (binout, d3plot), post-processing, measurement plotting, and objective scoring.

2.2 Finite Element Human Body Model

Finite Element (FE) Human Body Models (HBMs) are tools for evaluating injury during virtual crash testing. These models serve as highly detailed representation of the human body, incorporating detailed tissue, organ, and joint definitions to capture realistic biomechanical responses while maintaining computational efficiency and numerical robustness. The geometries are discretized using finite element meshes optimised for element size, structure, and stable time-step integration. Unlike ATD, HBM allows for detailed stress and strain analysis at the tissue level across internal organs and offering superior injury prediction irrespective of impact angle (John et al. 2022).

2.2.1 VIVA+ HBM

VIVA+ is a line-up of open-source finite element human body models representing vehicle occupants and vulnerable road users. It consists of 50th percentile male human body model (50M) and 50th percentile female human body model (50F) in both seated and standing posture (John et al. 2022).

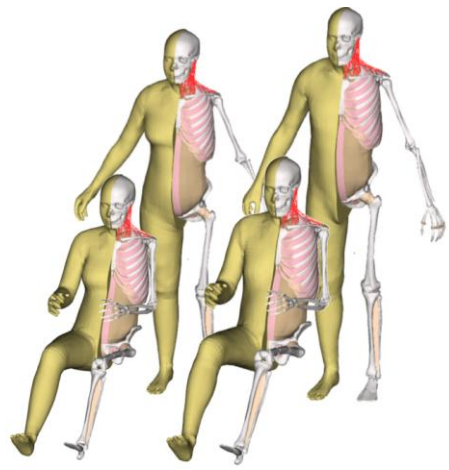

Figure 2 - VIVA+ Human Body Model (HBM) (John et al. 2022)

2.3 ARCGen

ARCGen is a software tool that implements the arc-length corridor method, designed to compute characteristic average curve and statistical response corridors essential for validating computational models and ATDs.

ARCGen uses arc-length reparameterization and signal registration to compute the average response and statistical corridors from experimental data. In simple terms, it re-parameterises experimental curves based on their arc length. Each experimental run performed on different subjects produces a different path due to varying timestamps. This results in misaligned peaks, valleys and endpoints across timestamps. ARCGen uses warping functions to automatically align peaks and valleys across all experimental data, producing an accurate final average. Once aligned, the tool uses a mathematical framework to calculate statistical corridors around the

average. These corridors quantify data variability across experiments (Hartlen and Cronin 2022).
ARCGen has various input parameters that control how the characteristic average and statistical corridor are generated:

- n – Number of input signals
- nResamplePoints – A user defined parameter which defines the number of points in re-parameterised signals. (fixed at 500 resampling points by HBM4VT)
- nWarpCtrlPts – Number of interior control points for warping function. This enables non-linear shifting of signals to align features such as peaks and valleys. This includes penalty factor (λ) to prevent non-monotonic or unrealistic warping.
- factor_cut_displacement – Set value which shows the unloading deflection values after reaching the maximum deflection. It eliminates (doesn't display) the data after the result has reached the set value.
- cut_simulation - The process where the simulation arc length is measured and if it is longer than the characteristic average arc length, then it is trimmed to its length.

Objective metric scores were calculated using the ARCGen tool by comparing simulation data against the generated experimental reference corridors (characteristic averages). The scores are evaluated using three scoring methodologies: Ellipse, Dynamic Arc-Length Warping (DALW), and ISO 18571.

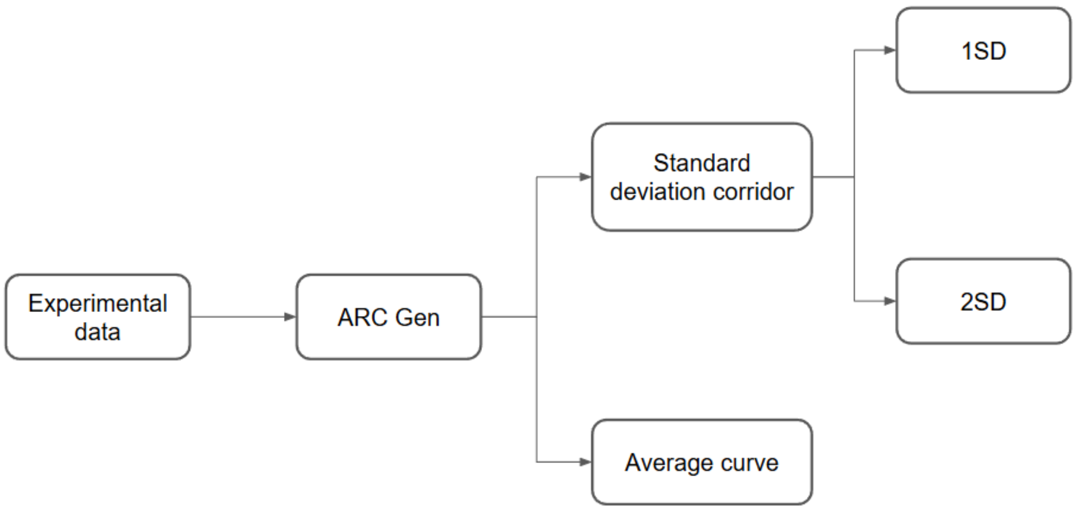

Figure 3 - Schematic workflow of the ARCGen process, showing the processing of experimental data to generate the average curve and standard deviation corridors (1SD and 2SD).

2.5 Scoring Methodology

The scores are evaluated using three scoring methodologies: Ellipse, Dynamic Arc-Length Warping (DALW), and ISO 18571. They are used to assess simulated HBM results against PMHS result by comparing simulation data against the experimental reference corridors generated (characteristic averages). The scores are calculated using measures derived from the results, such as force and deflection. The scoring methods use the ARCGen tool to compare results using the characteristic average curve and simulation curve.

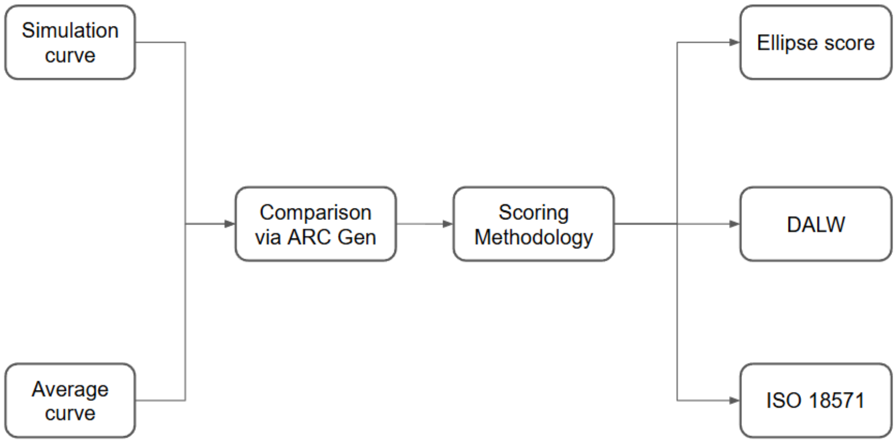

Figure 4 - Schematic overview of the biofidelity evaluation process, where ARC-Gen is utilised to generate the experimental average curve for subsequent objective scoring (Ellipse, DALW, and ISO 18571).

2.5.1 Ellipse score

The Ellipse score evaluates how well the simulation data matches the average PMHS response, including experimental variability. It uses the ARCGen generated characteristic average as the PMHS reference. The simulation curve is resampled into specific number of points based on normalized arc-length. The resampled simulation response and resampled average response are compared point-wise manner. Each simulation point is scored relative to its corresponding average response point. ARCGen statistical corridors, based on standard deviation boundaries (±1SD for the inner ellipse and ±2SD for the outer ellipse, respectively), define inner and outer ellipses. Point within the inner ellipse gives a score 1 and points beyond the outer ellipse score is 0. Points between the two ellipses are calculated with the formula (l_2/l_1+l_2), where l_1 and l_2 are the distances from the point to the inner and outer ellipse intersections respectively. The final score is the mean of all individual point scores. The ARCGen tool also creates the ellipse boundaries within the corridor which will help in determining the ellipse score (Ressi et al. 2025). The three cases and their respective score are shown in the Figure 5.

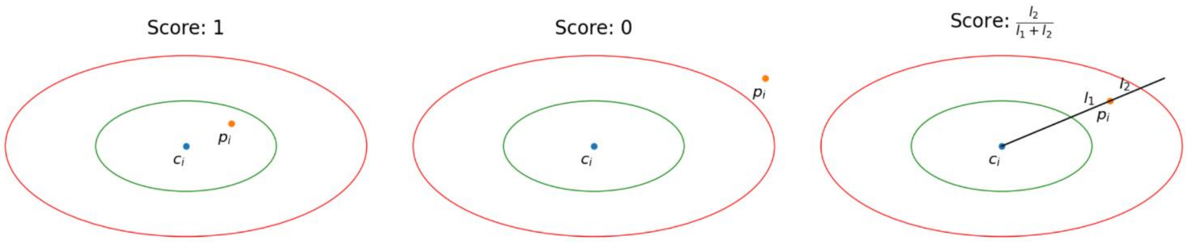

Figure 5 - Conceptual diagram of the Ellipse scoring algorithm showing boundary conditions (1SD and 2SD) and intermediate score calculation for data point relative to center.

2.5.2 Dynamic Arc-Length Warping (DALW)

Dynamic Arc-Length Warping is an extension of Ellipse score methodology. It optimises the alignment between simulation and test data. Unlike DTW, which uses time, DALW uses arc-length. DALW removes the time variable from the raw data coordinates. Then, it recalculates the points based on curve distances and resamples the curves with specific number of points with equal arc-length spacing. These new points are then processed by the warping function, which is similar to DTW (Ressi et al. 2025).

2.5.3 ISO 18571

ISO 18571 is a validation metric and rating procedure that calculates the correlation level between two non-ambiguous signals from physical tests and computational models for vehicle safety applications. It objectively compares time-history signals between models and tests. The method combines corridor and cross-correlation scores to evaluate the simulation accuracy against the experimental test results. Cross-correlation assesses phase shift, magnitude, and shape, providing a score between 0 and 1 for each aspect. Table 1 shows the scale for overall ISO rating within different ranges (Road vehicles - Objective rating metric for non-ambiguous signals 2024).

Table 1 - ISO rating with different range of scores.

Rank	Grade	Rating, R	Description
1	Excellent	$R > 0.94$	Captures almost all reference signal characteristics
2	Good	$0.8 < R \leq 0.94$	Captures main characteristics with noticeable differences
3	Fair	$0.58 < R \leq 0.8$	Captures basic characteristics with significant differences
4	Poor	$R \leq 0.58$	Virtually no correlation between signals

ISO 18571 specifically combines these four sub-ratings: corridor, phase, magnitude, and slope into an overall rating. The description here focuses on corridor and cross-correlation aspects.

3. Evaluated Loadcases

This section summarizes the evaluated loadcases including impactor characteristics and impact locations alongside the standardised HBM positioning guidelines specified by HBM4VT.

3.1 Kroell 1971, 1974 (Front Thoracic Impact):

This experiment aimed to characterise thoracic PMHS response during frontal impacts (Kroell, Schneider, and Nahum 1971);(Kroell, Schneider, and Nahum 1974). Further details regarding impactor specification and location are given in Table 2.

Table 2 - Impactor test parameters for Kroell frontal thoracic impact experiments

Impact location	Impactor size	Impactor weight (kg)	Impact speed (m/s)
4th intercostal space of the sternum	Circular (diameter of 150mm)	23.4	4.3, 6.7

According to HBM4VT setup guidelines, the HBM is positioned in a seated posture defined by the angle between the acetabulum center (AC) and the mid-T1 vertebra relative to the frontal plane, aligning the model in an erect posture. The thorax is subsequently subjected to a frontal impact directed at the mid-sternum. Figure 6 showing the resulting HBM posture replicating the physical test setup.

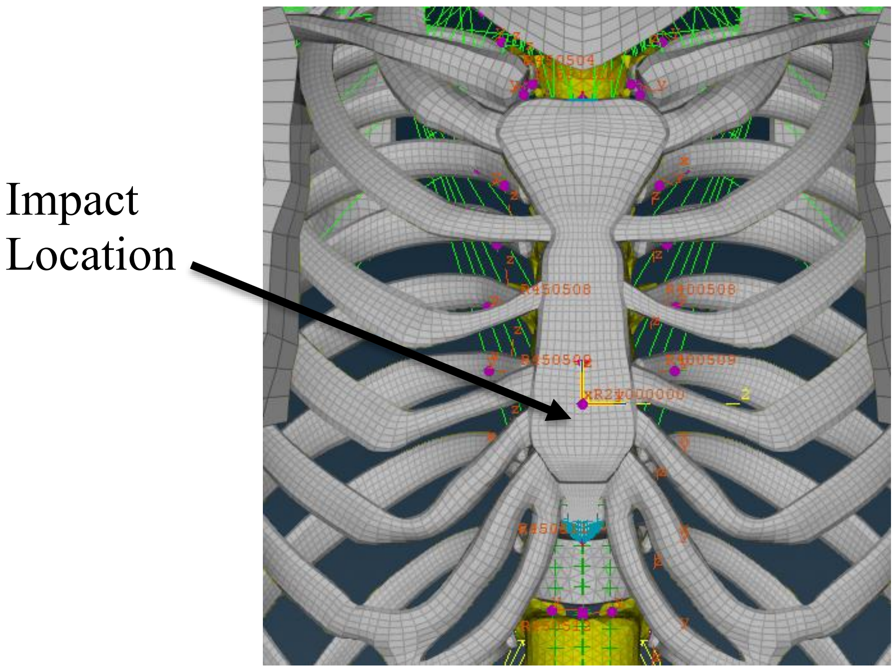

Figure 6 - Anterior view of the ribcage depicting the target impact location at the 4th intercostal space of the HBM.

3.2 Viano 1989 (Lateral Thoracic, Abdominal and Pelvic Impact):

This experiment aimed to study the biomechanical response of the thorax, abdomen and pelvis during lateral impacts (Viano 1989). Further details regarding impactor specification and location are given in Table 3.

Table 3 - Impactor test parameters for Viano lateral impact experiments across thoracic, abdominal, and pelvic locations

Impact location	Impactor size	Impactor weight (kg)	Impact speed
Thorax	Circular (diameter of 150mm)	23.4 kg	4.4, 6.5, 9.5
Abdomen			5.8, 6.8, 9.4
Pelvis			5.2, 9.8

According to HBM4VT setup guidelines, HBM is in a seated posture with active tissue definitions restricted to the pelvis, legs, and thorax, while the shoulder region is deactivated to exclude hub impactor contact. The impactor is then positioned to impact the lateral thorax and abdomen at specified impact angles. Figure 7 through Figure 9 show the resulting simulation setups across the different impact locations.

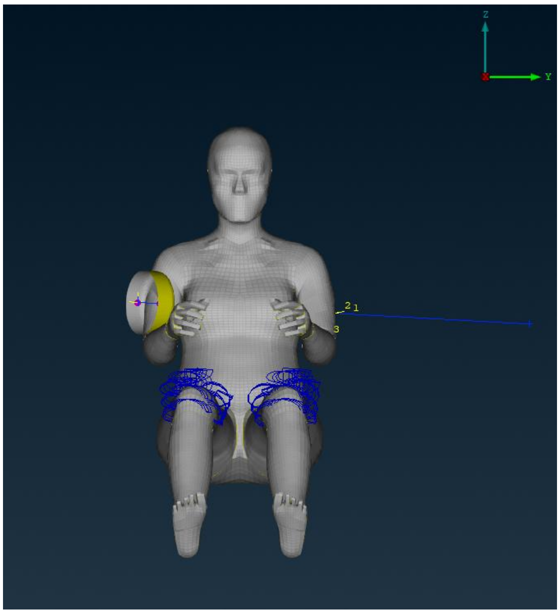

Figure 7 - Anterior view of the seated HBM depicting impactor positioning for the Viano lateral thoracic loadcase.

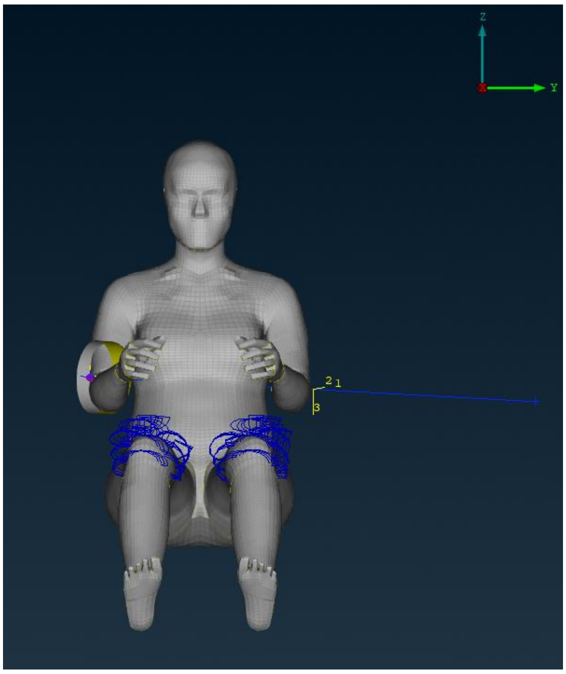

Figure 8 - Anterior view of the seated HBM depicting impactor positioning for the Viano lateral abdominal loadcase.

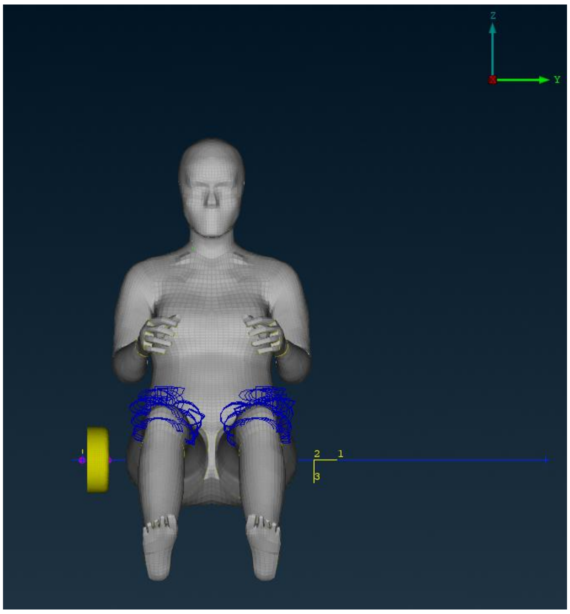

Figure 9 - Anterior view of the seated HBM depicting impactor positioning for the Viano lateral pelvic loadcase.

The detailed view of the different impact locations is shown in Figure 10. The thoracic loadcase targets an impact defined relative to the inferior end of the sternum via the positioning parameter XP_v, while the abdominal impact center is offset 75 mm lower along this thoracic reference point.

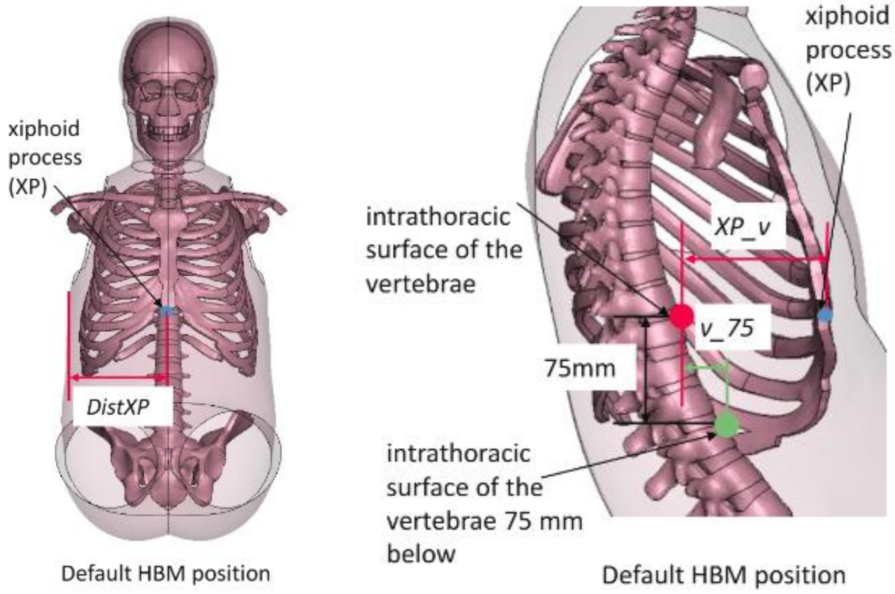

Figure 10 - Anatomical reference landmarks for thoracic and abdominal impactor positioning on the default HBM position (anterior and sagittal views)(Kofler, Ressi, and Klug 2025) [Source: HBM4VT OpenVT Euro NCAP report].

3.3 Compigne 2004 (Lateral Shoulder Impact):

This experiment evaluated shoulder impacts at different speeds and angles to establish biofidelity corridors (Compigne et al. 2004). Further details regarding impactor specification and location are given in Table 4.

Table 4 - Impactor test parameters for Compigne shoulder impact loadcase

Impact location	Impactor size	Impactor weight (kg)	Impact direction (deg)	Impact speed (m/s)
Left shoulder	Rectangular (150 mm x 80 mm)	23.4	0	3, 4, 6
Right shoulder			-15, 0, +15	1.5

The impact location is the center point of the greater tubercle region of the proximal humeral as shown in the Figure 11, with different impact angle and speed.

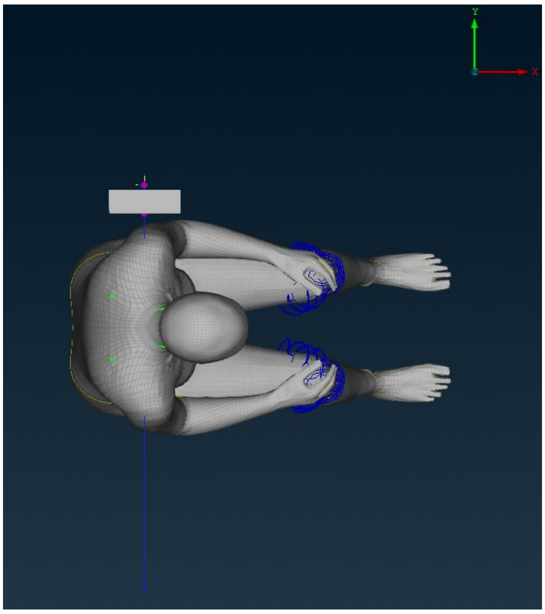

Figure 11 - Impactor positioning and alignment for lateral (0°) shoulder impact velocity conditions (3 m/s, 4 m/s, 6 m/s) on the seated HBM, superior view.

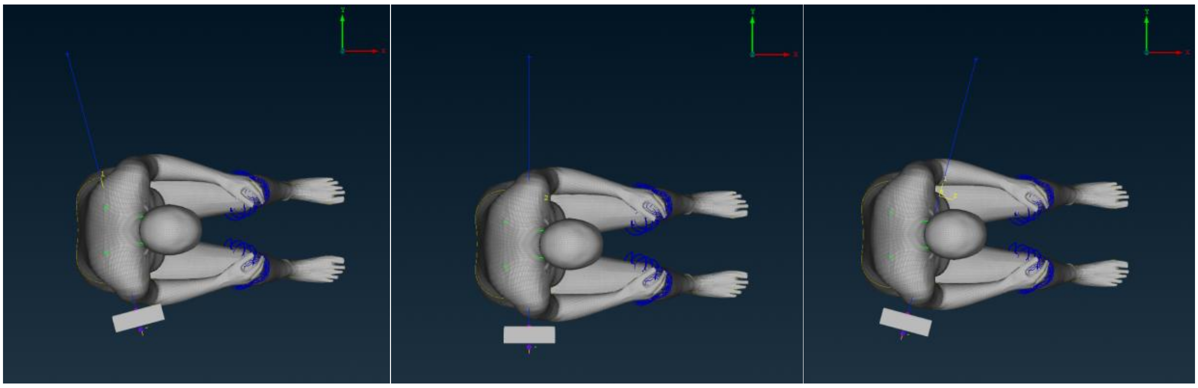

Figure 12 - Superior view of the seated HBM demonstrating parametric variations in shoulder impact angle (1.5 m/s Compigne loadcase): +15° anterior-oblique (left), 0° pure lateral (center), and -15° posterior-oblique (right).

The specific node locations defined to evaluate relative displacements across the upper torso, including acromion-to-acromion, acromion-to-sternum, acromion-to-T1, and impactor-to-T1 deflections, is shown in Figure 13.

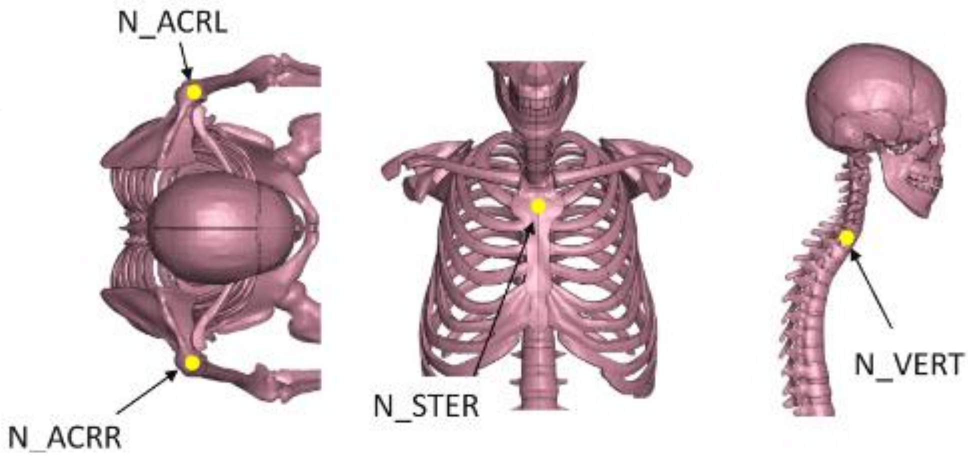

Figure 13 - Reference node locations for acromion-to-acromion, acromion-to-sternum, acromion-to-T1, and impactor-to-T1 relative deflection tracking (Kofler, Ressi, and Klug 2025)[Source: HBM4VT OpenVT Euro NCAP report].

3.4 Agnew 2024 (Lateral and Oblique Thoracic Impact):

This experiment aimed to collect biomechanical response data for small female PMHS during oblique and lateral thoracic impacts (Agnew et al. 2024). Further details regarding impactor specification and location are given in Table 5.

Table 5 - Impactor test parameters for Agnew small female thoracic impact experiments

Impact location	Impactor size	Impactor weight (kg)	Impact direction (deg)	Impact speed (m/s)
4th intercostal space of the sternum	Circular (diameter of 125mm)	14	Oblique, Lateral	2.5

Following HBM4VT guidelines, the HBM configuration mirrors the setup from (Shaw et al. 2006) having the same impact location. The only difference is lower impactor mass and with 2.5 m/s impact speed. Figure 14 highlights the HBM impact positioning, while Figure 15 showing the two evaluated impact directions: oblique (60°) and lateral (0°).

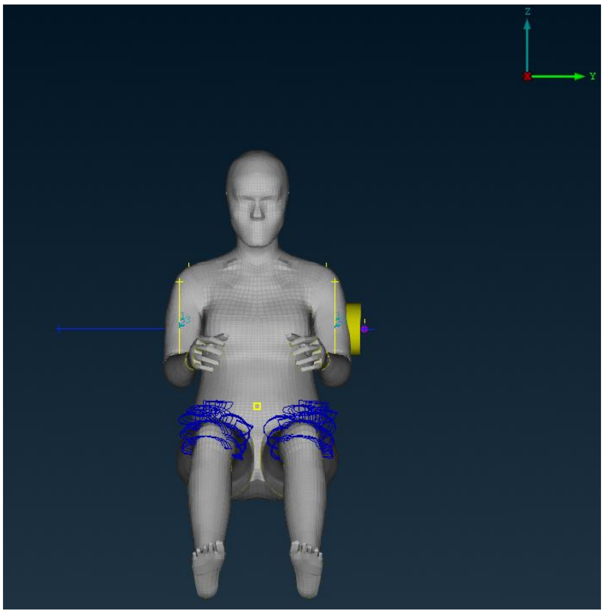

Figure 14 - Anterior view of the seated HBM and rigid impactor alignment for the Agnew thoracic impact loadcase.

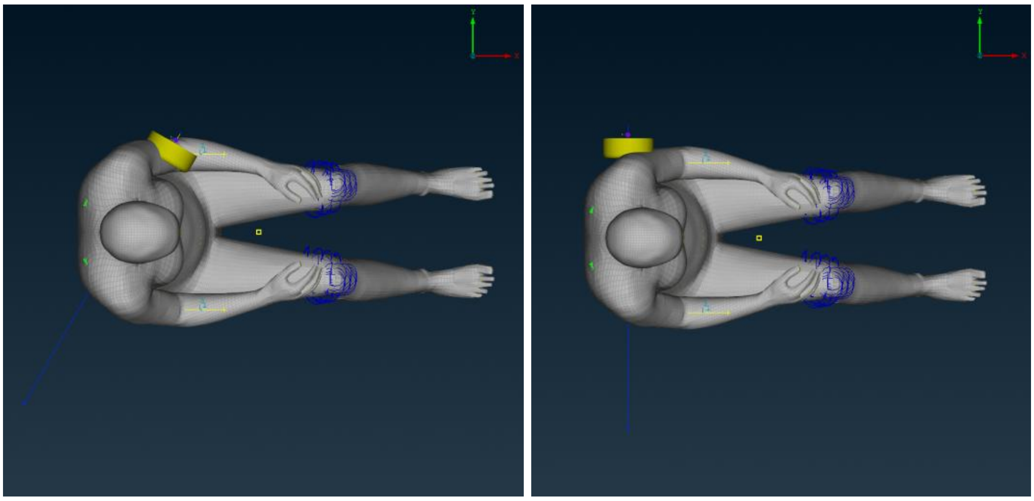

Figure 15 - Superior view of the seated HBM showing oblique (left) and lateral (right) impactor angles at 2.5 m/s for the Agnew thoracic impact setup.

4. Methodology

This section outlines the steps followed to address the objectives of the study. It covers the selection criteria for PMHS data used in female response corridor generation, the application of HBM4VT guidelines to configure the 50F HBM model across impact loadcases, and the parametric study framework detailing the selected design parameters and evaluation procedures.

4.1 Subject Selection

Each loadcase includes PMHS dataset with male and female subjects. The current CP 550 qualification compares 50M HBM responses against ARCGen corridor built using combined male and female data.

To evaluate the 50F HBM, only female-specific PMHS data should be included from the respective loadcases. However, due to limited female subjects, certain loadcases could not generate ARCGen corridor. Therefore, male subjects were also included in the female ARCGen corridor considering weight.

According to European population data, the mean body weight of a 50-year-old female (50F) is 68 kg, and one standard deviation above the mean corresponds to 79.8 kg. VIVA+ 50F HBM is based on the U.S. population anthropometry in the 1970s. However, since this study corresponds to the Euro NCAP initiative, the European population was considered as the target. To maintain anthropometric alignment with the target population, the final dataset includes all original female subjects, as well as male subjects weighing less than 79.8 kg, as shown in Table 6. It should, however, be noted that subjects with a body weight exceeding 50F HBM target weight may have an influence on the extent of the corridors, and subsequently influence the scores.

Table 6 - Anthropometric mean values and 1SD corridor limits used for PMHS selection.

Measure	Average	1SD
Height (in cm)	164.5	≥ 158.2 ≤ 170.8
Weight (in kg)	68	≥ 56.2 ≤ 79.6

4.2 Setup of 50 Percentile Female HBM

The first step involves setting up the 50th percentile female HBM with specific boundary conditions mentioned in the load case. The setup follows the procedure from the specific loadcase as described in CP 550 (Technical Bulletin CP 550 Qualification Procedure for HBM 2025). The key components include HBM, Impactor, and virtual environment involved in the procedure. Since the HBM4VT framework already specifies the setup protocols for 50M, the simulation setup was adapted by replacing the 50M HBM with the 50F HBM and adjusting the boundary conditions to match the average female anthropometry.

The impactor is configured with coordinates including positioning and orientation along with motion parameters such as travel direction, velocity and mass. All boundary conditions and parameters were defined relative to the global coordinate system (GCS) into which the HBM was imported.
HBM setup and pre-processing use ANSA for the given load case and boundary condition. The simulations were performed on Chalmers HPC. The output results produce d3plots and binout files. The results are post-processed using Jupyter notebooks adapted from the HBM4VT repositories (Technical Bulletin CP 550 Qualification Procedure for HBM 2025).

4.3 Parametric Study

Parametric study analyses how the variation in the input variables or parameters such as boundary condition, impactor positioning or influence of post-processing factors affect the results. Performing parametric sensitivity analysis helps to identify which inputs contribute to the HBM's responses and biofidelity scores.

This parametric study evaluates two distinct parameter categories: boundary condition and corridor parameters. To characterize their influences individually, the parameters were varied independently to isolate their specific influence on biofidelity scores relative to baseline results.

4.3.1 Boundary Condition Parameters

Boundary conditions parameters include possible variations in PMHS experiments due to uncertainties either in the physical test or reporting of the experiments. In the HBM4VT setups, these input variables are pre-defined, providing the starting point for evaluating the sensitivity of the setup on HBM outputs. For example, the Kroell experimental setup provided minimal support (securing the hands horizontally with tape) may have introduced variations in the initial torso posture of the PMHS. Consequently, evaluating HBM posture sensitivity is necessary to determine how initial positioning affects both kinematic response and biofidelity scores.

For the Kroell loadcase, the ACT angle (angle between acetabulum center to mid-T1 vertebrae) defines the HBM posture relative to the frontal plane. Minimal back support in the Kroell experimental setup caused postural variations (Kroell, Schneider, and Nahum 1971). Because physical test records lack exact quantitative posture measurements, a ± 5° tolerance relative to the ideal erect baseline (0°) was evaluated to quantify posture sensitivity. Furthermore, baseline posture definitions differ between HBMs, with the VIVA+ 50M model incorporated a 19.5° offset from erect posture for its qualification, as shown in Figure 16.

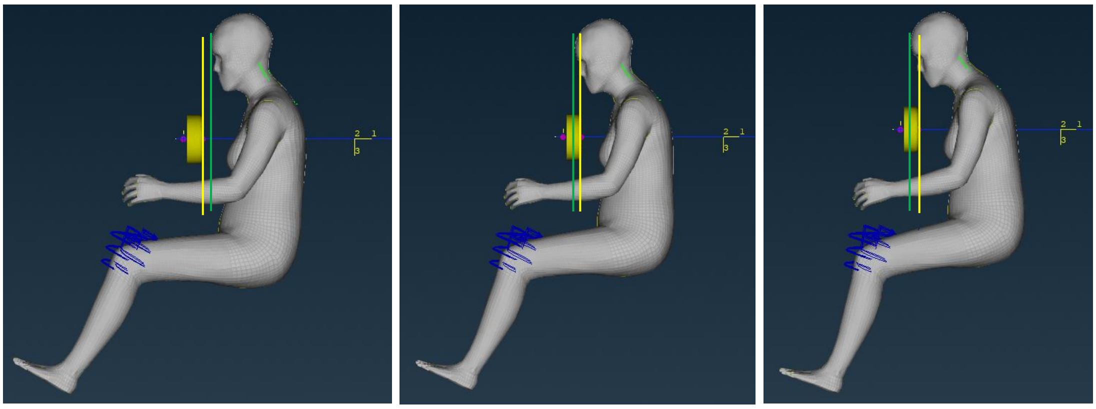

Figure 16 - HBM seating posture variations showing the ACT angle (from left to right): 14.5° (reclined/decreased angle), 19.5° (baseline configuration), and 24.5° (upright/increased angle). The coloured lines indicates the change in the distance between the impactor and HBM after change in ACT

In the Viano loadcase, the baseline HBM4VT setup for VIVA+ 50M assumed a seated HBM posture. In contrast, standing subjects were evaluated in physical experiments. To understand the influence of subject posture, the standing model of 50F was compared against the baseline seated configuration in this load case.

In the Compigne loadcase, the baseline HBM4VT setup positions the upper arm at a 19° angle between the glenohumeral joint and mid-epicondyle via a constrained beam element rotation. As this angle is not explicitly detailed in the original PMHS experimental documentation, it constitutes a positioning uncertainty. Consequently, a parametric study was performed comparing this baseline 19° configuration against a fully erect upper arm posture as shown in Figure 17.

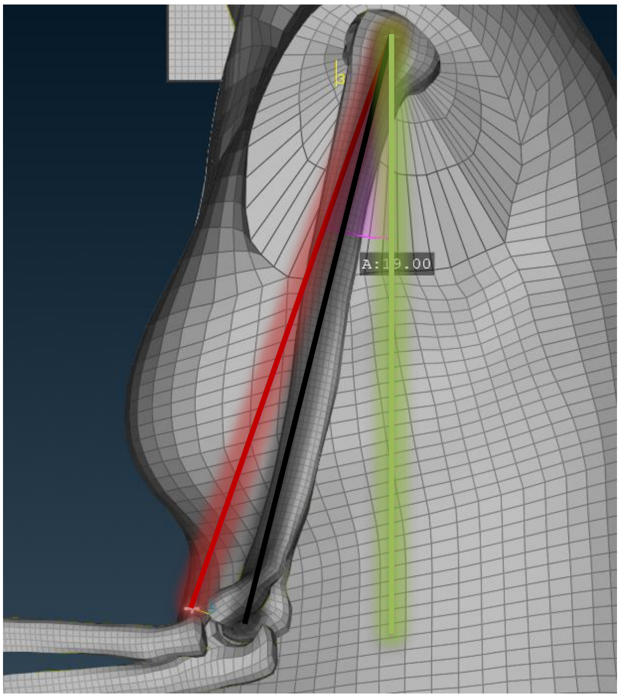

Figure 17 - HBM arm angle configurations for the Compigne loadcase: default initial arm angle (black), 19° baseline setup angle (red), and fully erect parametric arm angle aligned with the torso (green).

4.3.2 Corridor Parameters

Evaluating HBM biofidelity requires comparing simulation output curves against characteristic average responses and reference corridors generated from PMHS test data. Because ARCGen constructs these target curves, its algorithmic control settings directly dictate curve alignment, duration, and corridor width. Consequently, user-defined inputs introduce post-processing variability into the evaluation framework. Key ARCGen control parameters were identified and listed in Table 7, where they were systematically varied relative to default settings to evaluate their influence on baseline scores.

Table 7 - Identified parameters from ARCGen tool for parametric study.

Result Processing Parameters	Parameter	Description	Value
ARCGen	cut_simulation	Boolean value enabling truncation of the simulation response curve to match the maximum arc length of the characteristic reference curve.	True/False
	nWarpCtrlPts	Number of dynamic time-warping control points utilized to optimize feature alignment and phase correlation between time-history signals.	0, 1, 2, 3, 4, 5

5. Results

This section presents the simulation results for the 50F simulations across four loadcases; Kroell, Viano, Compigne and Agnew. The outputs evaluated include impactor force and deflection time-history curves (detailed in the appendix), alongside objective biofidelity rating scores calculated using the Ellipse, DALW, and ISO methods via the ARCGen tool. The baseline scores and the scores from parametric study for each loadcase are compared. To ensure clear attribution of score changes, the effects of physical setup variations and ARCGen parameter modifications are evaluated independently.

ARCGen corridors are generated from all PMHS test curves to establish a characteristic average response (cyan) and statistical boundaries (green and red). The simulation curve (blue) is subsequently compared against the average curve. Corresponding points at identical arc lengths are linked by reference lines (black), are used to compute the DALW score.

Parametric configurations of the 50F HBM were directly compared against the baseline 50F HBM setup. Model evaluation relied on objective biofidelity scores using an acceptance tolerance of ±0.1 relative to baseline scores, in accordance with (Technical Bulletin CP 550 Qualification Procedure for HBM 2025).

For the parametric studies, a threshold of ±0.1 was used to quantify if the scores changed with respect to the baseline condition. Sensitivity trends of the biofidelity scores for the Kroell, Viano, and Compigne loadcases are summarized in each loadcase section respectively, followed by an evaluation of the ARCGen algorithmic parameters. The increase or decrease in the score mentioned is based on the ±0.1 tolerance value mentioned in CP550 document.

5.1 Kroell 1971 and 1974

Following the subject selection criteria, ten subjects were selected for generating the corridors. The list of PMHS included in reference corridor generation and objective scoring calculation is shown in Table 21 in appendix A.

The biofidelity alignment between the simulation response and ARCGen corridors varies across the evaluated time-history curves and cross-plots. The force-time curve displays an early slope delay but subsequently aligns with the characteristic average response. In contrast, the deflection-time curve captures the initial slope accurately but underpredicts displacement near the end of the impact cycle. Consequently, the force-deflection plot shows continuous force underprediction across the deflection range up to maximum displacement. These response characteristics and corridor comparisons are shown in Figure 18 to Figure 20.

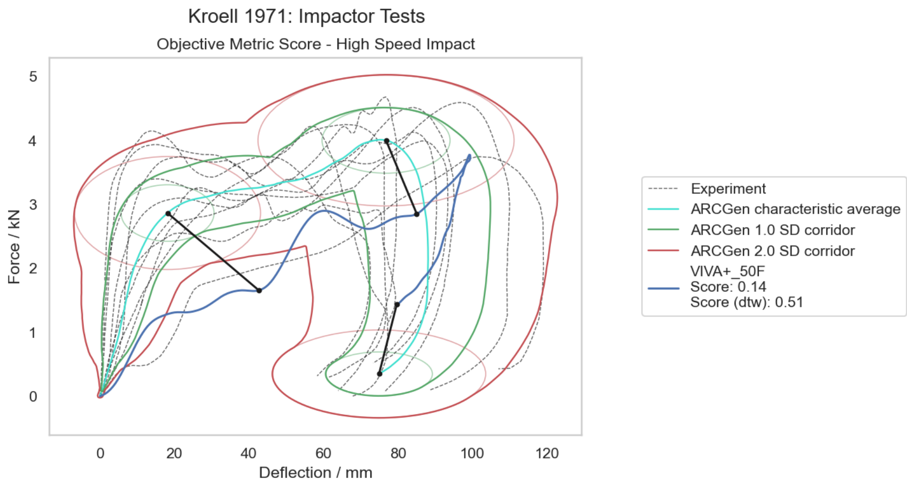

Figure 18 - Kroell loadcase - ARCGen Corridor and Objective Metric Score at 6.7 m/s impact speed (Force vs Deflection).

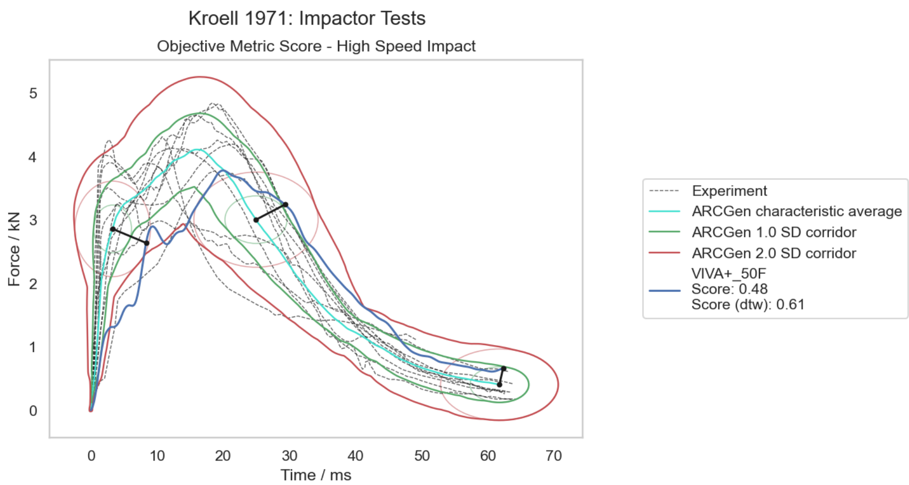

Figure 19 - Kroell loadcase - ARCGen Corridor and Objective Metric Score at 6.7 m/s impact speed (Force vs Time).

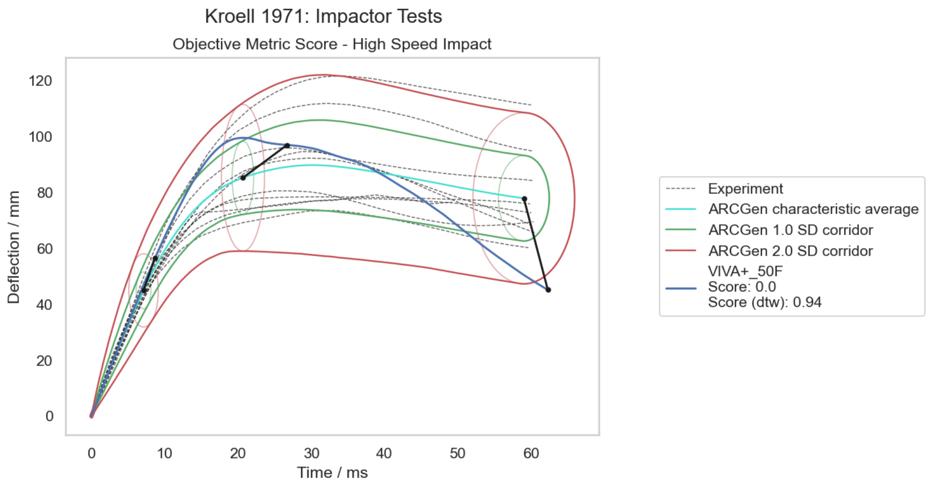

Figure 20 - Kroell loadcase - ARCGen Corridor and Objective Metric Score at 6.7 m/s speed impact (Deflection vs Time).

5.1.1 Parametric variation in boundary condition – ACT angle

The time histories and force-deflection cross-plot are shown in Figure 25 to Figure 27 in appendix A. Also, the comparison plots between the ACT angles are presented in Figure 28 to Figure 30. The scores calculated for the different ACT angles are given in Table 8.

Table 8 - Scores for ACT parametric variations (14.5°, 19.5° and 24.5°) under Kroell thoracic impact.

ACT	Plot Type	Ellipse	DALW	ISO
14.5	Force vs Deflection	0.08	0.48	NA
	Force vs Time	0.35	0.46	0.557
	Deflection vs Time	0.11	0.96	0.613
19.5	Force vs Deflection	0.14	0.51	NA
	Force vs Time	0.48	0.61	0.695
	Deflection vs Time	0.0	0.94	0.666
24.5	Force vs Deflection	0.22	0.58	NA
	Force vs Time	0.38	0.76	0.6
	Deflection vs Time	0.32	0.95	0.607

Note : ISO 18571 is not evaluated for force-deflection (FD) curves indicated with ("NA"). Green indicates an increase in the score, while red indicates a decrease in the score

The component-wise ISO score for different ACT angles is given in Table 14, appendix A. Also, the ISO score for each subject is given in Table 15 - Table 17, appendix A.

5.1.2 Corridor parameters – cut_simulation and nWarpCtrlPts

The score variation can be observed when the change in number of warping control points changes the ellipse and DALW scores. The trend in scores is shown in the plots (Figure 31 - Figure 38), appendix A.

The ISO scores for different warping points at 19.5° ACT angle showed no change in the scores, as shown in Table 9 along with component-wise scores in Table 19, appendix A. Similarly, the other ACT angles were evaluated and the variation in scores are given in Table 20 and Table 21, appendix A.

Table 9 - Influence of warping control points (nWarpCtrlPts) on ISO 18571 scores at 19.5° ACT angle.

nWarpCtrlPts	Measure	19.5°
0	Force-time	0.695
	Deflection-time	0.65
1	Force-time	0.695
	Deflection-time	0.666
2	Force-time	0.694
	Deflection-time	0.667
3	Force-time	0.697
	Deflection-time	0.671
4	Force-time	0.699
	Deflection-time	0.671
5	Force-time	0.697
	Deflection-time	0.666

Toggling the ARCGen cut_simulation parameter from FALSE to TRUE, altered the biofidelity scores across all evaluated ACT postures. For 19.5° ACT configurations, the deflection-time Ellipse scores increased upon enabling curve truncation, shown in Figure 38, appendix A. The cut_simulation parameter only takes effect when the simulation curve is longer than the reference average curve. The score variation for other ACT angles is shown in appendix A.

5.2 Viano 1989

Following the subject selection criteria in the methodology, the corridor includes both male and female subjects. The list of PMHS included in reference corridor generation and objective scoring calculation is shown in Table 22 in appendix B.

The force-compression ARCGen corridor spans a restricted section of the full response curve because the x-axis represents percentage compression, limiting objective rating calculations to this specific interval. In contrast, the force–time responses show anatomical variation: the thoracic simulation overpredicts force during the initial 15 ms before dropping below the characteristic average curve, whereas the abdominal responses closely align with the target average curves across the impact except the pelvic response, which can be observed in the Figure 50 through Figure 56, appendix B.

Structural responses under parametric variations are captured through force–time histories and force-hub displacement cross-plots, as shown in Figure 42 to Figure 49 in appendix B. Furthermore, comprehensive performance comparisons incorporating both force–compression cross-plots and force–time histories highlight the precise influence of these parameter modifications on overall structural behavior, as shown by the corresponding response curve shifts in Figure 57 to Figure 64 in appendix B.

5.2.1 Parametric variation in boundary condition – Seated and Standing 50F HBM

The scores calculated for seated and standing 50F HBM posture are in Table 10 and Table 11.

Table 10 – Scores of seated and standing 50F for force–deflection responses under Viano loadcase.

Part	Impact Speed (m/s)	Seated 50F		Standing 50F	
		Ellipse	DALW	Ellipse	DALW
Thorax	4.4	0.94	0.99	0.78	0.89
	6.5	0.72	0.87	0.93	0.99
	9.5	0.59	0.73	0.64	0.85
Abdomen	4.8	0.63	0.92	0.96	0.98
	6.8	0.48	0.77	0.61	0.97
	9.4	0.84	0.96	0.83	0.98
Pelvis	9.8	0.12	0.21	0.11	0.23

Table 11 – Scores of seated and standing 50F for force–time responses under Viano loadcase.

Part	Impact Speed (m/s)	Seated 50F			Standing 50F		
		Ellipse	DALW	ISO (force-time plot)	Ellipse	DALW	ISO (force-time plot)
Thorax	4.4	0.22	0.86	0.668	0.67	0.86	0.764
	6.5	0	0.29	0.429	0.1	0.6	0.621
	9.5	0.03	0.7	0.575	0.33	0.8	0.709
Abdomen	4.8	0.56	0.91	0.671	0.81	0.98	0.832
	6.8	0.17	0.86	0.783	0.38	0.85	0.849
	9.4	0.43	0.94	0.793	0.47	0.95	0.856
Pelvis	9.8	0.03	0.26	0.778	0.06	0.38	0.795

Note : Green indicates an increase in the score, while red indicates a decrease in the score.

The component-wise ISO scores for the seated and standing 50F simulations are presented in Table 23 and Table 24 , respectively, in appendix B. Additionally, the individual subject ISO scores for the experimental dataset are provided in Table 25 and Table 26 of appendix B.

5.2.2 Corridor parameters – cut_simulation and nWarpCtrlPts

Objective metric scores demonstrated high sensitivity to variations in the warping control points (nWarpCtrlPts) relative to the default setting (nWarpCtrlPts = 1).

- Thoracic Impact :
  - 4.4 m/s (Force-time) : Setting nWarpCtrlPts = 0 led to a reduction in the Ellipse score across both seated and standing simulation runs.
  - 6.5 m/s (Force-time) : DALW scores improved when nWarpCtrlPts was expanded to 2, 3, 4, and 5 control points.
  - 9.5 m/s (Force-time) : Ellipse scores consistently decreased across all alternative nWarpCtrlPts settings.
- Abdominal Impact Loadcases :
  - 5.8 m/s (Force-time) : The Ellipse score dropped at nWarpCtrlPts = 5.
  - 6.8 m/s (Force-time) : The DALW score decreased at nWarpCtrlPts = 0 but increased at nWarpCtrlPts = 2.
  - 9.4 m/s (Force-compression & Force-time) : Setting nWarpCtrlPts = 0 caused a reduction in Ellipse scores for both force-compression and force-time responses.

For reference, Figure 65 through Figure 71 in appendix B shows all the variations in seated Ellipse and DALW scores resulting from adjustments to the nWarpCtrlPts parameter. Similarly,

Figure 72 through Figure 78 in appendix B shows the corresponding score changes with standing 50F across varying nWarpCtrlPts values.

Enforcing curve truncation by setting cut_simulation from FALSE to TRUE is both physically and algorithmically counterintuitive. Because the experimental PMHS reference data span a specific evaluation window that naturally corresponds to the uncut simulation profile (cut_simulation = FALSE). Enabling truncation reduces curve length alignment, leading to a severe drop in scores due to comparing non-equivalent arc lengths.

5.3 Compigne 2004

Following the subject selection criteria in the methodology, it includes both male and female subjects. The list of PMHS included in the reference corridor generation and objective scoring calculation is shown in Table 27 in appendix C.

Across the shoulder impacts, simulation curve behavior varies relative to the characteristic average response. The 0° impact model captures early stiffness but underestimates mid-deflection force, while the ±15° oblique configurations display delayed stiffness and a plateaued peak before converging during unloading, as shown in Figure 82 through Figure 85, appendix C. Also, the time history plots are presented in Figure 79 to Figure 81 in appendix C.

5.3.1 Parametric variation in boundary condition – Arm angle

The scores calculated with the help of the corridors generated for two arm angles are given in the Table 12.

Table 12 – Scores of Compigne shoulder impact across varying impact speeds (3 m/s, 4 m/s, 6 m/s) and impact angles (-15°, 0°, +15°) with 19° arm angle and erect arm (0°) posture.

Location	Impactor Speed (m/s) / Angle (deg)		19° arm angle		Erect arm angle (0°)	
			Ellipse	DALW	Ellipse	DALW
Left shoulder	3	0°	-	-	-	-
	4		0.26	0.48	0.18	0.5
	6		-	-	-	-
Right Shoulder	1.5	+15°	0.6	0.79	0.08	0.25
		0°	0.18	0.64	0.46	0.91
		-15°	0.0	0.21	0.29	0.66

Note : (" - ") indicate conditions where metric scores could not be calculated. Green indicates an increase in the score, while red indicates a decrease in the score

The scores get better from angled arm position to erect-angled position of the HBM. Only the right shoulder impact at -15° has reduced the score.

5.3.2 Corridor parameters – cut_simulation and nWarpCtrlPts

Modifying the warping control points (nWarpCtrlPts) influenced metric stability; across all control point settings except the default value (nWarpCtrlPts = 1), the Ellipse score decreased for the Compigne 4 m/s lateral shoulder impact at 0° as shown in Figure 21.

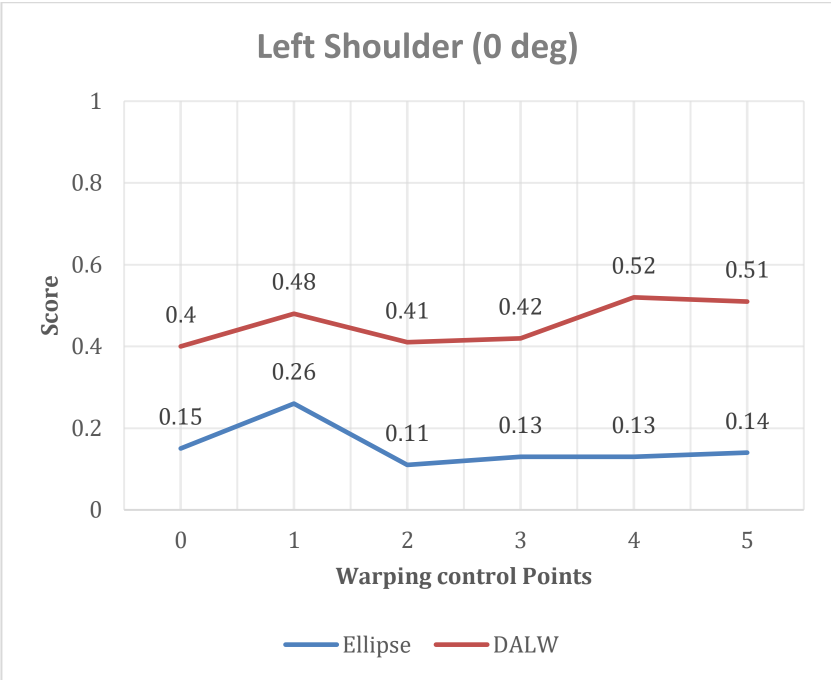

Figure 21 - Change in scores with nWarpCtrlPts results on left shoulder impact at 4 m/s and 0° angle.

The variation in scores with arm angled at 19° with different number of warping control points are shown in the Figure 86 through Figure 89 in appendix C. Similarly, the results of the parametric study, in which the arm angle was adjusted to be aligned with the upper torso and change in number of warping control points, are presented in Figure 90 to Figure 93 in appendix C.

For the 19° arm angle, enabling or disabling this parameter (true or false) produced identical scores. However, differences were observed for the erect arm angle, specifically for the 1.5 m/s impact at an impact angle of -15°. These results are summarized in the Figure 22 bar graphs below.

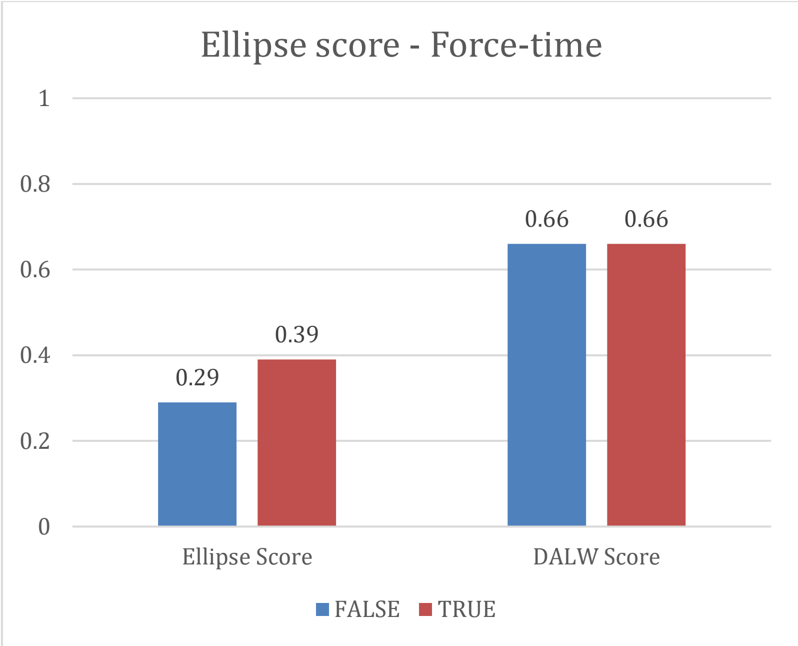

Figure 22 - Influence of cut_simulation on force–time objective scores for the Compigne oblique shoulder impact at 1.5 m/s and -15° angle.

5.4 Agnew 2024

Following the subject selection criteria, it includes the Agnew and Shaw load cases from (Shaw et al. 2006), which are used in the corridor to calculate the score, shown in Table 28.

The ARCGen corridor generated for lateral impacts, the model's peak force is close to the average response and overestimates maximum deflection before diverging in late unloading. In oblique impacts, the force-time response closely follows the characteristic average curve, whereas the deflection-time history exhibits a phase-shifted peak and rapid late-stage attenuation as shown in the Figure 98 to Figure 101 in appendix D. Furthermore, the time history plots are presented in Figure 94 to Figure 97 in appendix D.

The scores obtained via ARCGen corridor with the comparison of average curve with simulation curve is calculated and presented in the Table 13.

Table 13 - Objective biofidelity rating scores evaluated across force–time and deflection–time responses in the Agnew thoracic impact loadcases.

Plot Type	Angle	Ellipse	DALW	ISO
Force vs Time	Oblique	0.58	0.98	0.309
	Lateral	0.45	0.72	0.438
Deflection vs Time	Oblique	0.12	0.4	0.356
	Lateral	0.45	0.85	0.562

The component-wise ISO scores for all simulations are detailed in appendix D, Table 29. Additionally, the individual subject ISO scores for the Agnew experiment are listed in Table 30 and Table 31 for force–time and deflection–time responses, respectively.

6. Discussion

6.1 Subject selection

As mentioned in the subject selection, experimental reference corridors generated via ARCGen were derived from female subjects where available (e.g., Compigne). However, other loadcases contained very few experimental datasets due to which ARCGen couldn't generate statistical corridors and compute objective metric scores. To address this data insufficiency, male subjects were selectively integrated into the corridor generation process. The inclusion criterion for male PMHS data was that subject weight fell within the allowable boundaries representing the average female population weight distribution. Stature was not considered because in impact biomechanics and impulse response scaling, key responses such as contact force and deflection can be predominantly governed by tissue inertia and mass distribution rather than overall body stature.

6.2 Score Variation

Score variations across all loadcases exhibited no single overall trend, as score sensitivity was governed entirely by the mechanics of the chosen rating method. The Ellipse score relies on point-by-point spatial alignment within elliptical corridors and remains sensitive to phase shifts over time. Conversely, the DALW score measures structural curve similarity based on dynamic arc length, remaining decoupled from absolute time dependency. Thus, both metrics offer distinct yet equally valid perspectives on model biofidelity rather than one being strictly superior to the other.

6.3 ISO 18571 evaluation for loadcases

Evaluating the results under the ISO 18571 rating scale demonstrates that the majority of force-time and deflection-time responses in Kroell loadcase fall within the fair biofidelity band. The baseline parameters yield a fair correlation, whereas a -5° reduction in seating angle (14.5°) reduces force-time biofidelity to poor. In the Viano loadcase, transitioning the HBM from a seated to a standing posture improves overall signal correlation, notably elevating abdominal biofidelity from fair to good across all impact speeds.

6.4 Loadcase corridor construction limitation

For the Kroell loadcase, reference corridors could not be constructed for 4.3 m/s condition due to data processing limitations within ARCGen. Specifically, the software was unable to parse the experimental dataset required to synthesise the characteristic average response curve and statistical deviation corridors. Consequently, only the 6.7 m/s impact speed was evaluated in this study. Similarly, for Viano loadcase, an ARCGen corridor could not be generated for the 5.2 m/s pelvis impact configuration because only two subjects met the criteria for inclusion in this speed condition.

6.5 Parametric angle changes in Kroell

Objective scores vary across impact angles due to differences in local kinematics between soft tissue and sternal displacement. At a 24.5° impact angle, initial tissue deflection precedes sternal displacement relative to the impactor. Conversely, at a 14.5° angle, initial engagement occurs simultaneously at skin contact, leading to a delayed sternal response relative to the soft tissue deformation. This comparison of the impact is shown in Figure 23. Consequently, the objective score for the deflection–time history decreases as the impact angle is reduced, as shown in Figure 28 - Figure 30 in appendix A.

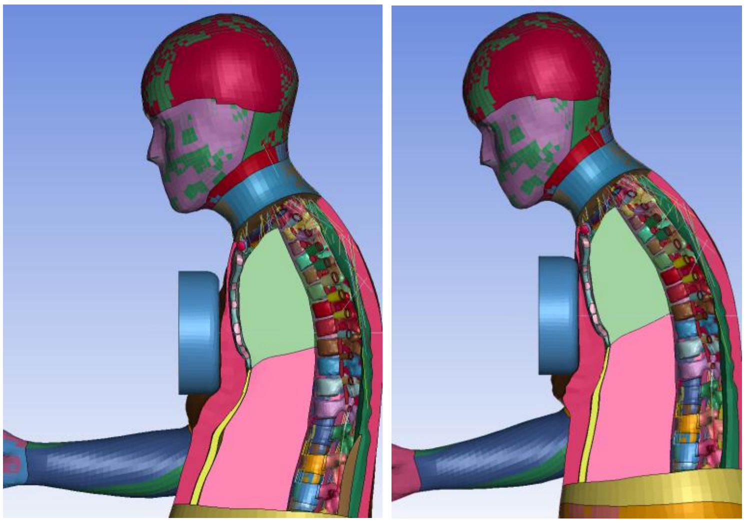

Figure 23 - Hub impact on the sternum at 14.5° and 24.5° impact angle

6.6 Evaluation of ARCGen algorithmic parameters

Following CP 550 guidelines (Technical Bulletin CP 550 Qualification Procedure for HBM 2025), factor_cut_displacement was held constant and omitted from the parametric study due to its deterministic value given in the CP 550 document. The simulation dataset is exclusively affected by nWarpCtrlPts and cut_simulation, whereas both the simulation and experimental datasets are influenced by factor_cut_displacement, as illustrated by the color-coded flowchart in Figure 24.

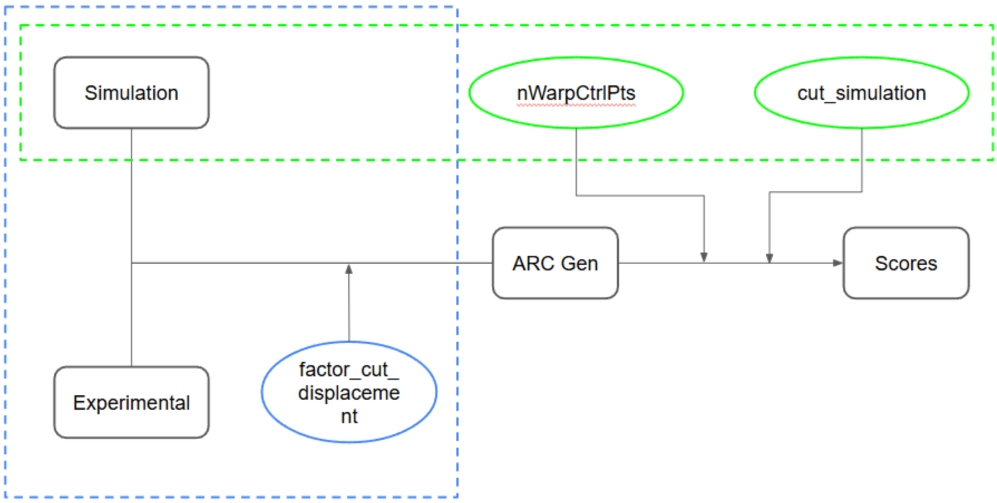

Figure 24 - Flowchart showing ARCGen parameter dependencies, with color-coded sections indicating which datasets are affected by each parameter.

The cut_simulation parameter is defined as a Boolean variable, limiting its possible values to simply true or false. Meanwhile, nWarpCtrlPts was varied from 0 to 5 based on (Ressi et al. 2025). While (Hartlen and Cronin 2026) showed that nWarpCtrlPts can extend up to 8, adjustments to this parameter directly alter response corridors and objective ratings. Stable objective rating scores across varying warping point counts signify that the curve is fully fitted, whereas adding extra control points may lead to overfitting. In contrast, score variations across point densities indicate that higher point resolution is needed for an accurate fit. Selecting an appropriate number of warping points in ARCGen is important: too few (≤ 2) fail to align local extrema, producing poor trends and artificially wide corridors, while too many (> 5) risk over-registration. This selection of number of warping points can be considered in future work.

6.6 Future Work

Future work will need to focus on expanding the qualification framework for the 50F across additional loadcases featuring varied experimental setups and boundary conditions, such as tabletop configurations and full-scale sled tests. Alongside loadcase expansion, future work will integrate the recommendations of (Hartlen and Cronin 2026) to optimise the selection of the nWarpCtrlPts parameter in the ARCGen setting.

7. Conclusion

This thesis initiates a step towards qualification of the 50th percentile female HBM across the Kroell, Viano, Compigne, and Agnew loadcases under the HBM4VT framework. The study was structured around three core objectives: setting up HBM4VT loadcases for 50F VIVA+ HBMs, conducting parametric study on uncertain variables to evaluate the influence of uncertainties in the boundary conditions and scoring methodology factors, and evaluating the objective metric scores along with the effect of parametric study on it using scoring methodology such as Ellipse, DALW and ISO 18571.

For the first objective, VIVA+ 50F HBM were simulated for setup conditions replicating the physical experimental environments. The ARCGen tool was used to generate characteristic average curve and statistical reference corridors from experimental PMHS data. To address additional data for female corridor, selective male subjects meeting mass criteria were also considered to generate the corridors.

For the second objective, uncertain parameters pertaining to boundary conditions across the loadcases were evaluated. For Kroell loadcase, the ACT angle (representing seating posture) was varied by ±5°. For Viano loadcase, the baseline seated HBM posture was replaced with a standing posture to better replicate the experimental setup. For Compigne loadcase, the upper arm angle initially defined at 19° in the baseline framework was adjusted to align erect with the upper torso.

Finally, the objective biofidelity scores across Ellipse, DALW, and ISO 18571 metrics were evaluated for both baseline and parametric configurations. Variations in metric scores were analyzed and reported in accordance with Technical Bulletin CP 550 evaluation guidelines. All the results were compared to understand the influence of boundary conditions with uncertainty in how to select parameters in the post-processing phase, and relate this to the specified tolerance of the EuroNCAP protocol.

8. References

Agnew, A, G Baker, A Marcallini Jr, A Bendig, K Moorhouse, H Rhule, J Bolte Iv, and Y-S Kang. 2024. “Small Female Post-Mortem Human Subject (PMHS) Thoracic Responses to Simplified Oblique and Lateral Loading.”

Compigne, Sabine, Yves Caire, Thierry Quesnel, and Jean-Pierre Verries. 2004. “Non-Injurious and Injurious Impact Response of the Human Shoulder Three-Dimensional Analysis of Kinematics and Determination of Injury Threshold.” In , 2004-22–0005. doi:10.4271/2004-22-0005.

“CP550 HBM Qualification_v11.” 2025.

Gayzik, F Scott, Daniel P Moreno, Nicholas A Vavalle, Ashley C Rhyne, and Joel D Stitzel. 2005. “Development of a Full Human Body Finite Element Model for Blunt Injury Prediction Utilizing a Multi-Modality Medical Imaging Protocol.” In Prague, Czech Republic.

Global Status Report on Road Safety. 2023. 1st ed. Geneva: World Health Organization.

Hartlen, Devon C., and Duane S. Cronin. 2022. “Arc-Length Re-Parametrization and Signal Registration to Determine a Characteristic Average and Statistical Response Corridors of Biomechanical Data.” *Frontiers in Bioengineering and Biotechnology* 10: 843148. doi:10.3389/fbioe.2022.843148.

Hartlen, Devon C., and Duane S. Cronin. 2026. “Warping Points in Arc-Length-Based Averages Have a Substantial Effect on Computed Biomechanical Response Corridors and Objective Ratings Methods.” In Munich, Germany: Devon C. Hartlen, Duane S. Cronin, 2.

Iraeus, Johan, Erik Brynskog, Jobin John, Jonas Östh, Bengt Pipkorn, and Johan Davidsson. 2024. *Development of SAFER HBM V11*. Sweden.

John, Jobin, Corina Klug, Matej Kranjec, Erik Svenning, and Johan Iraeus. 2022. “Hello, World! VIVA+: A Human Body Model Lineup to Evaluate Sex-Differences in Crash Protection.” *Frontiers in Bioengineering and Biotechnology* 10: 918904. doi:10.3389/fbioe.2022.918904.

Klug, Corina, Martin Schachner, Andre Eggers, Jakub Galazka, Simon Gargallo, Cristian Jimenez, Jessica Kirch, et al. 2023. “EURO NCAP VIRTUAL TESTING - CRASHWORTHINESS.” In Yokohama, Japan: ESV.

Kofler, Desiree, Felix Ressi, and Corina Klug. 2025a. “HBM4VT - Compigne Hub Simulation Setup.”

Kofler, Desiree, Felix Ressi, and Corina Klug. 2025b. “HBM4VT - Viano Hub Simulation Setup.”

Kroell, Charles K., Dennis C. Schneider, and Alan M. Nahum. 1971. "Impact Tolerance and Response of the Human Thorax." In San Diego, California, United States, 710851. doi:10.4271/710851.

Kroell, Charles K., Dennis C. Schneider, and Alan M. Nahum. 1974. "Impact Tolerance and Response of the Human Thorax II." In Ann Arbor, Michigan, United States, 741187. doi:10.4271/741187.

Lebarbé, M, and P Petit. 2012. "New Biofidelity Targets for the Thorax of a 50th Percentile Adult Male in Frontal Impact."

Ressi, F, B Schneider, D Kofler, V Kannan, D Hartlen, D Cronin, and C Klug. 2025. "Development of a Robust Human Body Model Qualification Methodology: Ensuring Biofidelity for Occupant Protection Assessments in Virtual Testing." In Vilnius, Lithuania.

"Road Vehicles - Objective Rating Metric for Non-Ambiguous Signals." 2024.

Shaw, Joshua M., Rodney G. Herriott, Joseph D. McFadden, Bruce R. Donnelly, and John H. Bolte. 2006. "Oblique and Lateral Impact Response of the PMHS Thorax." In , 2006-22–0007. doi:10.4271/2006-22-0007.

Viano, David C. 1989. "Biomechanical Responses and Injuries in Blunt Lateral Impact." In Washington, District of Columbia, United States, 892432. doi:10.4271/892432.

Appendix A

Table 21 – Kroell experimental PMHS subject demographics, impact test speed at 6.7 m/s, and corridor acceptance criteria for 50F qualification.

Subject	Impact Speed	Gender	Age (years)	Height (in cm)	Weight (in kg)	50 F Corridor	Currently used by HBM4VT
Speed (6.7 m/s)							
15FM	7.33	M	80	165.1	53.1		
13FM	7.42	M	81	167.6	76.2		
18FM	6.71	M	78	175.2	65.8		
20FM	6.71	M	29	180.3	56.7		
19FM	6.71	M	19	172.7	65.8		
22FM	6.71	M	72	182.8	74.8		
63FM	6.93	M	53	183	88		
64FM	6.93	M	72	163	63		
12FF	7.24	F	67	162.5	62.6		
14FF	7.33	F	76	154.9	57.6		
21FF	6.83	F	45	172.7	68.5		
Average			61	170.8	66.5		

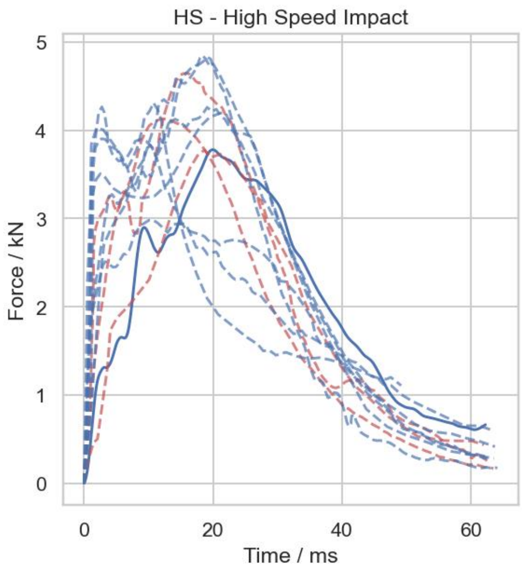

Figure 25 - Kroell loadcase - force-time plot.

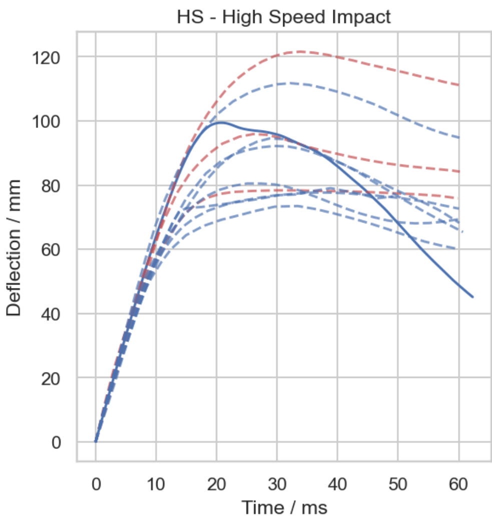

Figure 26 - Kroell loadcase - deflection-time plot.

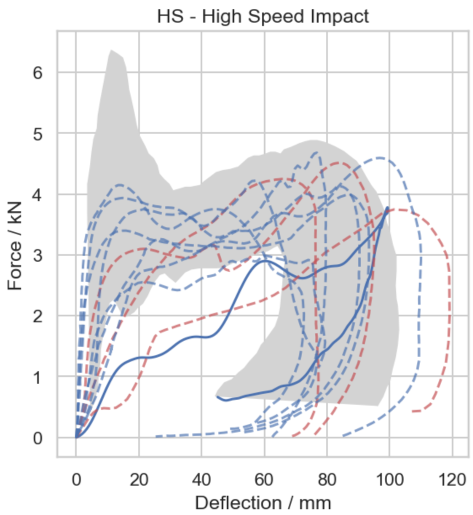

Figure 27 - Kroell loadcase - force-deflection plot.

In Figure 25 to Figure 27 graphs, the blue line is the simulation curve generated from simulation, the dotted red and blue line is the experimental data curves of females and males respectively, performed with PMHS. All the experimental data is normalized to make it compatible to compare with the simulation curve.

Figure 25 graph shows the force vs time plot, representing the simulation curve compared with the seven male and three female subjects. As mentioned in the experimental graphs, the initial force peak, the dip and the plateau can be similarly observed in this plot. Figure 26 graph represents the deflection vs time it is important to mention that the deflection here is the relative displacement of the impactor and vertebrae.

Figure 27 graph has a grey corridor is defined as Lebarbe corridor which is the performance benchmark, representing the statistical range of human response derived from the PMHS testing. The corridor is an area and not a single curve since the specification of the PMHS vary in age, size, muscle and bones condition (Lebarbé and Petit 2012).

Table 14 - Kroell's *component-wise ISO 18571 scores for different ACT angles for Kroell loadcase.*

ACT	Measure	Corridor	Phase	Magnitude	Slope	Overall
14.5	Force-time	0.443	0.256	0.927	0.718	0.557
	Deflection-time	0.502	0.814	0.67	0.58	0.613
19.5	Force-time	0.563	0.42	0.943	0.703	0.638
	Deflection-time	0.861	0.54	0.907	0.576	0.749
24.5	Force-time	0.646	0.523	0.954	0.708	0.695
	Deflection-time	0.785	0.484	0.885	0.392	0.666

Table 15 - Individual ISO scores for each subject of Kroell loadcase at 14.5° ACT angle.

Subject	Measure	Corridor	Phase	Magnitude	Slope	Overall
12FF	Force-time	0.34	0.242	0.901	0.718	0.508
	Deflection-time	0.375	0.702	0.488	0.024	0.393
14FF	Force-time	0.485	0.282	0.851	0.650	0.551
	Deflection-time	0.641	0.831	0.779	0.592	0.697
21FF	Force-time	0.646	0.637	0.948	0.673	0.71
	Deflection-time	0.824	0.444	0.88	0.619	0.718
13FM	Force-time	0.505	0.403	0.812	0.677	0.580
	Deflection-time	0.904	0.694	0.941	0.689	0.826
64FM	Force-time	0.414	0.194	0.827	0.516	0.473
	Deflection-time	0.375	0	0.293	0	0.208
15FM	Force-time	0.37	0.258	0.798	0.632	0.486
	Deflection-time	0.318	0.968	0.463	0.586	0.53
18FM	Force-time	0.522	0.226	0.831	0.617	0.544
	Deflection-time	0.503	0.911	0.703	0.721	0.668
20FM	Force-time	0.534	0	0.914	0.55	0.506
	Deflection-time	0.220	0.887	0.26	0.409	0.399
19FM	Force-time	0.443	0	0.774	0.492	0.43
	Deflection-time	0.347	0.435	0.397	0	0.305
22FM	Force-time	0.539	0.306	0.878	0.557	0.564
	Deflection-time	0.49	0.927	0.711	0.742	0.672

Table 16 - Individual ISO scores for each subject of Kroell loadcase at 19.5° ACT angle

Subject	Measure	Corridor	Phase	Magnitude	Slope	Overall
12FF	Force-time	0.518	0.516	0.922	0.706	0.636
	Deflection-time	0.578	0.339	0.741	0	0.447
14FF	Force-time	0.678	0.548	0.874	0.642	0.684
	Deflection-time	0.795	0.54	0.884	0.435	0.69
21FF	Force-time	0.882	0.919	0.972	0.654	0.862
	Deflection-time	0.506	0.097	0.486	0.426	0.404
13FM	Force-time	0.709	0.702	0.852	0.661	0.726

	Deflection-time	0.607	0.403	0.674	0.576	0.573
64FM	Force-time	0.506	0.476	0.787	0.513	0.558
	Deflection-time	0.575	0	0.651	0	0.36
15FM	Force-time	0.537	0.540	0.829	0.669	0.622
	Deflection-time	0.635	0.702	0.777	0.4	0.63
18FM	Force-time	0.739	0.492	0.866	0.617	0.691
	Deflection-time	0.821	0.645	0.934	0.669	0.778
20FM	Force-time	0.647	0	0.876	0.499	0.534
	Deflection-time	0.523	0.613	0.683	0.161	0.501
19FM	Force-time	0.51	0	0.856	0.472	0.47
	Deflection-time	0.556	0.145	0.691	0	0.39
22FM	Force-time	0.769	0.645	0.899	0.543	0.725
	Deflection-time	0.835	0.661	0.953	0.701	0.797

Table 17 - Individual ISO scores for each subject of Kroell loadcase at 24.5° ACT angle

Subject	Measure	Corridor	Phase	Magnitude	Slope	Overall
12FF	Force-time	0.375	0.339	0.93	0.687	0.541
	Deflection-time	0.389	0.685	0.5	0	0.393
14FF	Force-time	0.557	0.395	0.888	0.642	0.608
	Deflection-time	0.657	0.806	0.788	0.58	0.698
21FF	Force-time	0.689	0.694	0.968	0.619	0.732
	Deflection-time	0.796	0.395	0.859	0.582	0.686
13FM	Force-time	0.592	0.5	0.862	0.692	0.648
	Deflection-time	0.887	0.653	0.937	0.664	0.806
64FM	Force-time	0.444	0.306	0.773	0.465	0.487
	Deflection-time	0.389	0	0.303	0	0.216
15FM	Force-time	0.426	0.379	0.846	0.669	0.549
	Deflection-time	0.325	0.96	0.474	0.55	0.527
18FM	Force-time	0.613	0.339	0.879	0.6	0.609
	Deflection-time	0.521	0.887	0.711	0.711	0.67
20FM	Force-time	0.568	0	0.903	0.462	0.5

	Deflection-time	0.223	0.855	0.273	0.366	0.388
19FM	Force-time	0.47	0	0.833	0.457	0.446
	Deflection-time	0.362	0.371	0.397	0	0.298
22FM	Force-time	0.645	0.444	0.909	0.53	0.635
	Deflection-time	0.506	0.895	0.716	0.742	0.673

Table 18 - Influence of ARCGen warping control points (nWarpCtrlPts) on ISO 18571 scores across ACT angles.

		ISO 18571		
nWarpCtrlPts	Measure	14.5°	19.5°	24.5°
0	Force-time	0.558	0.695	0.598
	Deflection-time	0.599	0.65	0.592
1	Force-time	0.557	0.695	0.6
	Deflection-time	0.613	0.666	0.607
2	Force-time	0.554	0.694	0.597
	Deflection-time	0.614	0.667	0.611
3	Force-time	0.558	0.697	0.599
	Deflection-time	0.617	0.671	0.611
4	Force-time	0.561	0.699	0.602
	Deflection-time	0.618	0.671	0.611
5	Force-time	0.56	0.697	0.598
	Deflection-time	0.615	0.666	0.608

Table 19 - Component-wise ISO 18571 scores for 19.5° angle for different warping control points.

nWarpCtrlPts	Measure	Corridor	Phase	Magnitude	Slope	Overall
0	Force-time	0.645	0.523	0.962	0.699	0.695
	Deflection-time	0.773	0.467	0.878	0.358	0.65
1	Force-time	0.646	0.523	0.954	0.708	0.695
	Deflection-time	0.785	0.484	0.885	0.392	0.666
2	Force-time	0.642	0.531	0.951	0.703	0.694
	Deflection-time	0.785	0.484	0.886	0.395	0.667
3	Force-time	0.646	0.531	0.95	0.711	0.697

	Deflection-time	0.785	0.492	0.888	0.403	0.671
4	Force-time	0.65	0.531	0.951	0.715	0.699
	Deflection-time	0.785	0.492	0.888	0.403	0.671
5	Force-time	0.648	0.531	0.952	0.709	0.697
	Deflection-time	0.783	0.484	0.885	0.394	0.666

Table 20 - Component-wise ISO 18571 scores for 14.5° angle for different warping control points.

nWarpCtrlPts	Measure	Corridor	Phase	Magnitude	Slope	Overall
0	Force-time	0.442	0.256	0.934	0.718	0.558
	Deflection-time	0.49	0.797	0.659	0.558	0.599
1	Force-time	0.443	0.256	0.927	0.718	0.557
	Deflection-time	0.502	0.814	0.67	0.58	0.613
2	Force-time	0.439	0.256	0.924	0.711	0.554
	Deflection-time	0.503	0.814	0.671	0.582	0.614
3	Force-time	0.442	0.264	0.922	0.721	0.558
	Deflection-time	0.503	0.822	0.672	0.586	0.617
4	Force-time	0.444	0.264	0.925	0.726	0.561
	Deflection-time	0.503	0.822	0.672	0.587	0.618
5	Force-time	0.442	0.264	0.926	0.727	0.56
	Deflection-time	0.504	0.814	0.672	0.581	0.615

Table 21 - Component-wise ISO 18571 scores for 24.5° angle for different warping control points.

nWarpCtrlPts	Measure	Corridor	Phase	Magnitude	Slope	Overall
0	Force-time	0.494	0.369	0.957	0.678	0.598
	Deflection-time	0.51	0.755	0.668	0.516	0.592
1	Force-time	0.496	0.369	0.955	0.682	0.6
	Deflection-time	0.521	0.772	0.678	0.542	0.607
2	Force-time	0.491	0.369	0.954	0.681	0.597
	Deflection-time	0.522	0.78	0.68	0.55	0.611
3	Force-time	0.493	0.377	0.953	0.679	0.599
	Deflection-time	0.522	0.78	0.68	0.549	0.611
4	Force-time	0.496	0.377	0.954	0.686	0.602

	Deflection-time	0.523	0.78	0.68	0.549	0.611
5	Force-time	0.494	0.377	0.956	0.669	0.598
	Deflection-time	0.524	0.772	0.68	0.543	0.608

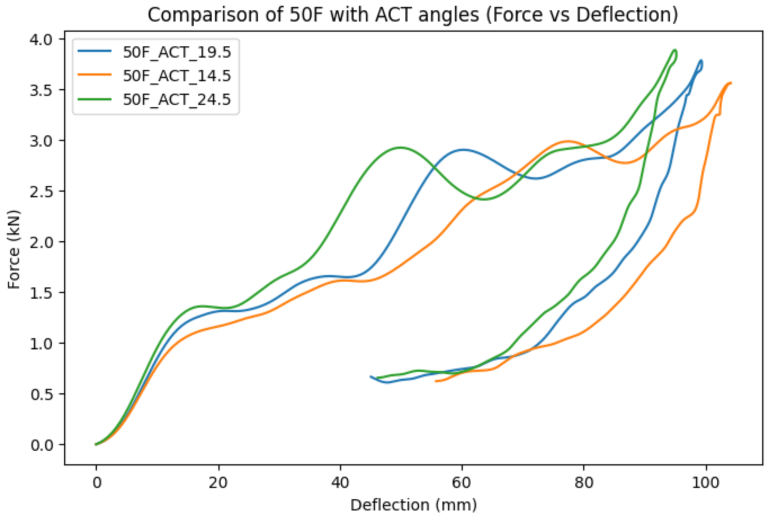

Figure 28 - Kroell loadcase - Comparison of different ACT angles (force-deflection).

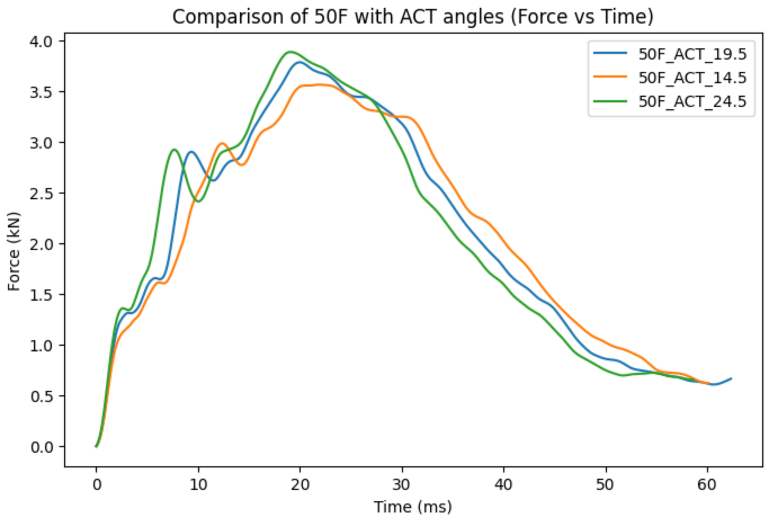

Figure 29 - Kroell loadcase - Comparison of different ACT angles (force-time).

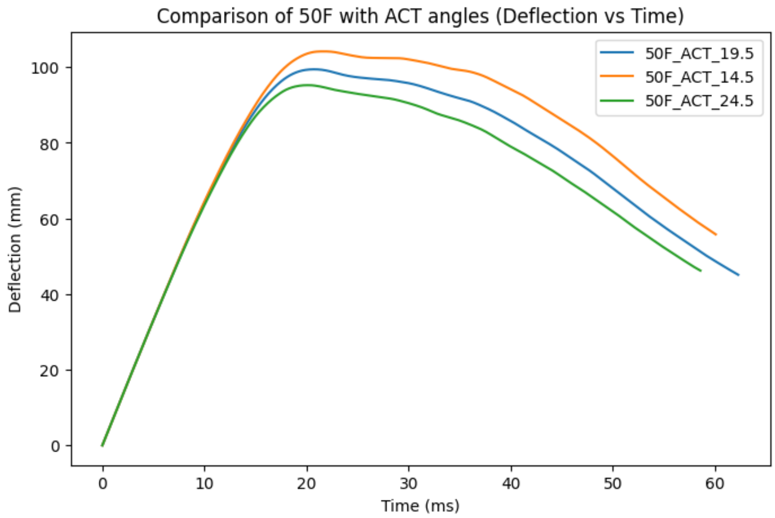

Figure 30 - Kroell loadcase - Comparison of different ACT angles (deflection-time).

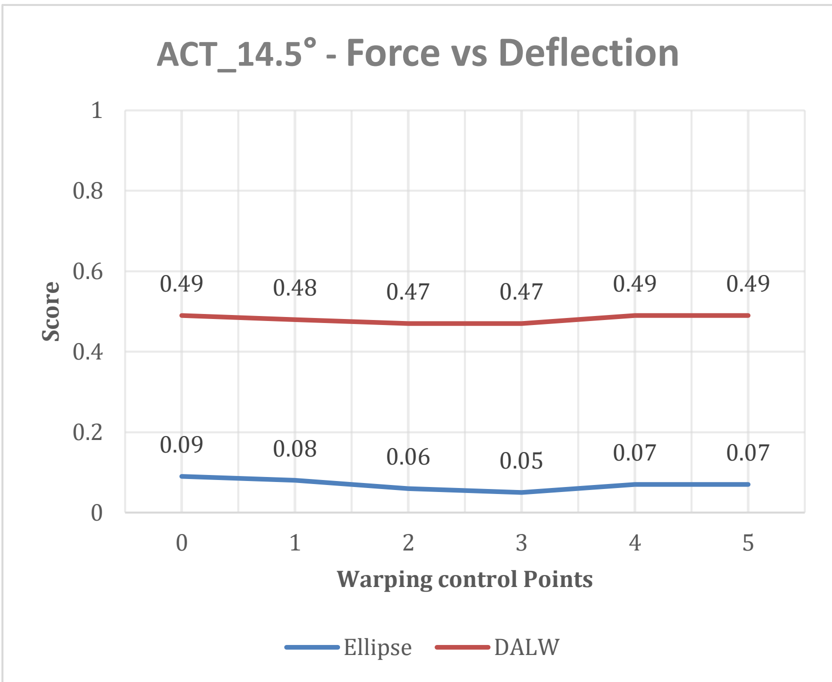

Figure 31 - Kroell loadcase - nWarpCtrlPts results at 14.5° ACT angle on force- deflection plot.

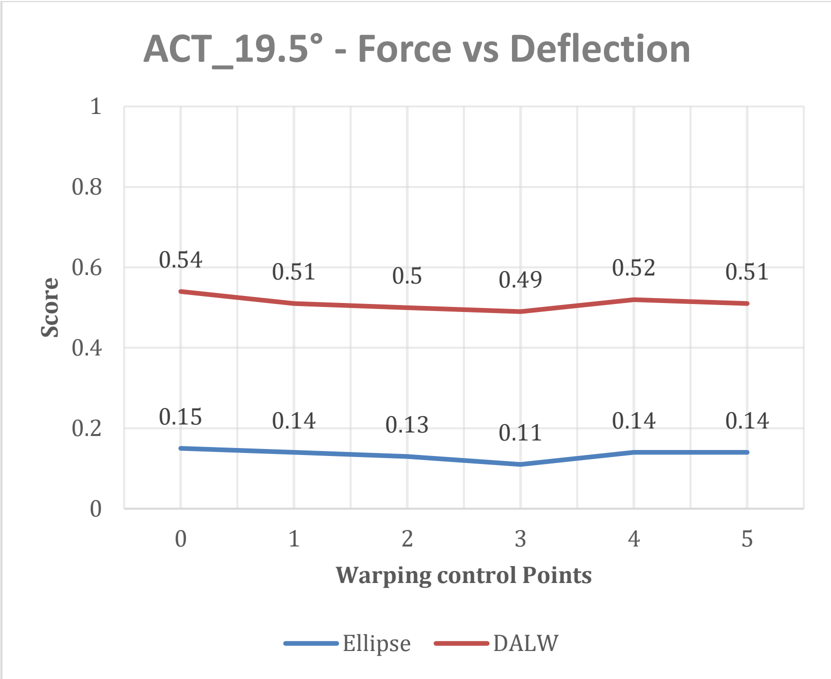

Figure 32 - Kroell loadcase - nWarpCtrlPts results at 19.5° ACT angle on force-deflection plot.

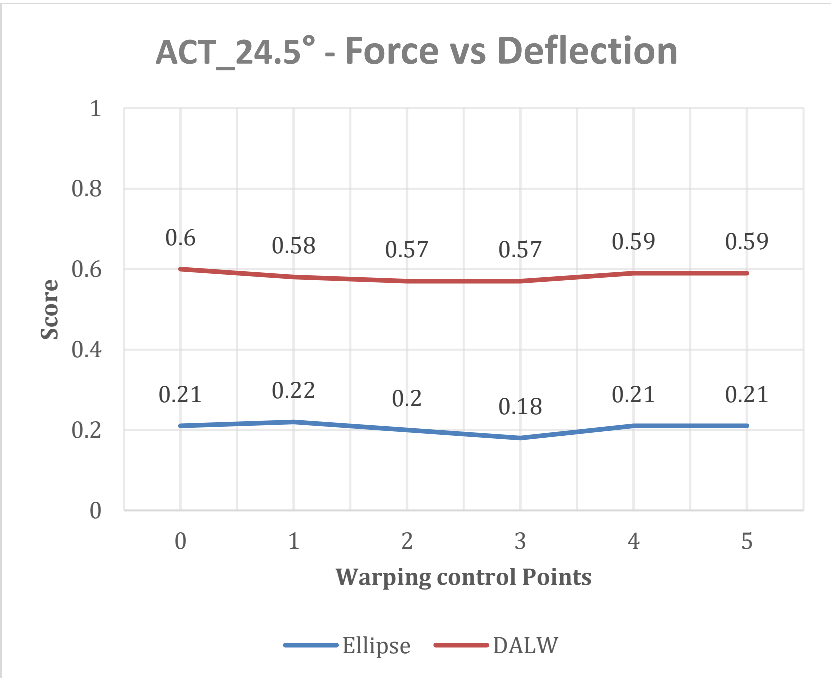

Figure 33 - Kroell loadcase - nWarpCtrlPts results at 24.5° ACT angle on force-deflection plot.

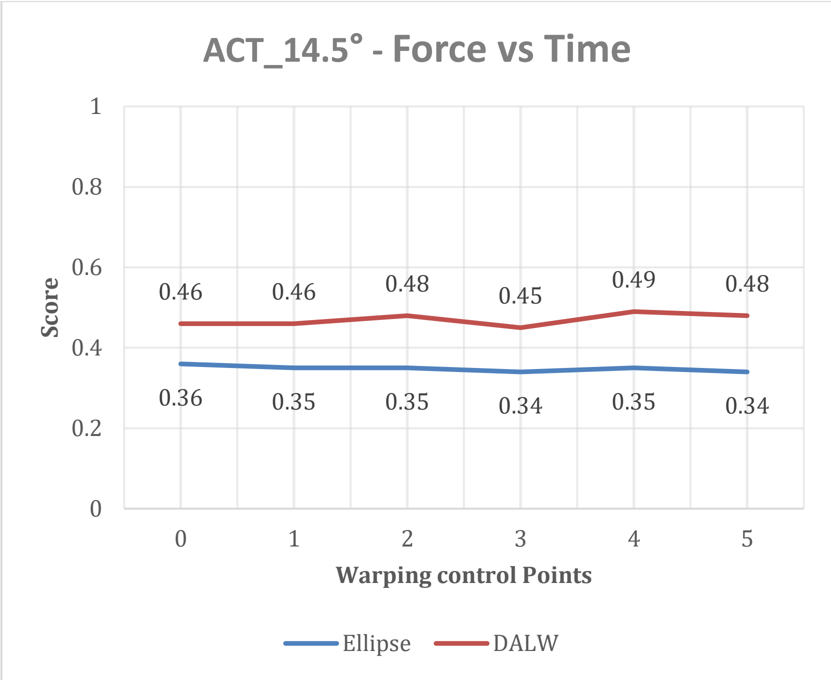

Figure 34 - Kroell loadcase - nWarpCtrlPts results at 14.5° ACT angle on force-time plot.

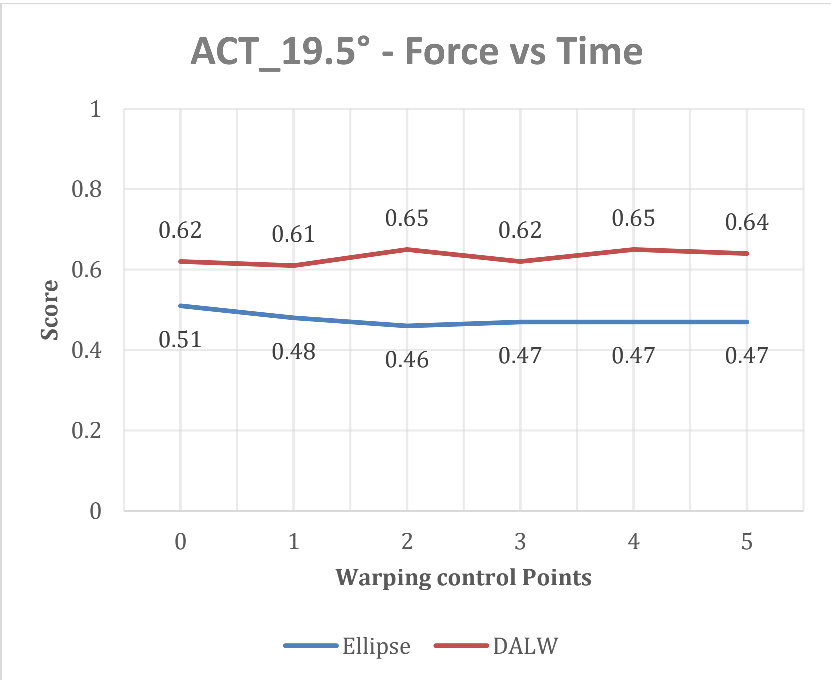

Figure 35 - Kroell loadcase - nWarpCtrlPts results at 19.5° ACT angle on force-time plot

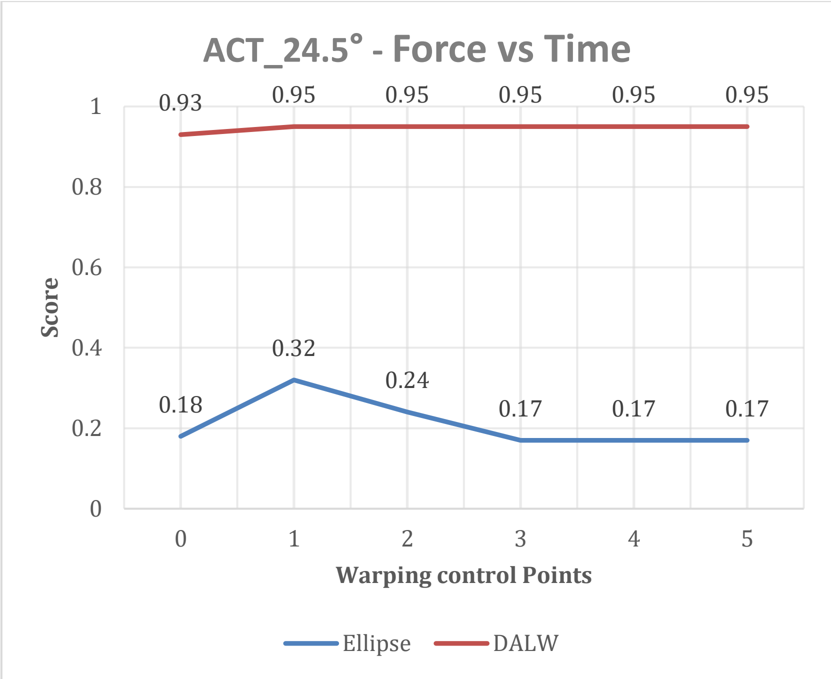

Figure 36 - Kroell loadcase - nWarpCtrlPts results at 24.5° ACT angle on force-time plot

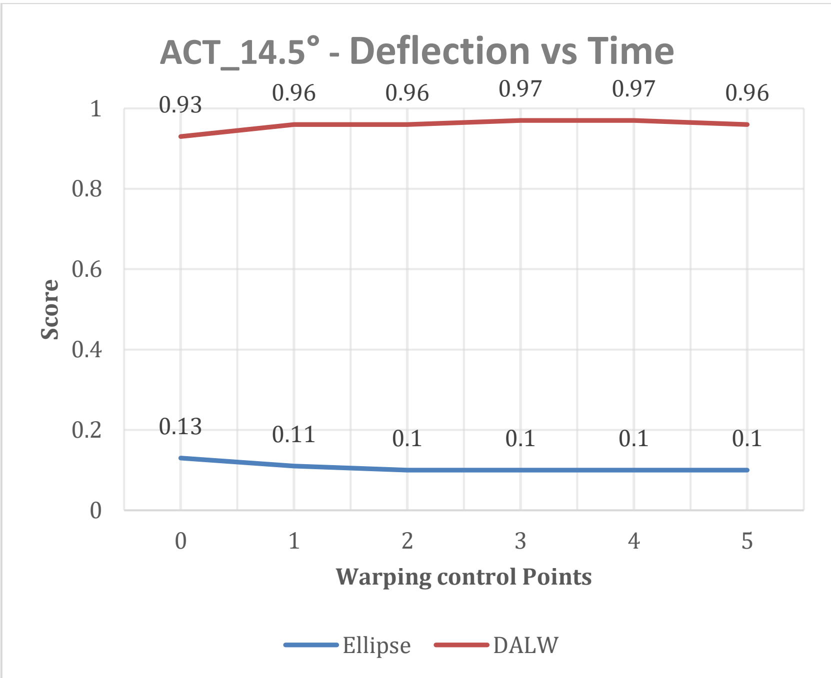

Figure 37 - Kroell loadcase - nWarpCtrlPts results at 14.5° ACT angle on deflection-time plot.

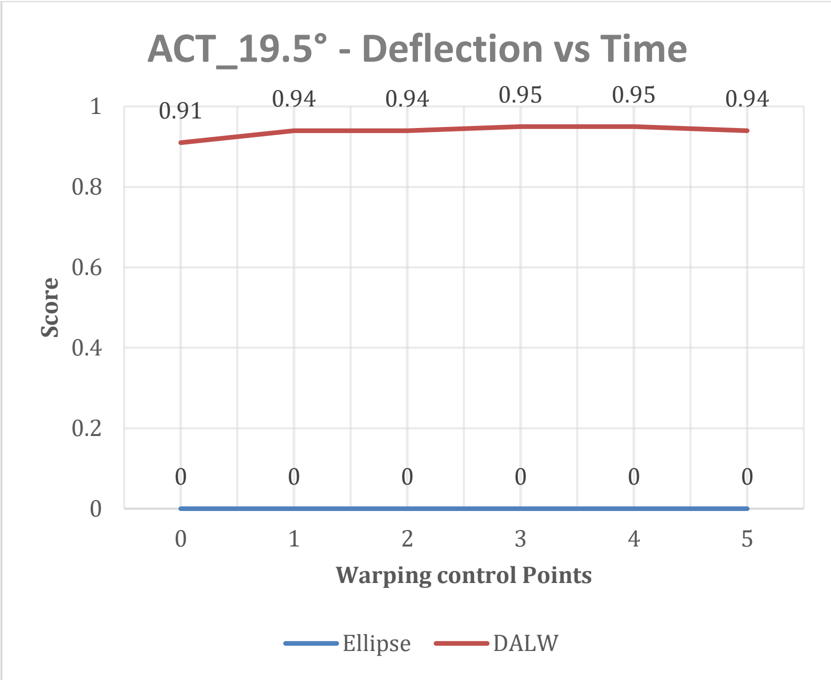

Figure 38 - Kroell loadcase - nWarpCtrlPts results at 19.5° ACT angle on deflection-time plot.

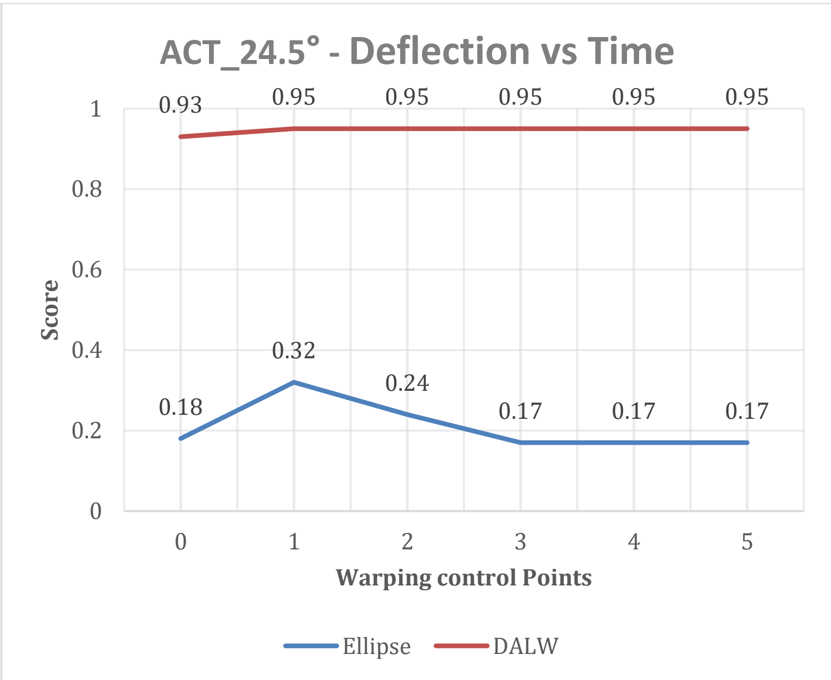

Figure 39 - Kroell loadcase - nWarpCtrlPts results at 24.5° ACT angle on deflection-time plot.

Altering the warping control points (nWarpCtrlPts) sensitive to the 24.5° ACT deflection-time response revealed that setting nWarpCtrlPts to 0, 3, 4, or 5 control points led to a score reduction compared to the baseline setting (nWarpCtrlPts = 1).

When cut_simulation parameter is set to true, its impact varies across parameters and signals:

- Deflection-time: Scores were affected across all ACT values.
- 19.5° (Baseline Angle): Force-deflection and force-time scores remained identical.
- 14.5° Parametric Angle: Force-deflection and force-time scores were unaffected, while deflection–time scores changed.
- 24.5° Parametric angle: Only force-deflection scores remained unchanged; both force-time and deflection–time scores were affected.

The exact score changes are summarized in Figure 40 and Figure 41 in the form of bar graphs.

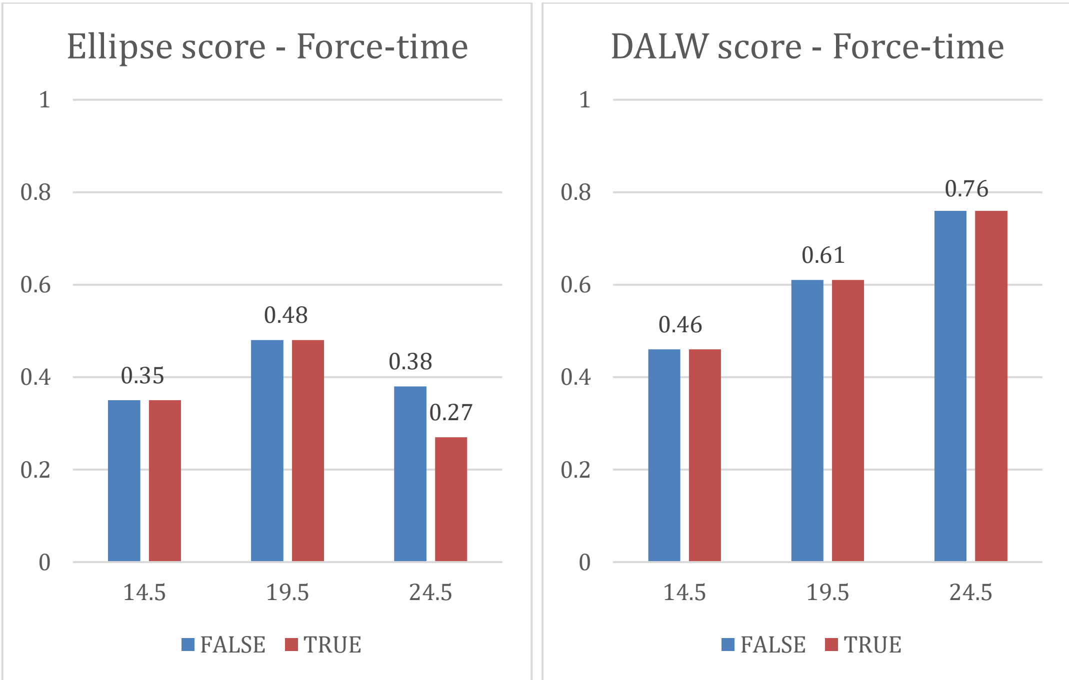

Figure 40 - Kroell loadcase - Comparison of force–time Ellipse and DALW scores across different impact angles for enabled (true) and disabled (false) cut_simulation settings in ARCGen.

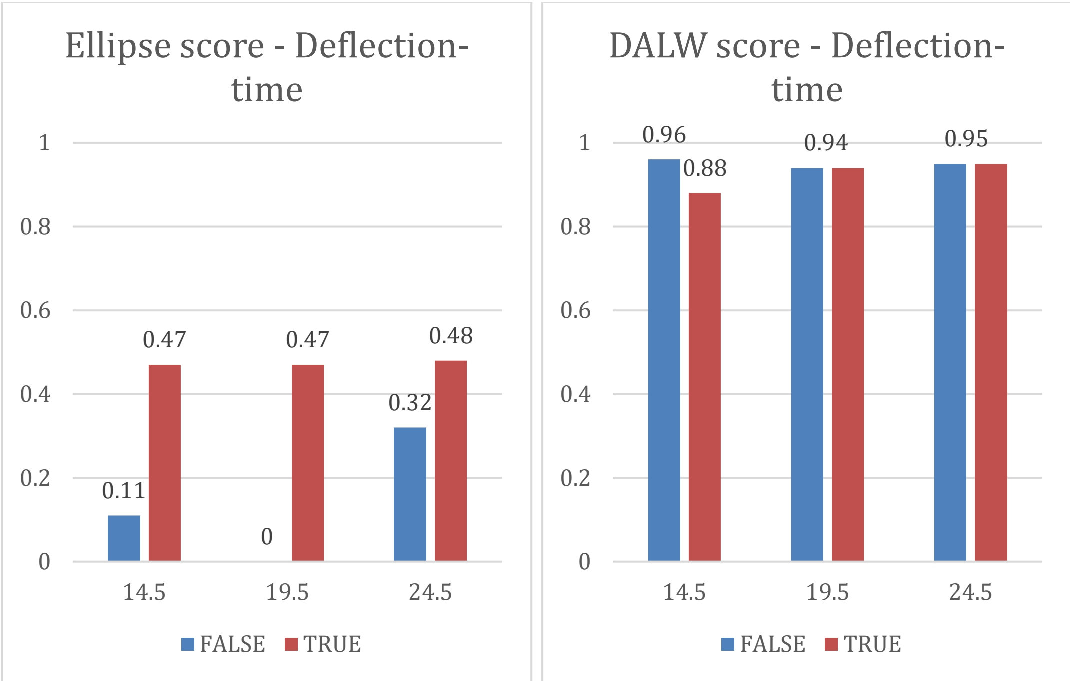

Figure 41 - Kroell loadcase - Comparison of deflection–time Ellipse and DALW scores across different impact angles for enabled (true) and disabled (false) cut_simulation settings in ARCGen.

Appendix B

Table 22 - Cadaveric subject metadata, test velocity classification, and corridor inclusion criteria for Viano lateral thoracic, abdominal, and pelvic impact configurations.

Subject	Impact Speed (m/s)	Gender	Age (years)	Height (in cm)	Weight (in kg)	50 F Corridor	Currently used by HBM4VT
Abdomen LS (4.8 m/s)							
986	5.1	M	29	173	70.3		
47	5.5	M	62	176.5	83.91		Twice
8	5.1	F	52	157	53.07		
UOM2	3.8	M	64	178.5	75.76	Twice	Twice
Average			51	171.2	70.76		
Abdomen MS (6.8 m/s)							
947	6.79	M	38	166.5	56.25		
954	6.73	M	66	159	56.25		
RNY2	6.75	M	64	171	61.69		
956	7.06	F	40	175	76.2		
Average			52	167.8	62.59		
Abdomen HS (9.4 m/s)							
993	8.1	M	49	173	70.76		
986	9.8	M	29	173	70.3		
47	9.9	M	62	176.5	83.91		
63	9.8	M	64	173	48.54		
Average			51	173.8	68.37		
Thorax LS (4.4 m/s)							
986	5.5	M	29	173	70.3		
8	5.2	F	52	157	53.07		
UOM1	4	M	37	186.5	67.59		
UOM2	3.8	M	64	178.5	75.76	Twice	Twice

Average			45	173.75	66.68		
Thorax MS (6.5 m/s)							
935	5.99	M	63	174	69.85		
947	6.48	M	38	166.5	56.25		
954	6.73	M	66	159	56.25		
RNY2	6.71	M	64	171	61.69		
956	6.71	F	40	175	76.2		
Average			54	169.1	64		
Thorax HS (9.5 m/s)							
863	9.4	M	49	176	107		
RNY1	8.7	F	76	153.5	44		Another female subject
993	8.3	M	49	173	70.76		
986	9.7	M	29	173	70.3		
63	9.7	M	64	173	48.54		
UOM1	10.2	M	37	186.5	67.59		
Average			50	172.5	68		
Pelvis HS (9.8 m/s)							
993	8.5	M	49	173	70.76		
986	9.6	M	29	173	70.3		
47	9.9	M	62	176.5	83.91		
8	9.5	F	52	157	53.07		
63	10.1	M	64	173	48.54		
UOM1	10.3	M	37	186.5	67.59		
Average			49	173.1	65.69		

Note : The red marked subjects are the ones with no data available to consider in the corridor.

In the Figure 42 - Viano loadcase - force vs hub displacement and force-time plot at 4.4 m/s impact speed on thorax.Figure 42 to Figure 49 graphs, the blue line is the simulation curve generated from simulation, the dotted red and blue line is the experimental data curves of females and males respectively, performed with PMHS. All the experimental data is normalized to make it compatible to compare with the simulation curve. The pattern of the peak and dip of the force can be observed here too, as mentioned in Kroell simulation results.

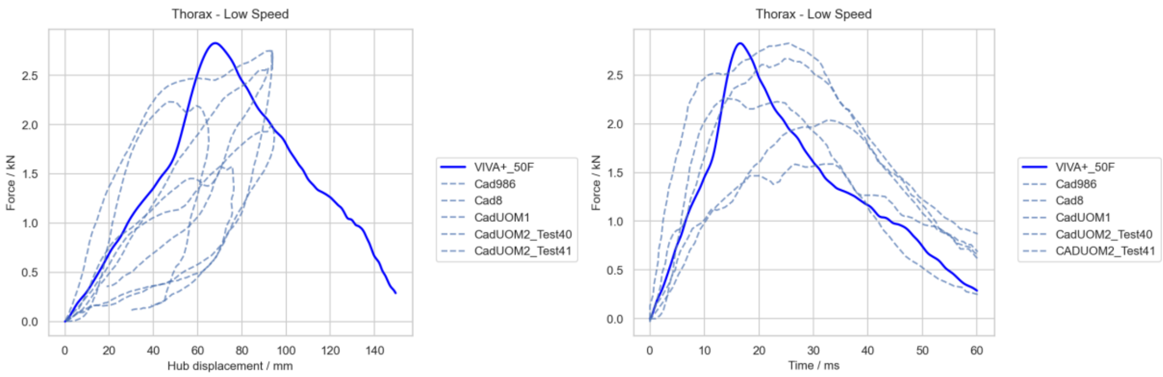

Figure 42 - Viano loadcase - force vs hub displacement and force-time plot at 4.4 m/s impact speed on thorax.

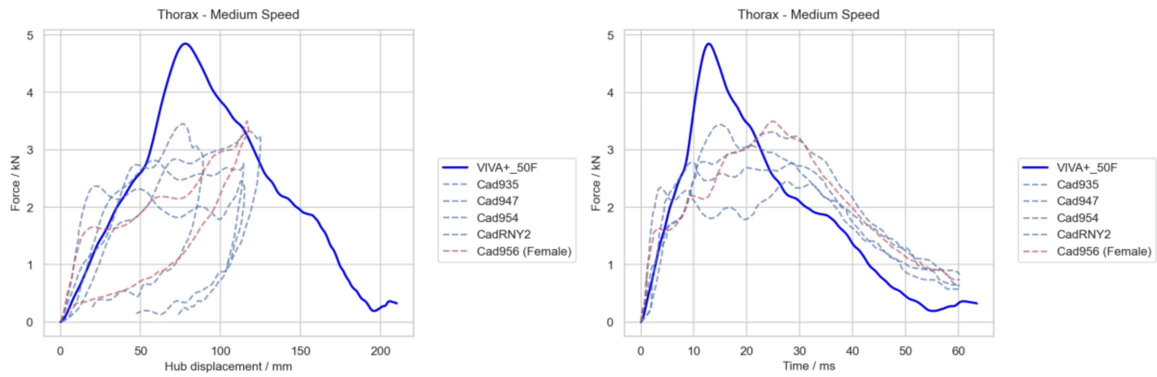

Figure 43 - Viano loadcase – force vs hub displacement and force-time plot at 6.5 m/s impact speed on thorax.

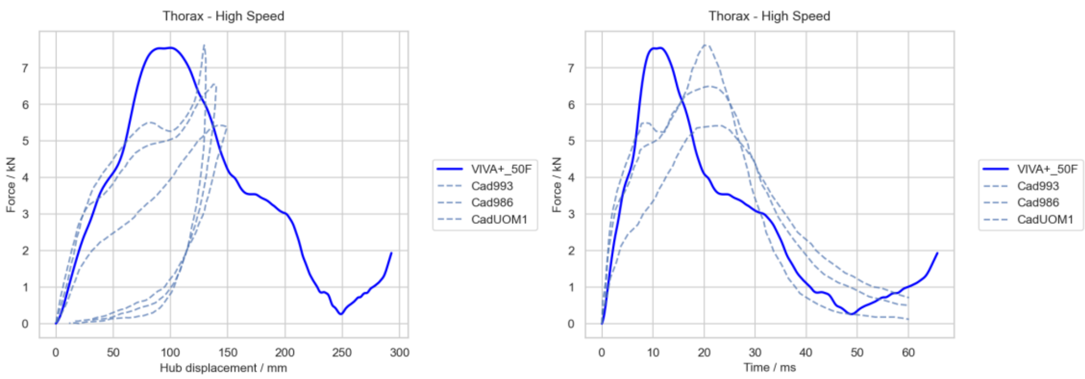

Figure 44 - Viano loadcase - force vs hub displacement and force-time plot at 9.5 m/s impact speed on thorax.

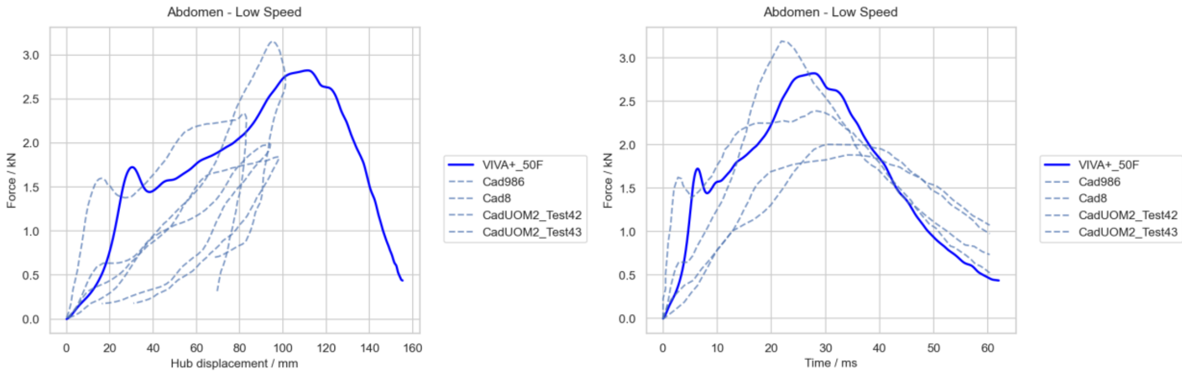

Figure 45 - Viano loadcase - force vs hub displacement and force-time plot at 5.8 m/s impact speed on abdomen.

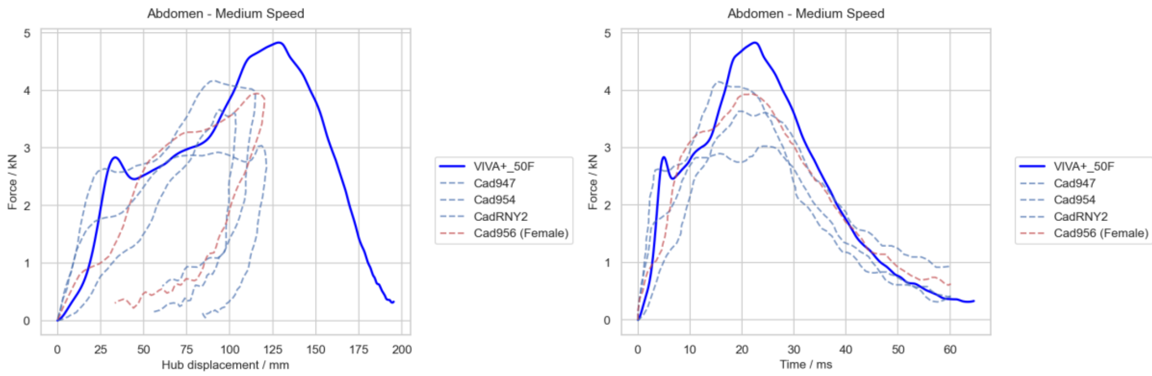

Figure 46 - Viano loadcase - force vs hub displacement and force-time plot at 6.8 m/s impact speed on abdomen.

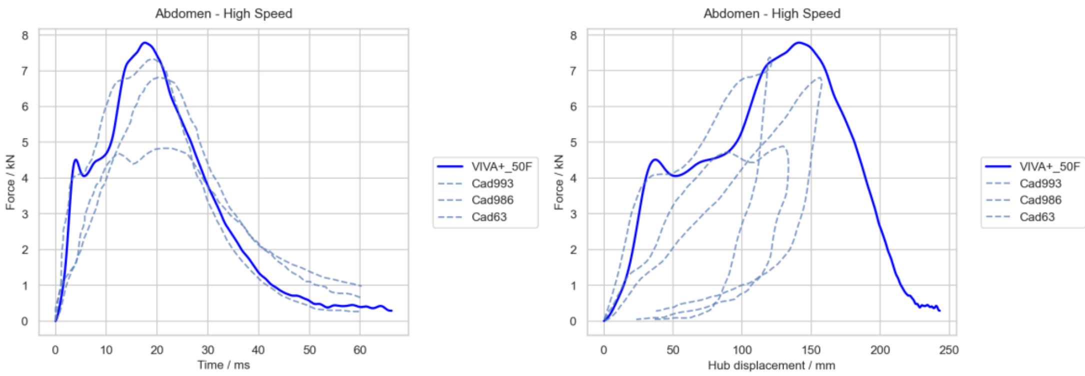

Figure 47 - Viano loadcase - force vs hub displacement and force-time plot at 9.4 m/s impact speed on abdomen.

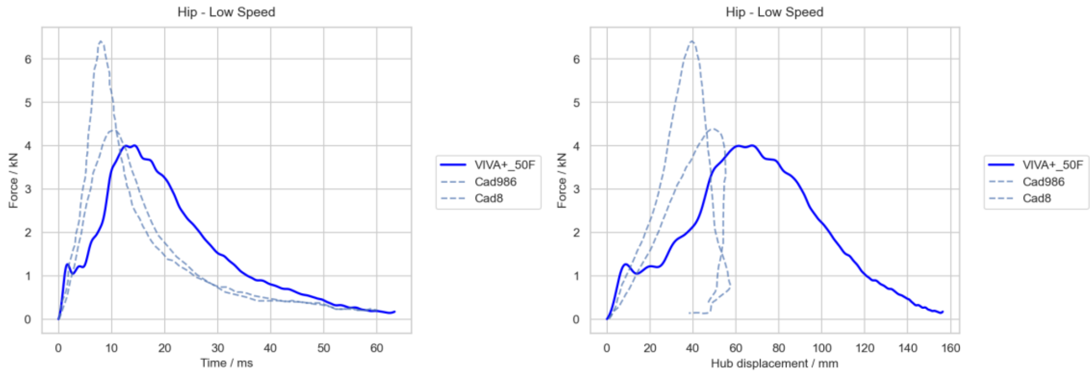

Figure 48 - Viano loadcase - force vs hub displacement and force-time plot at 5.2 m/s impact speed on pelvis.

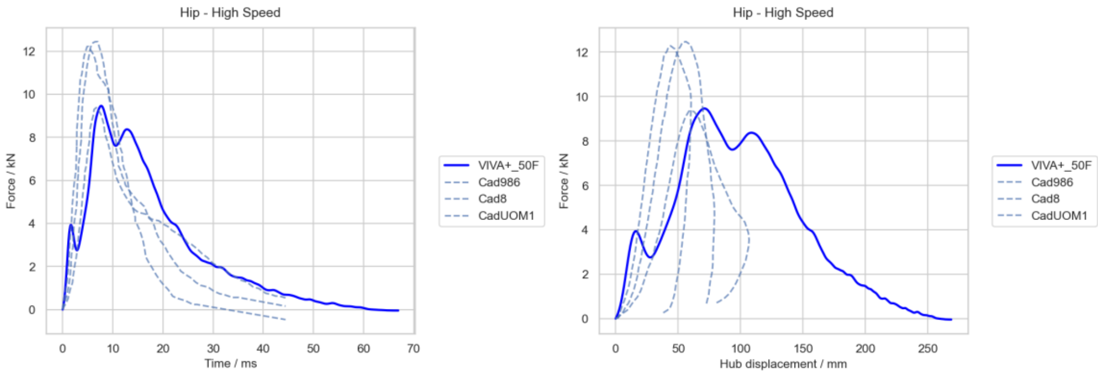

Figure 49 - Viano loadcase - force vs hub displacement and force-time plot at 9.8 m/s impact speed on pelvis.

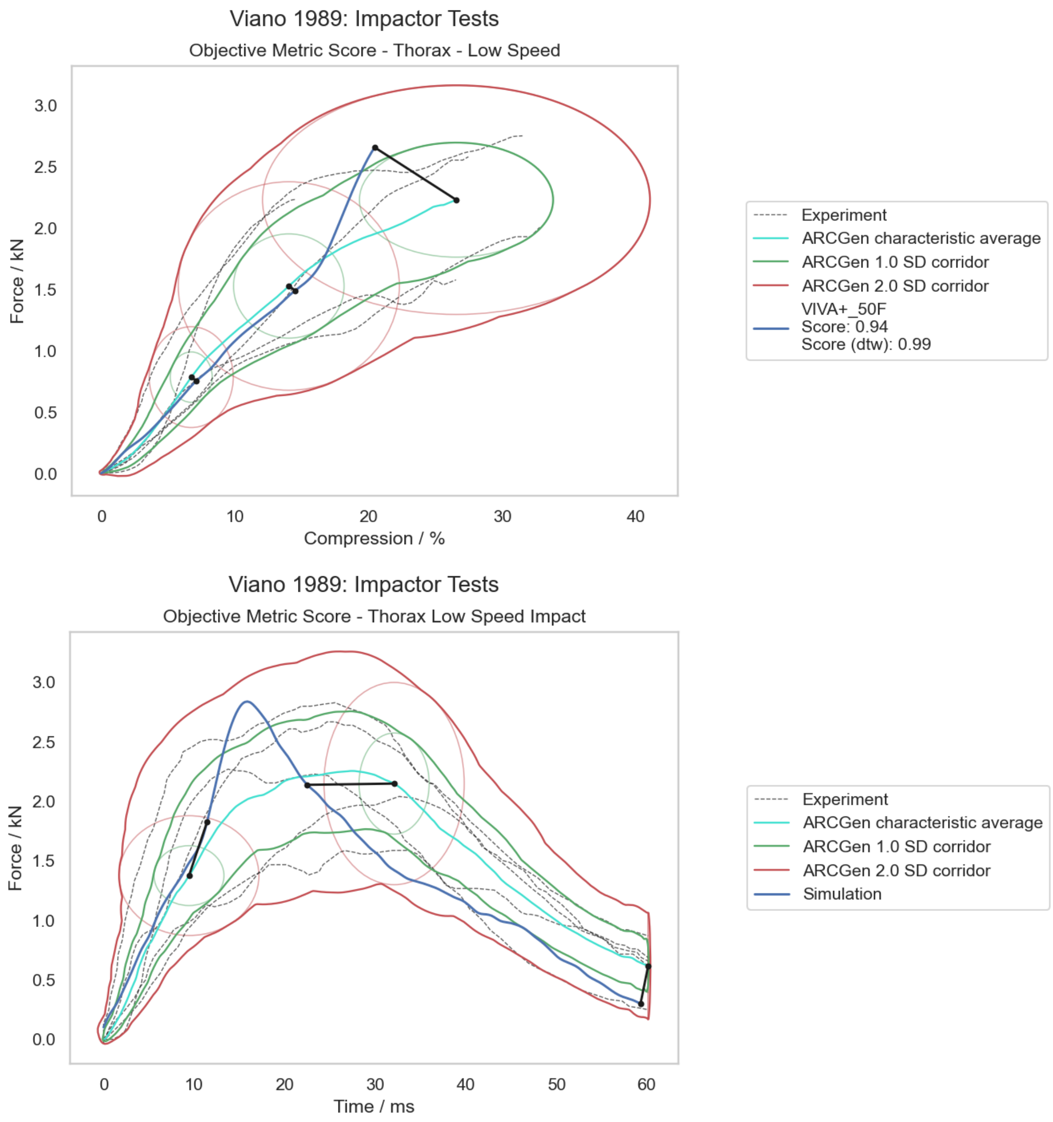

Figure 50 - Viano loadcase - ARCGen corridor for thorax at 4.4 m/s impact speed.

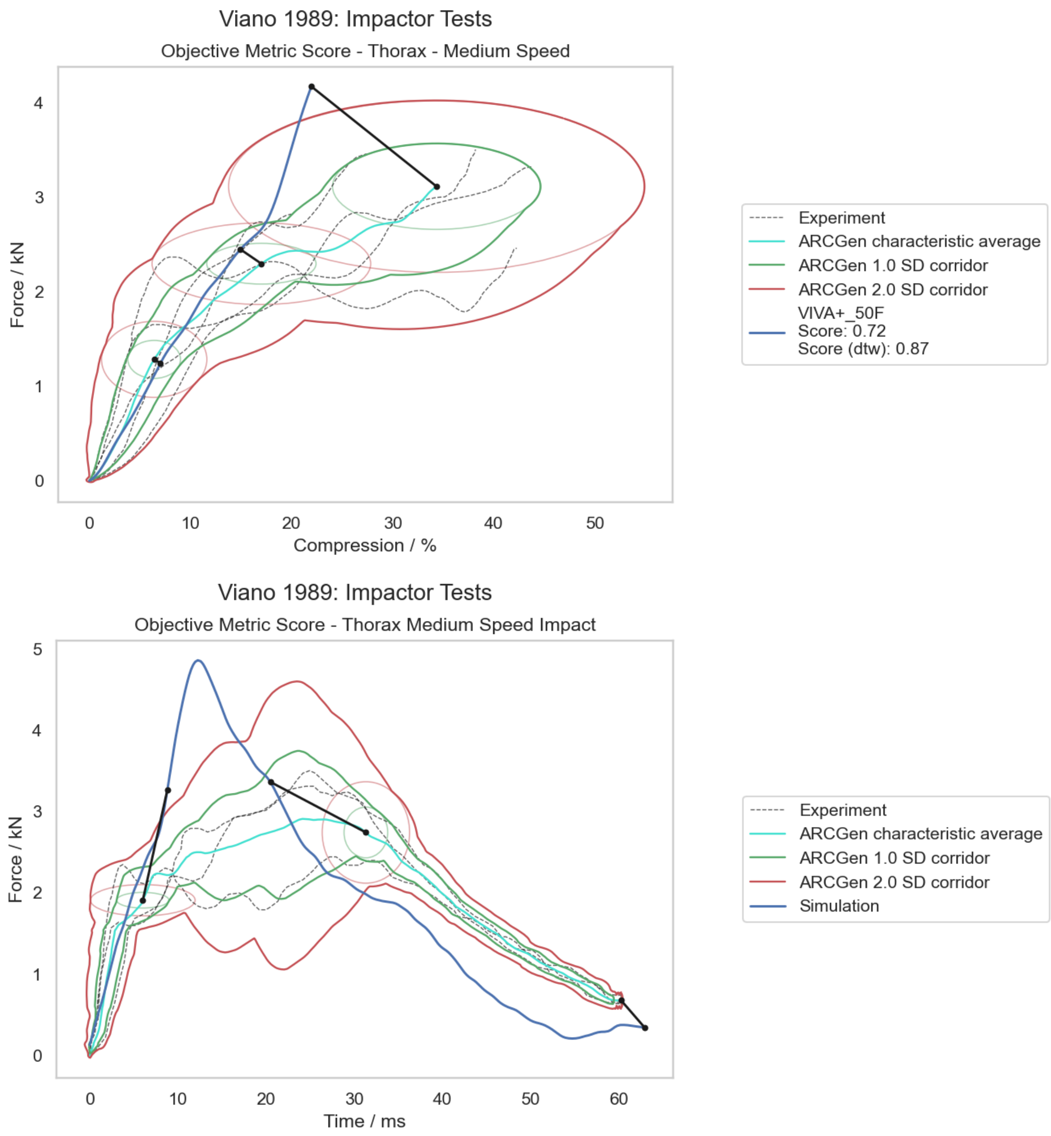

Figure 51 - Viano loadcase - ARCGen corridor for thorax at 6.5 m/s impact speed.

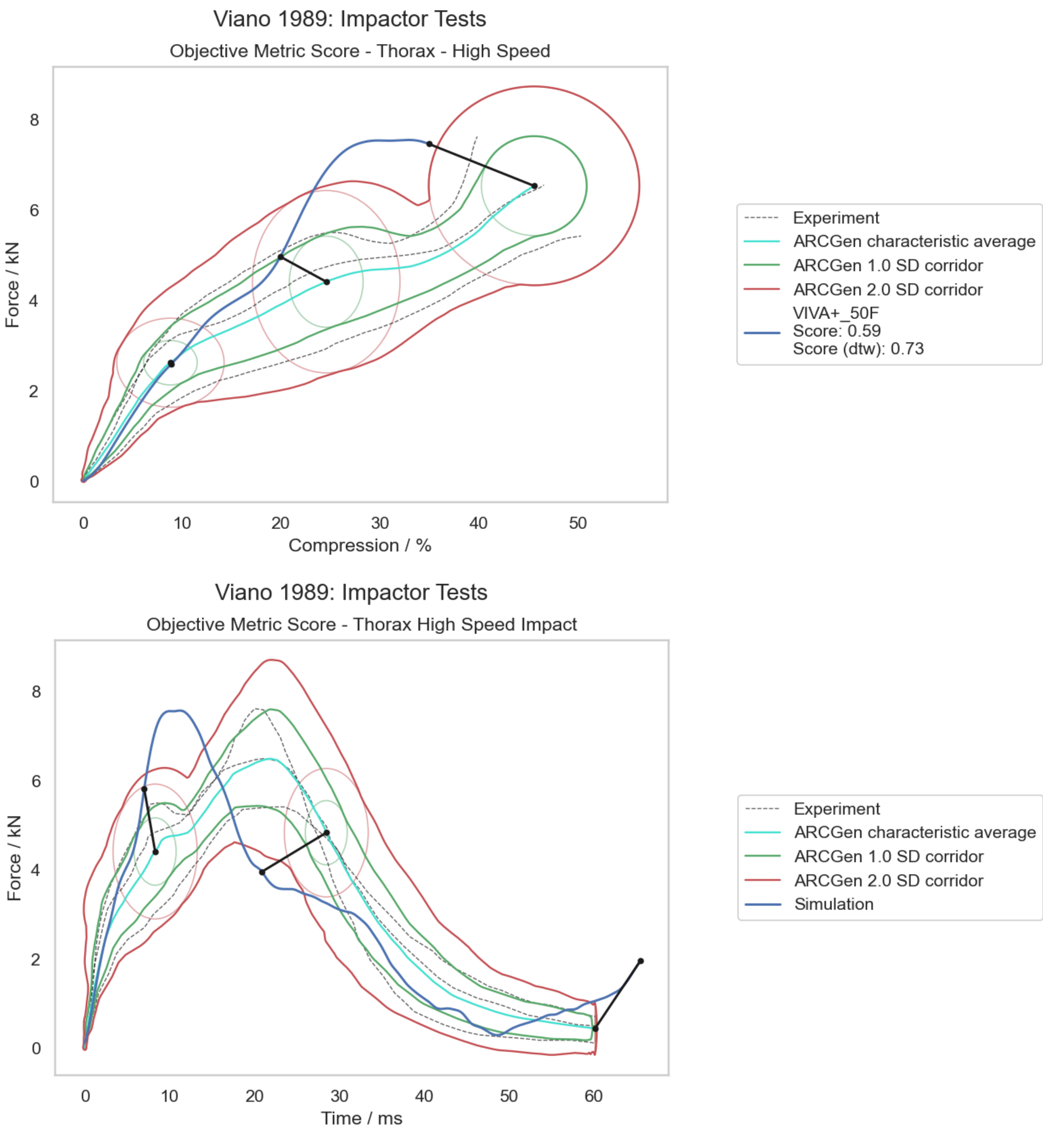

Figure 52 - Viano loadcase - ARCGen corridor for thorax at 9.5 m/s impact speed.

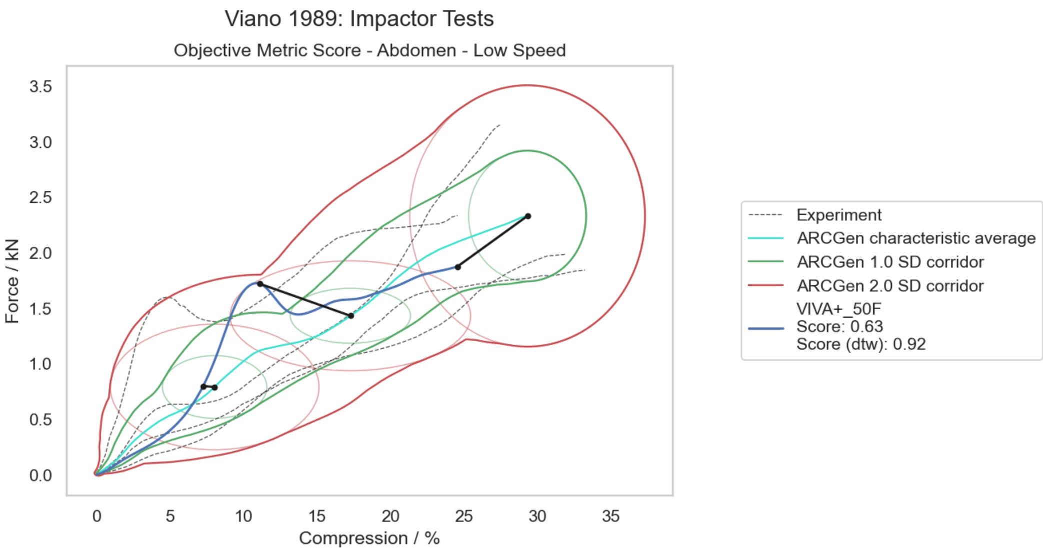

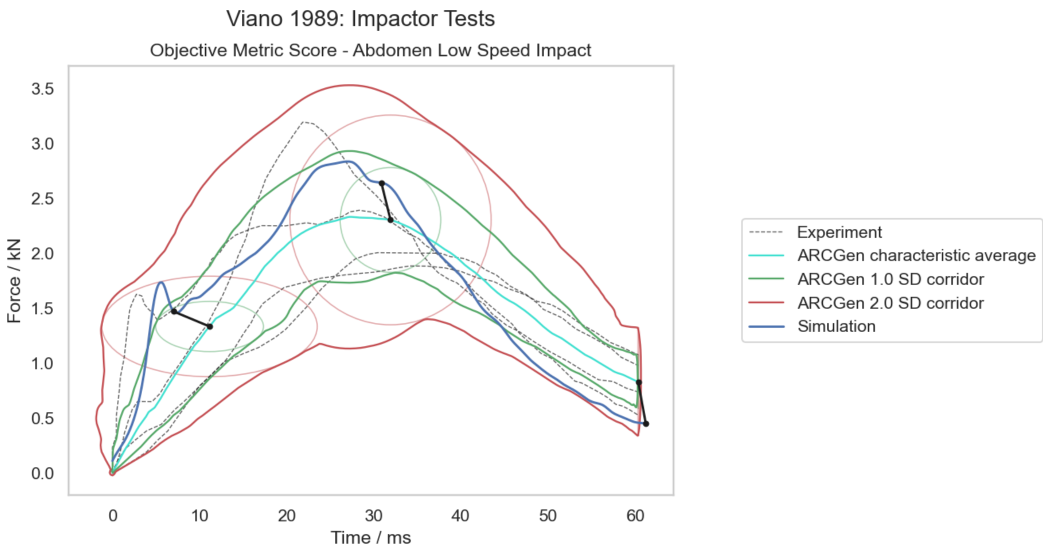

Figure 53 - Viano loadcase - ARCGen corridor for abdomen at 5.8 m/s impact speed.

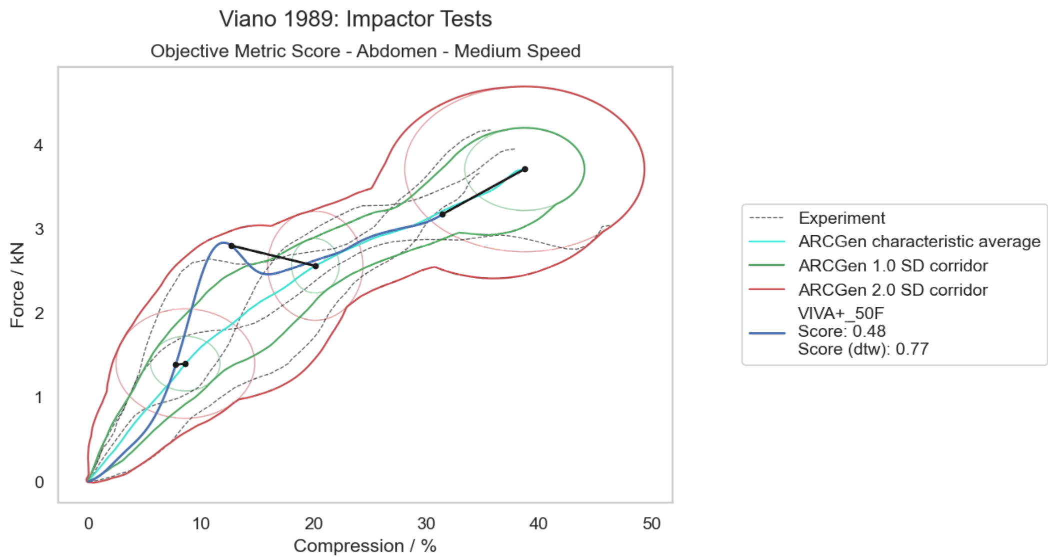

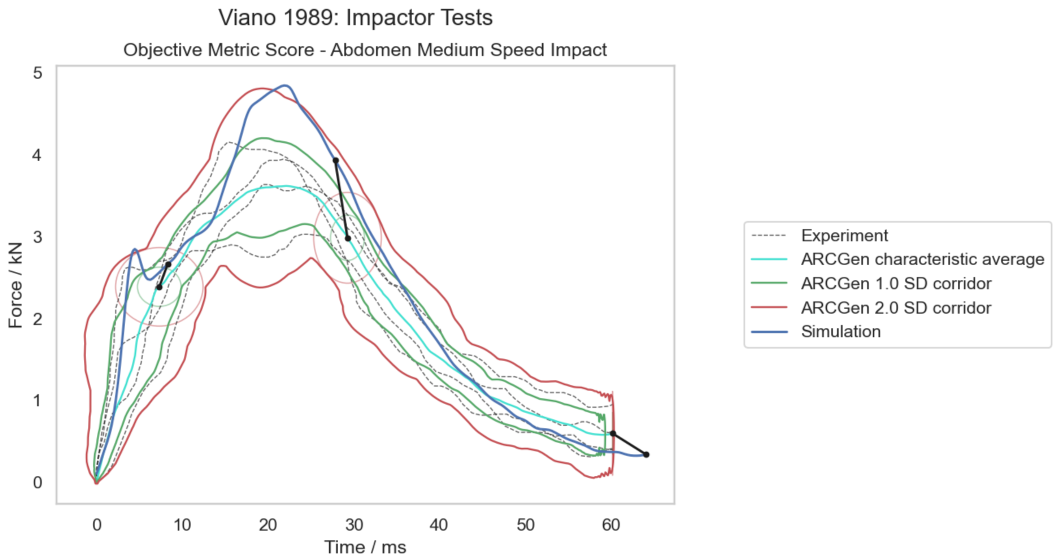

Figure 54 - Viano loadcase - ARCGen corridor for abdomen at 6.8 m/s impact speed.

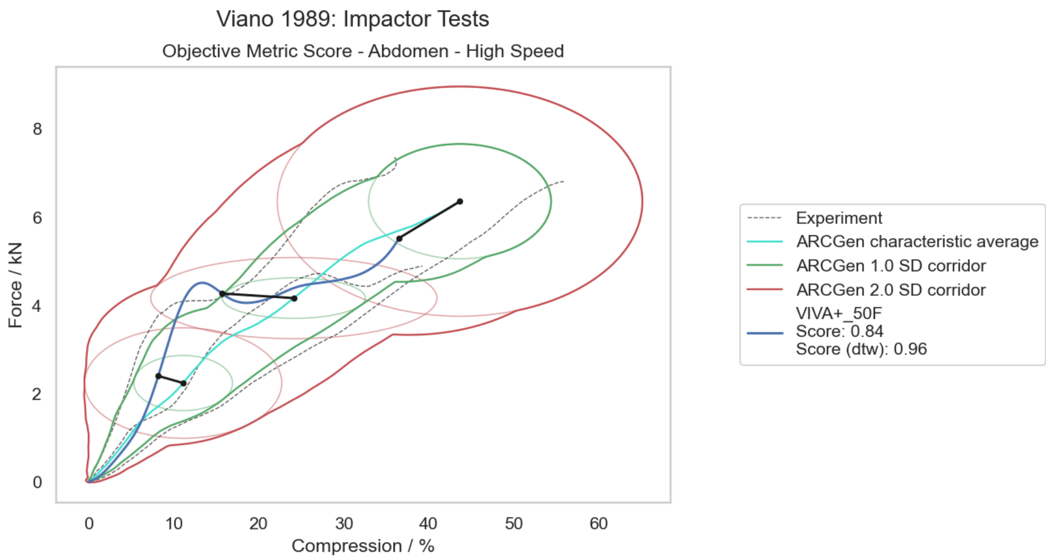

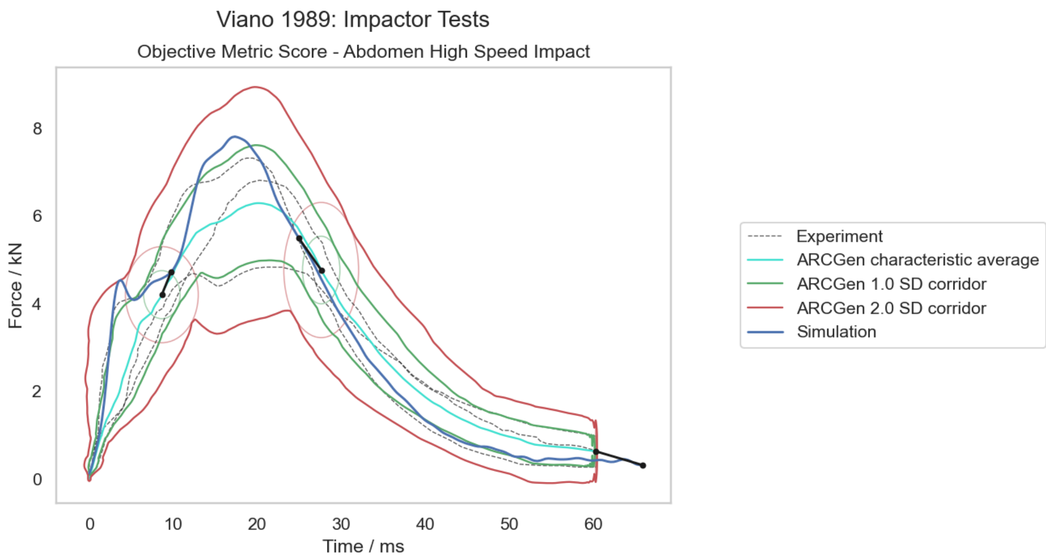

Figure 55 - Viano loadcase - ARCGen corridor for abdomen at 9.4 m/s impact speed.

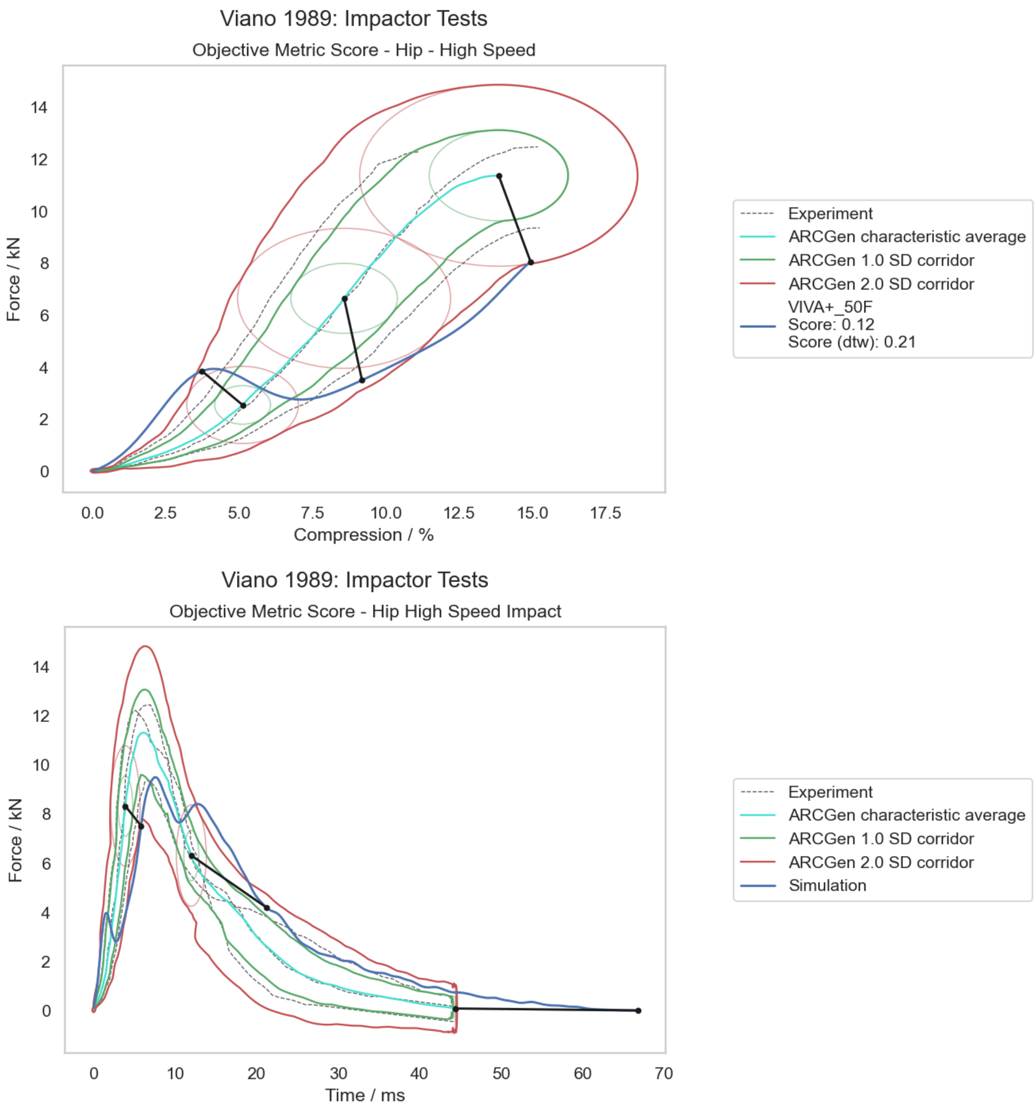

Figure 56 - Viano loadcase - ARCGen corridor for pelvis at 9.8 m/s impact speed.

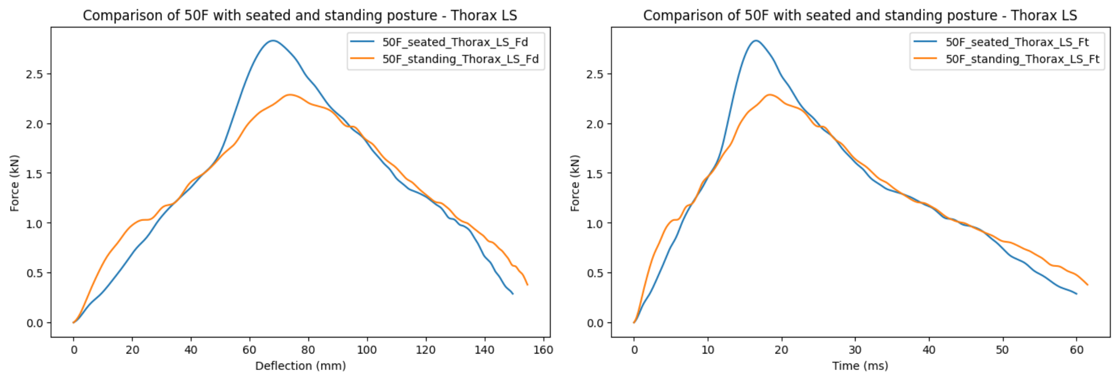

Figure 57 - Comparison of seated and standing position of 50F – force-deflection and force-time plot at 4.4 m/s impact speed on thorax.

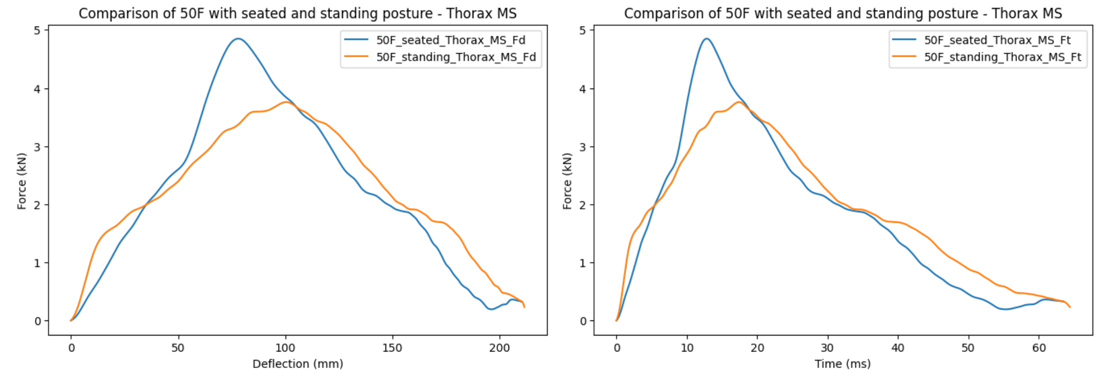

Figure 58 - Comparison of seated and standing position of 50F - force-deflection and force-time plot at 6.5 m/s impact speed on thorax.

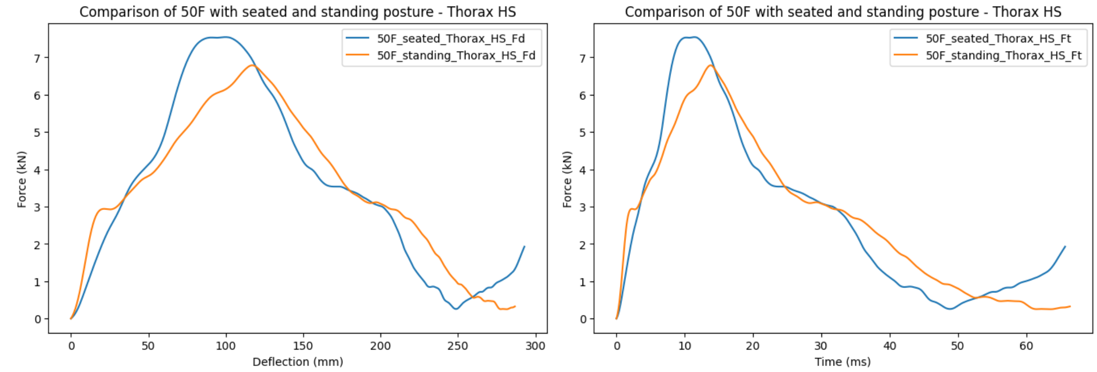

Figure 59 - Comparison of seated and standing position of 50F - force-deflection and force-time plot at 9.5 m/s impact speed on thorax.

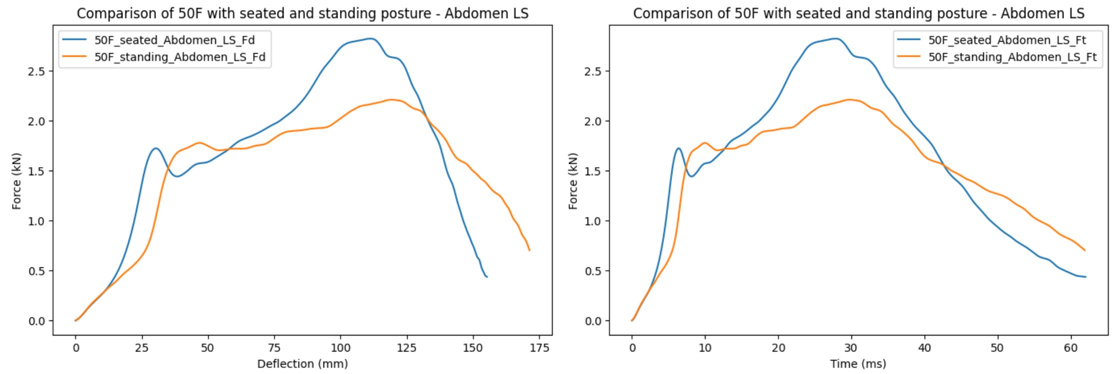

Figure 60 - Comparison of seated and standing position of 50F - force-deflection and force-time plot at 5.8 m/s impact speed on abdomen.

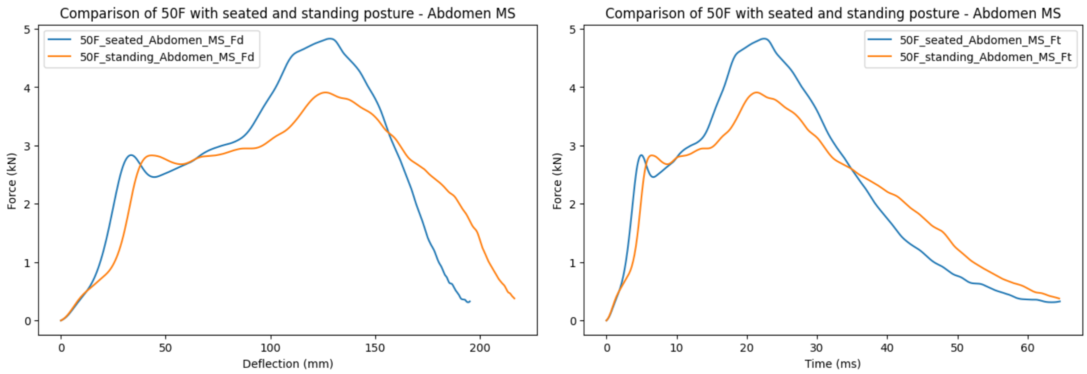

Figure 61 - Comparison of seated and standing position of 50F - force-deflection and force-time plot at 6.8 m/s impact speed on abdomen.

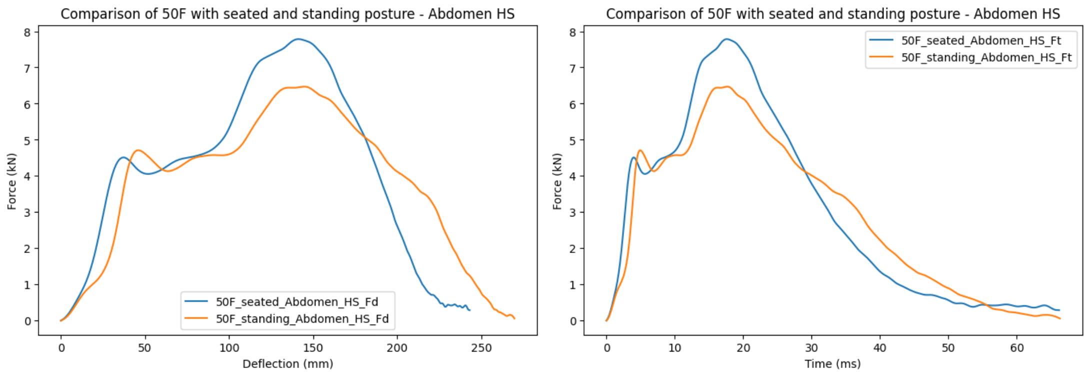

Figure 62 - Comparison of seated and standing position of 50F - force-deflection and force-time plot at 9.4 m/s impact speed on abdomen.

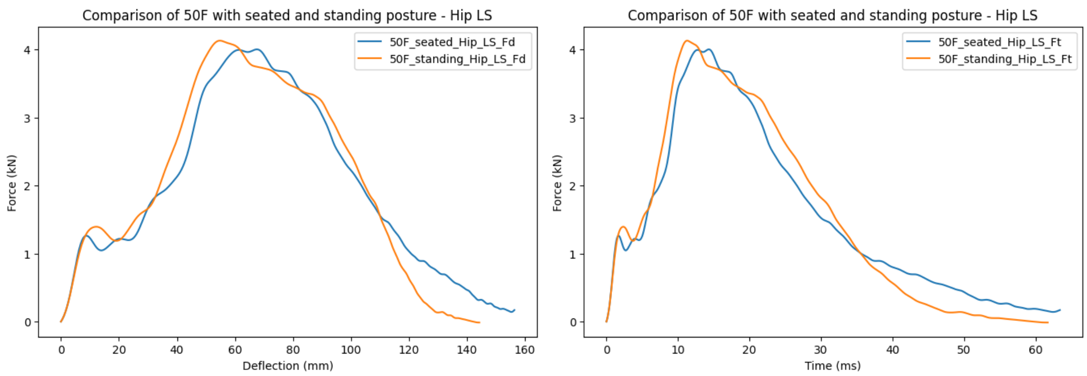

Figure 63 - Comparison of seated and standing position of 50F - force-deflection and force-time plot at 5.2 m/s impact speed on pelvis.

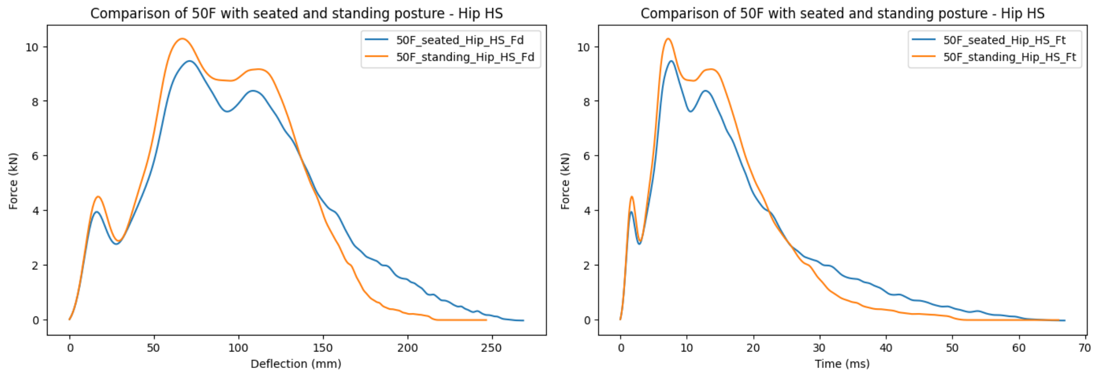

Figure 64 - Comparison of seated and standing position of 50F - force-deflection and force-time plot at 9.8 m/s impact speed on pelvis.

Table 23 – Component-wise ISO 18571 scores for seated 50F of Viano loadcase.

	Impactor Speed (m/s)	Corridor	Phase	Magnitude	Slope	Overall
Thorax	4.4	0.595	0.717	0.896	0.54	0.668
	6.5	0.397	0.633	0.717	0	0.429
	9.5	0.641	0.467	0.884	0.242	0.575
Abdomen	5.8	0.63	0.675	0.898	0.522	0.671
	6.8	0.752	0.975	0.866	0.571	0.783
	9.4	0.816	0.85	0.899	0.582	0.793
Pelvis	5.2	-	-	-	-	-
	9.8	0.765	0.817	0.847	0.697	0.778

Table 24 - Component-wise ISO 18571 scores for standing 50F for Viano loadcase.

	Impactor Speed (m/s)	Corridor	Phase	Magnitude	Slope	Overall
Thorax	4.4	0.711	0.717	0.976	0.706	0.764
	6.5	0.615	0.708	0.869	0.297	0.621
	9.5	0.747	0.625	0.947	0.479	0.709
Abdomen	5.8	0.853	0.8	0.977	0.676	0.832
	6.8	0.835	0.958	0.974	0.646	0.849
	9.4	0.907	0.917	0.972	0.578	0.856
Pelvis	5.2	-	-	-	-	-
	9.8	0.781	0.817	0.925	0.669	0.795

Table 25 - Individual ISO scores for each subject of Viano loadcase for seated HBM.

Subject	Corridor	Phase	Magnitude	Slope	Overall
Thorax (4.5 m/s)					
986	0.461	1	0.775	0.529	0.645
8	0.522	0.683	0.817	0.582	0.625
UOM1	0.775	1	0.936	0.538	0.805
UOM2	0.432	0.508	0.698	0.146	0.443
UOM2	0.382	0.192	0.835	0.276	0.413
Thorax (6.7 m/s)					
935	0.336	0	0.502	0	0.235
RNY2	0.368	0.533	0.806	0.152	0.445
956	0.428	0.417	0.829	0.226	0.465
Thorax (9.4 m/s)					
993	0.453	0.333	0.81	0.187	0.447
986	0.628	0.558	0.885	0.237	0.587
UOM1	0.716	0.45	0.759	0.292	0.587
Abdomen (4.5 m/s)					
986	0.816	0.85	0.927	0.593	0.8
8	0.846	1	0.946	0.596	0.847
UOM2	0.258	0.258	0.756	0.29	0.364
UOM2	0.253	0.253	0.71	0	0.288
Abdomen (6.7 m/s)					
947	0.605	0.792	0.83	0.45	0.656
954	0.59	0.95	0.709	0.435	0.655
RNY2	0.736	0.842	0.935	0.687	0.787
956	0.815	0.933	0.913	0.529	0.801
Abdomen (9.4 m/s)					
993	0.567	0.767	0.716	0.332	0.59
986	0.961	0.958	0.97	0.712	0.913
63	0.659	0.717	0.896	0.598	0.706
Pelvis (9.4 m/s)					
986	0.609	0.742	0.568	0.7	0.646
8	0.851	0.908	0.905	0.623	0.828

UOM1	0.769	0.817	0.816	0.657	0.765

Table 26 - Individual ISO scores for each subject of Viano loadcase for standing HBM.

Subject	Corridor	Phase	Magnitude	Slope	Overall
Thorax (4.5 m/s)					
986	0.478	0.983	0.711	0.648	0.66
8	0.56	0.683	0.796	0.657	651
UOM1	0.753	1	0.957	0.592	0.811
UOM2	0.475	0.483	0.797	0.363	0.519
UOM2	0.427	0.225	0.931	0.519	0.506
Thorax (6.7 m/s)					
935	0.555	0.033	0.554	0.179	0.375
RNY2	0.605	0.692	0.95	0.476	0.666
956	0.662	0.525	0.961	0.547	0.672
Thorax (9.4 m/s)					
993	0.597	0.45	0.913	0.454	0.602
986	0.779	0.683	0.959	0.458	0.732
UOM1	0.704	0.792	0.811	0.467	0.696
Abdomen (4.5 m/s)					
986	0.795	0.7	0.96	0.598	0.77
8	0.781	0.975	0.844	0.574	0.791
UOM2	0.518	0.4	0.92	0.533	0.578
UOM2	0.548	0.317	0.903	0.49	0.561
Abdomen (6.7 m/s)					
947	0.838	0.842	0.969	0.536	0.805
954	0.543	0.85	0.861	0.497	0.659
RNY2	0.665	0.767	0.945	0.701	0.748
956	0.89	1	0.993	0.642	0.883
Abdomen (9.4 m/s)					
993	0.771	0.85	0.869	0.448	0.742
986	0.775	0.892	0.946	0.625	0.802
63	0.802	0.767	0.947	0.579	0.779
Pelvis (9.4 m/s)					

986	0.696	0.742	0.77	0.698	0.721
8	0.779	0.942	0.823	0.523	0.769
UOM1	0.775	0.817	0.889	0.637	0.779

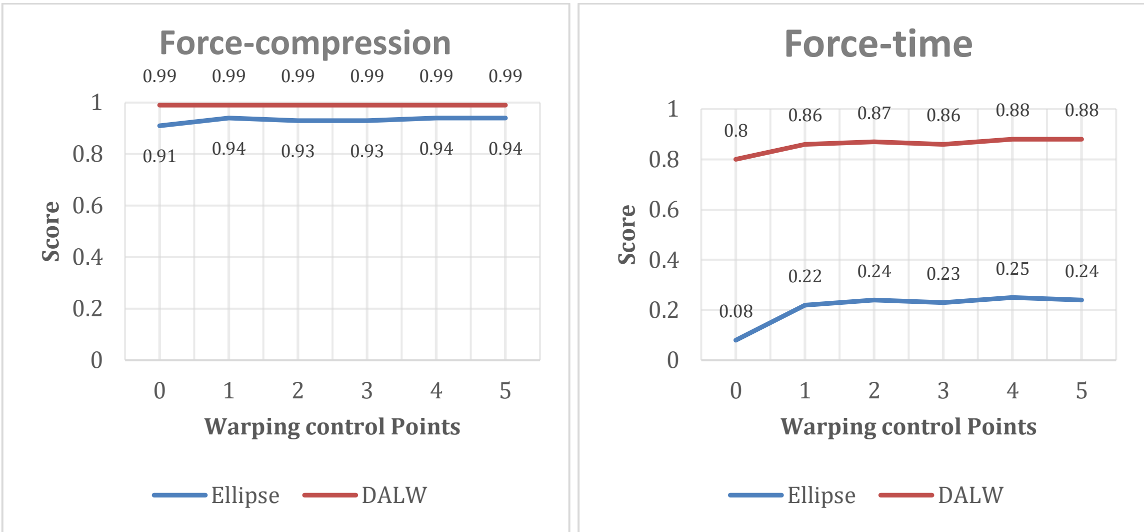

Figure 65 - Viano loadcase – Scores of seated 50F with nWarpCtrlPts results on Thorax at 4.4 m/s impact speed.

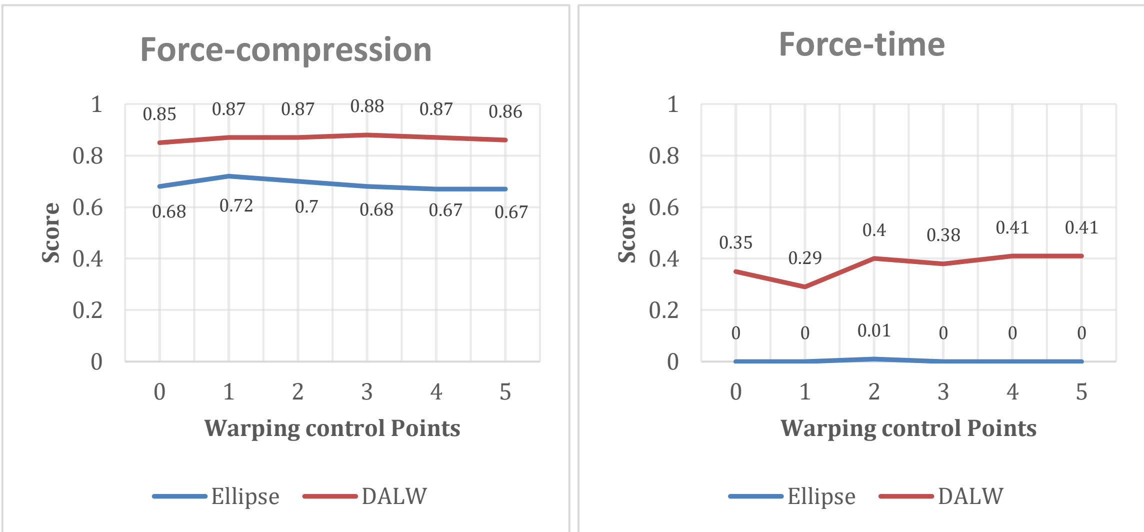

Figure 66 - Viano loadcase - Scores of seated 50F with nWarpCtrlPts results on Thorax at 6.5 m/s impact speed.

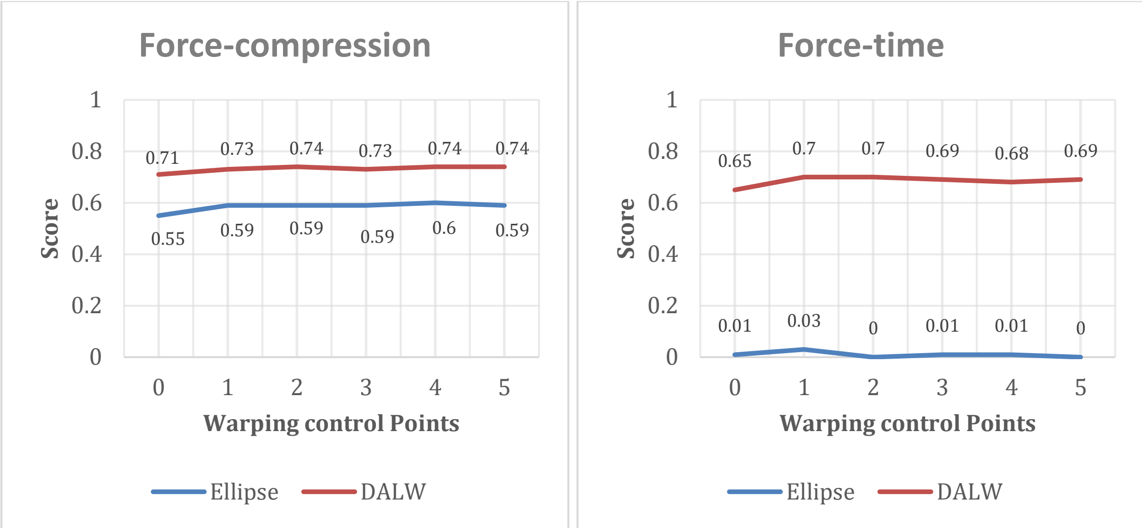

Figure 67 - Viano loadcase - Scores of seated 50F with nWarpCtrlPts results on Thorax at 9.5 m/s impact speed.

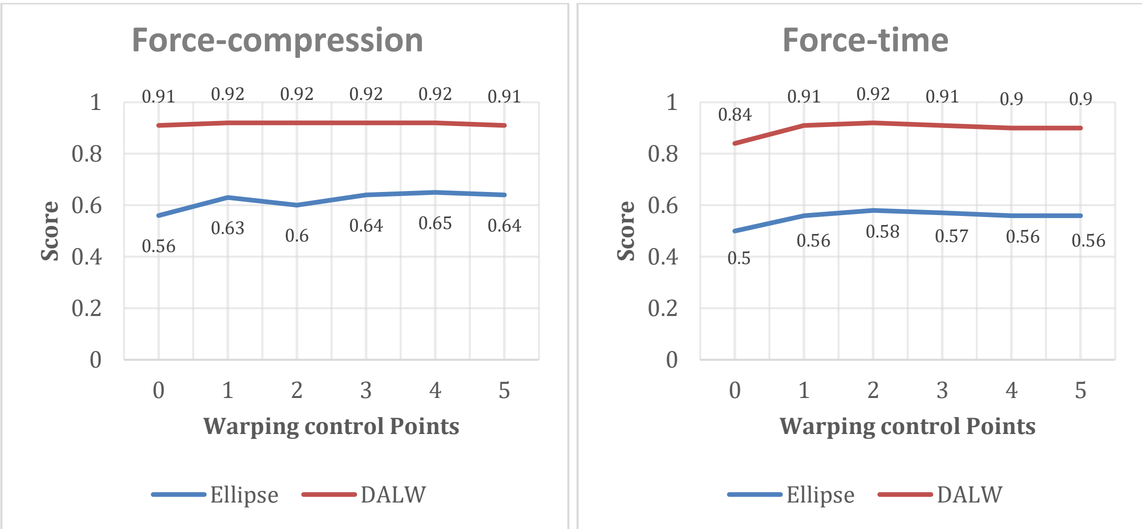

Figure 68 - Viano loadcase - Scores of seated 50F with nWarpCtrlPts results on Abdomen at 5.8 m/s impact speed.

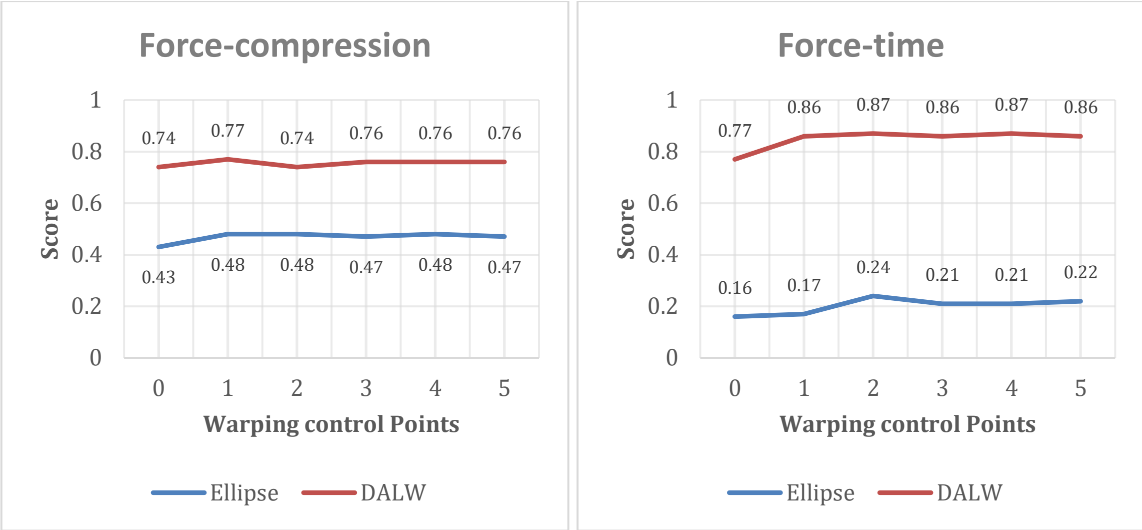

Figure 69 - Viano loadcase - Scores of seated 50F with nWarpCtrlPts results on Abdomen at 6.8 m/s impact speed.

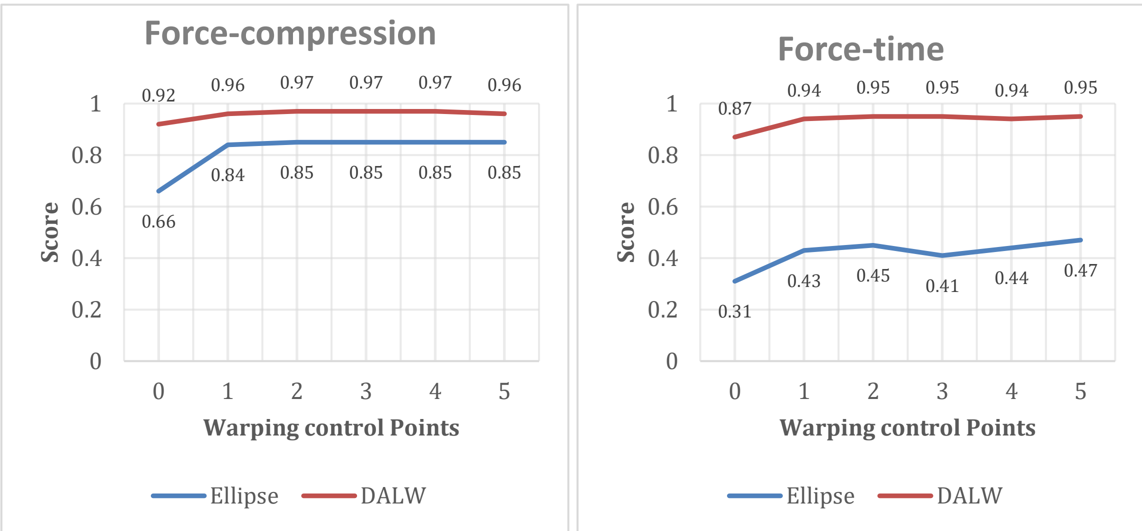

Figure 70 - Viano loadcase - Scores of seated 50F with nWarpCtrlPts results on Abdomen at 9.4 m/s impact speed.

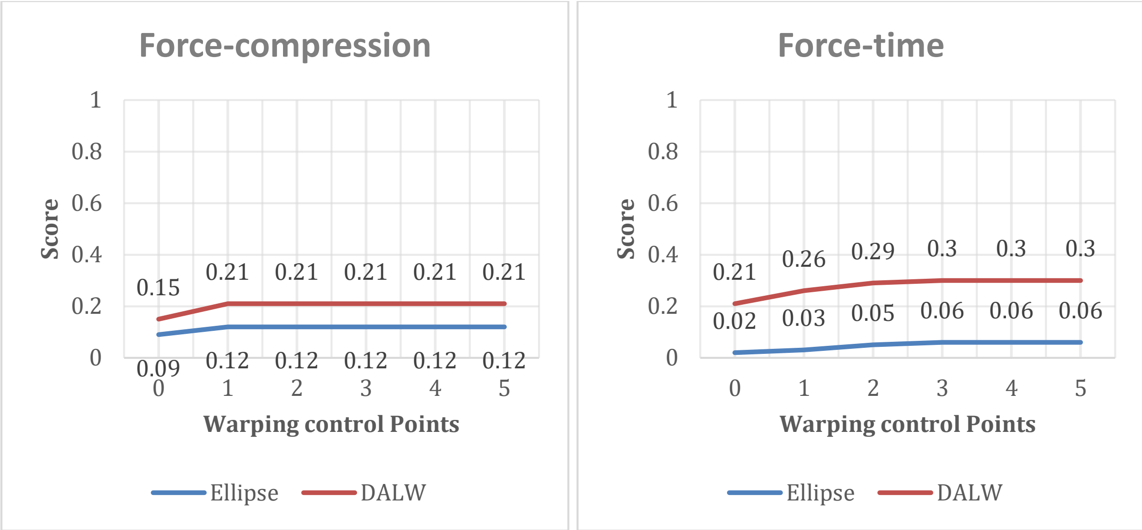

Figure 71 - Viano loadcase - Scores of seated 50F with nWarpCtrlPts results on Pelvis at 9.8 m/s impact speed.

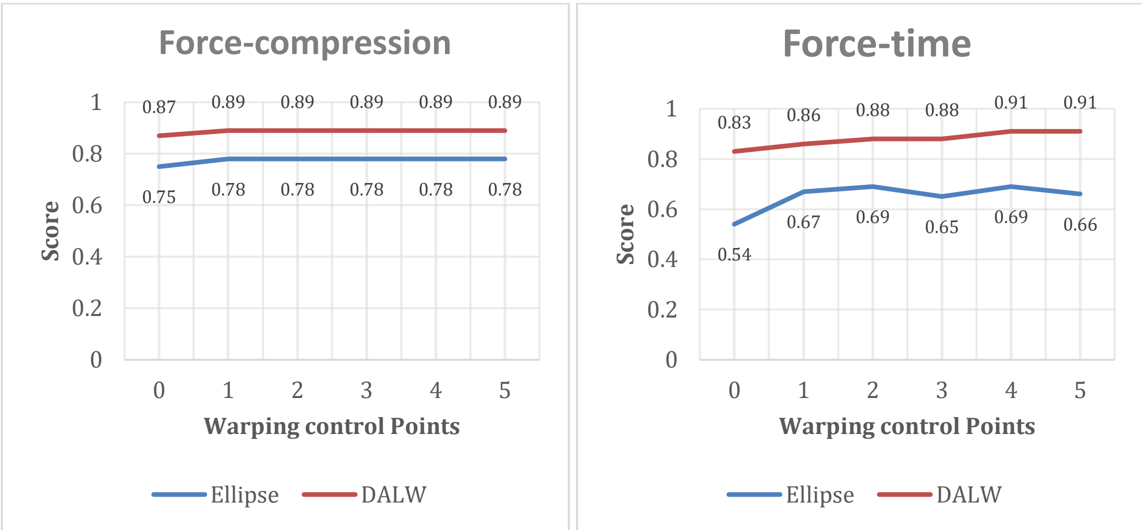

Figure 72 - Viano loadcase - Scores of standing 50F with nWarpCtrlPts results on Thorax at 4.4 m/s impact speed.

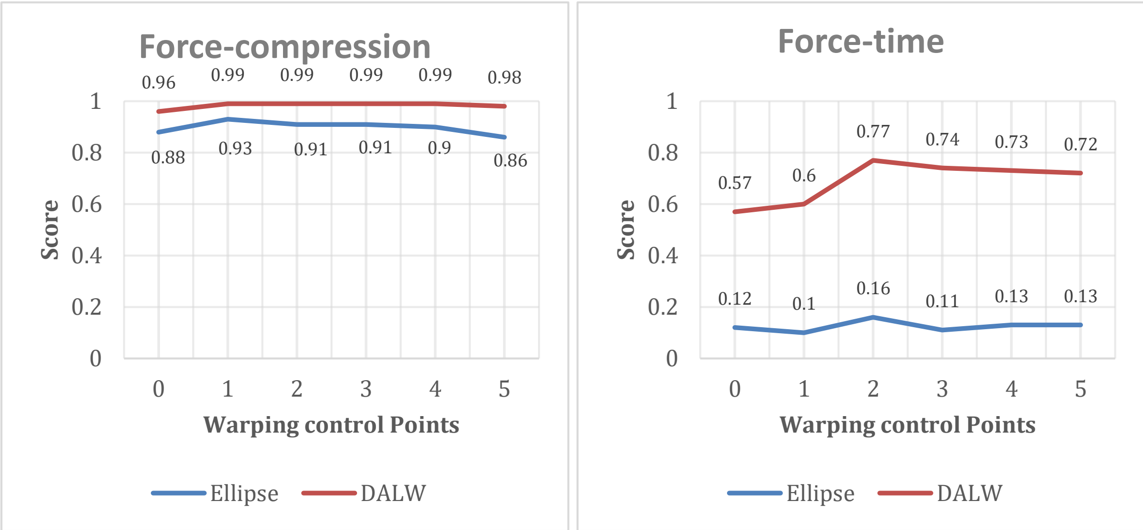

Figure 73 - Viano loadcase - Scores of standing with nWarpCtrlPts results on Thorax at 6.5 m/s impact speed.

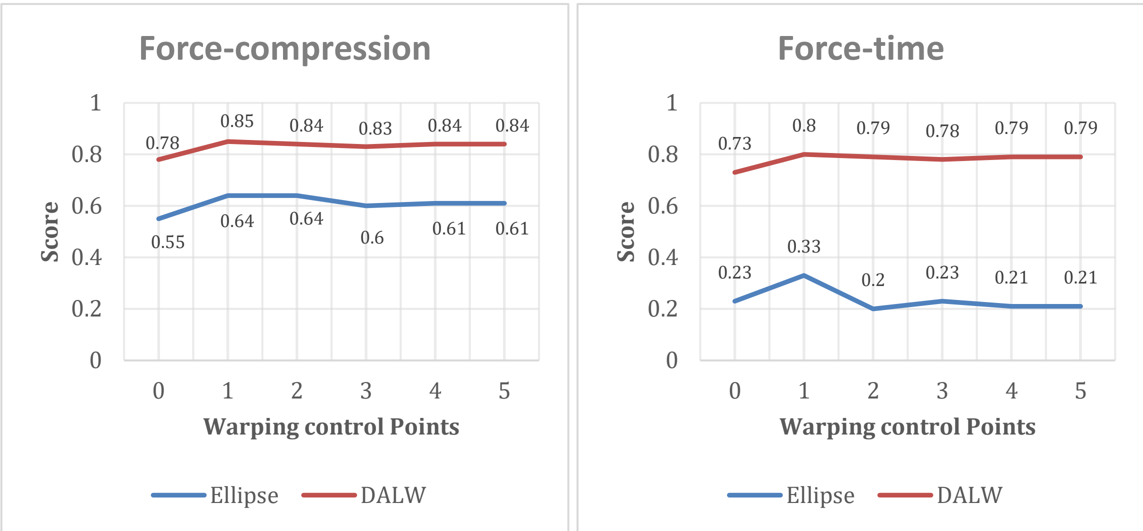

Figure 74 - Viano loadcase - Scores of standing with nWarpCtrlPts results on Thorax at 9.5 m/s impact speed.

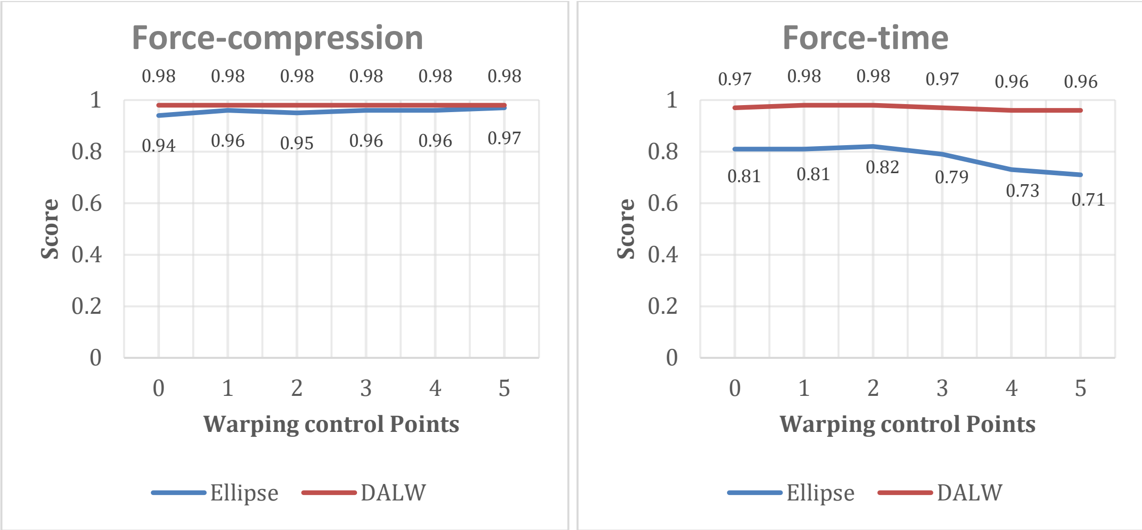

Figure 75 - Viano loadcase - Scores of standing with nWarpCtrlPts results on Abdomen at 5.8 m/s impact speed.

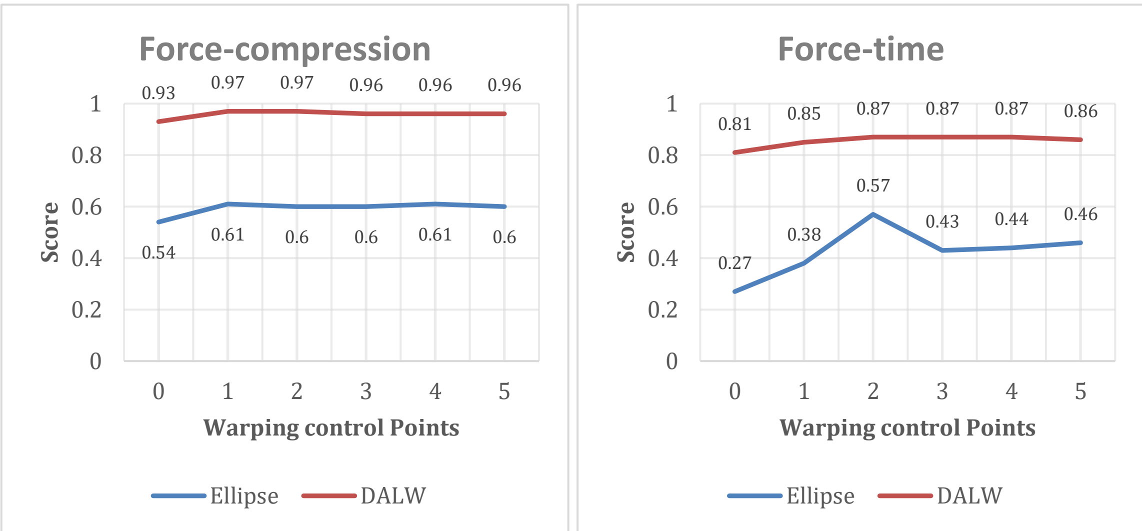

Figure 76 - Viano loadcase - Scores of standing with nWarpCtrlPts results on Abdomen at 6.8 m/s impact speed.

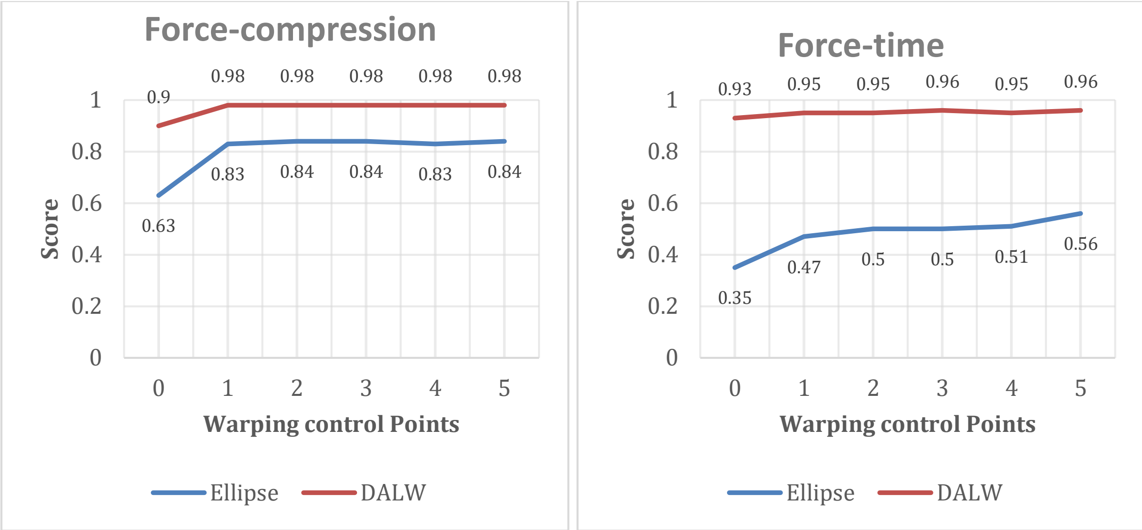

Figure 77 - Viano loadcase - Scores of standing with nWarpCtrlPts results on Abdomen at 9.4 m/s impact speed.

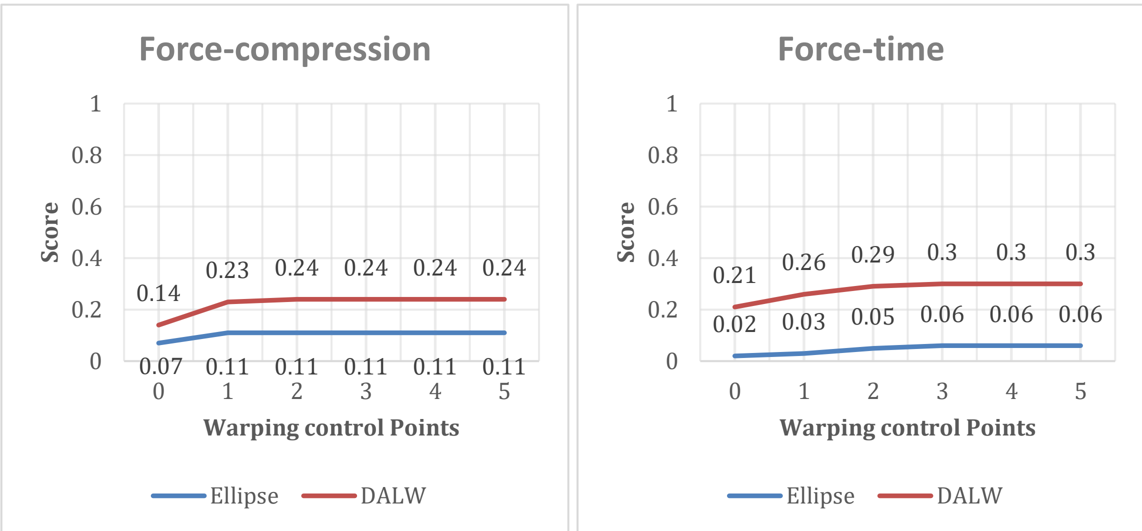

Figure 78 - Viano loadcase - Scores of standing with nWarpCtrlPts results on Pelvis at 9.8 m/s impact speed.

Appendix C

Table 27 - PMHS subject inclusion criteria and test setup matrix across Compigne shoulder impacts (right shoulder variations at 1.5 m/s and left shoulder impacts at 3 m/s, 4 m/s and 6 m/s).

Subject	Gender	Age (years)	Height (in cm)	Weight (in kg)	50 F Corridor	Currently used by HBM4VT
RS - 0 / +15 / -15° (1.5 m/s)						
2	M	88	163	33		
5	M	91	165	50		
1	F	77	161	67		
3	F	79	159	52		
4	F	82	155	50		
6	F	94	148	50		
7	F	93	152	66.5		
Average		86	157.5	52.6		
LS - 3 m/s (0°)						
5	M	91	165	50		
6	F	94	148	50		
Average		92	156.5	50		
LS - 4 m/s (0°)						
3	F	79	159	52		
4	F	82	155	50		
7	F	93	152	66.5		
Average		84	155.3	56.1		
LS - 6 m/s (0°)						
1	F	77	161	67		
2	M	88	163	33		
Average		82	162	50		

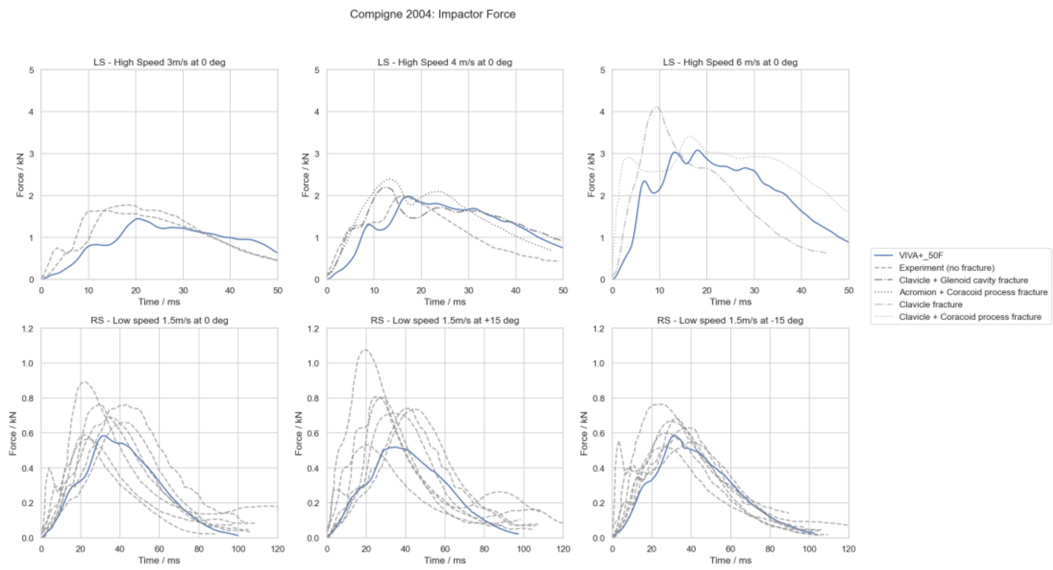

Figure 79 - Compigne loadcase – Impactor force plot

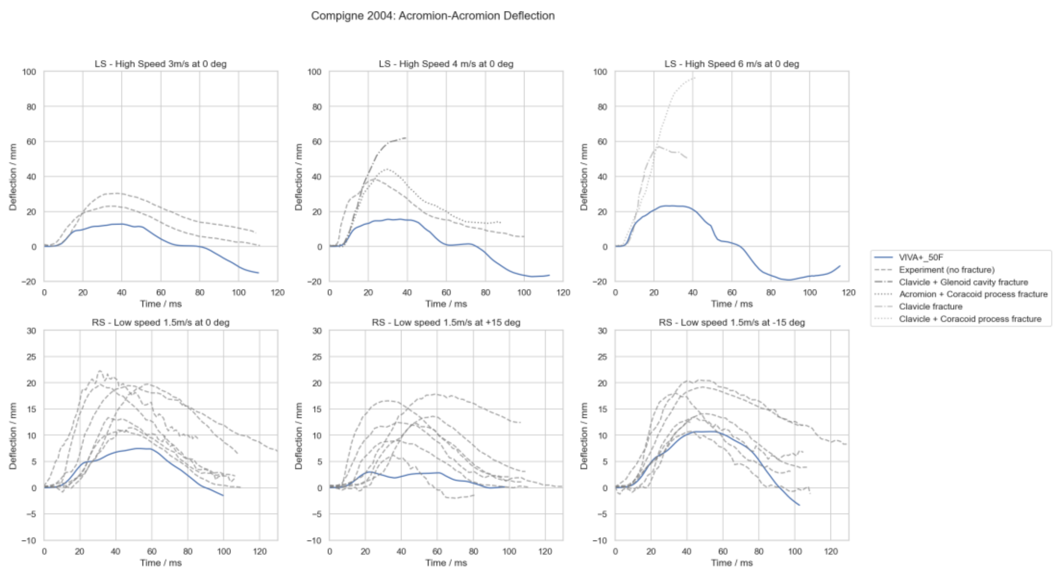

Figure 80 - Compigne loadcase – Acromion-to-Acromion deflection plot.

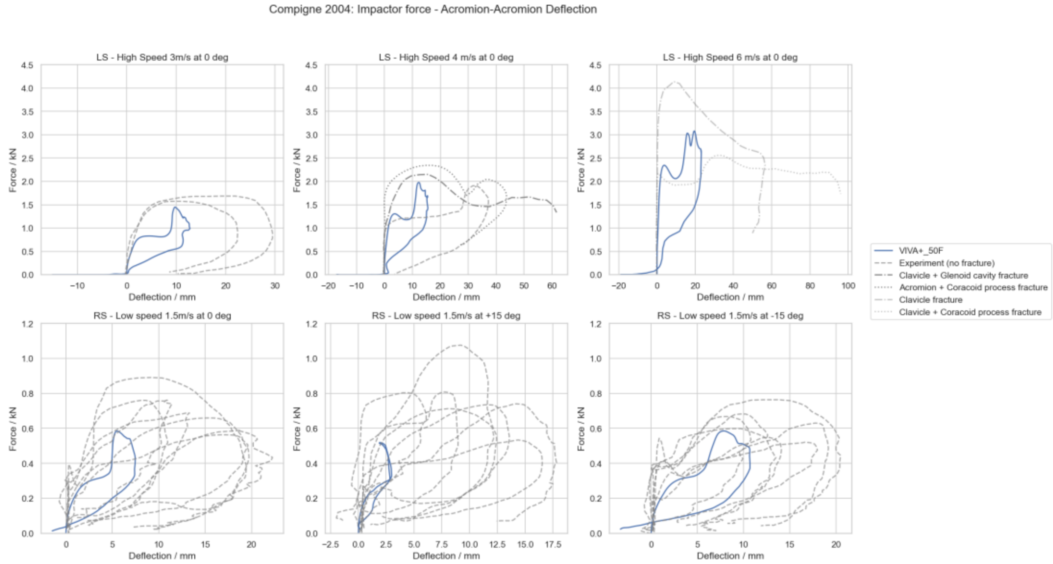

Figure 81 - Compigne loadcase - Impactor force vs Acromion-to-Acromion plot.

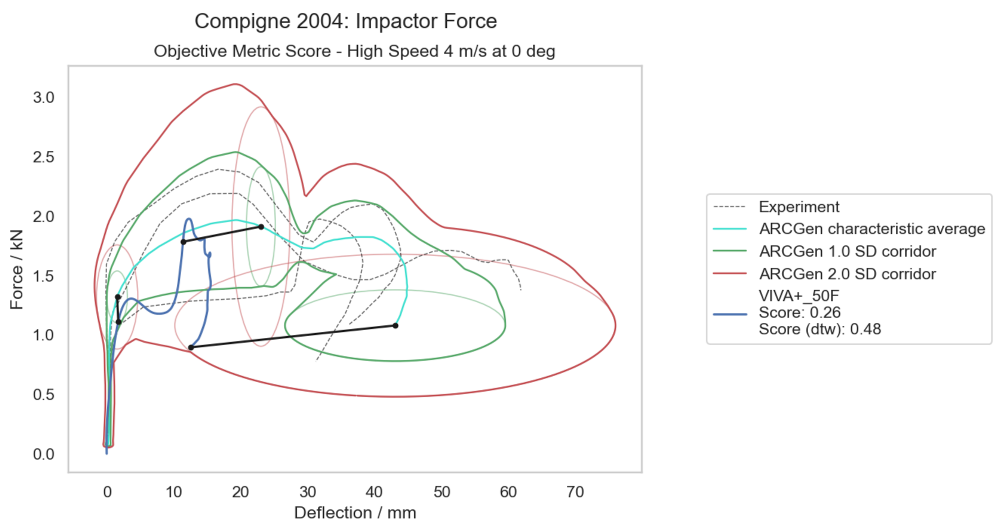

Figure 82 - Compigne loadcase - ARCGen corridor for left shoulder impact at 4 m/s and 0° angle.

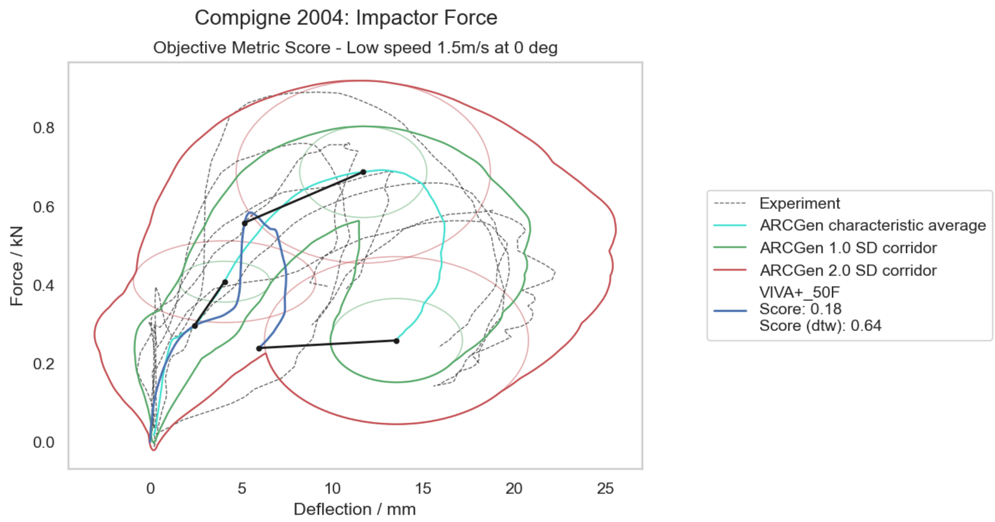

Figure 83 - Compigne loadcase - ARCGen corridor for right shoulder impact at 1.5 m/s and 0° angle.

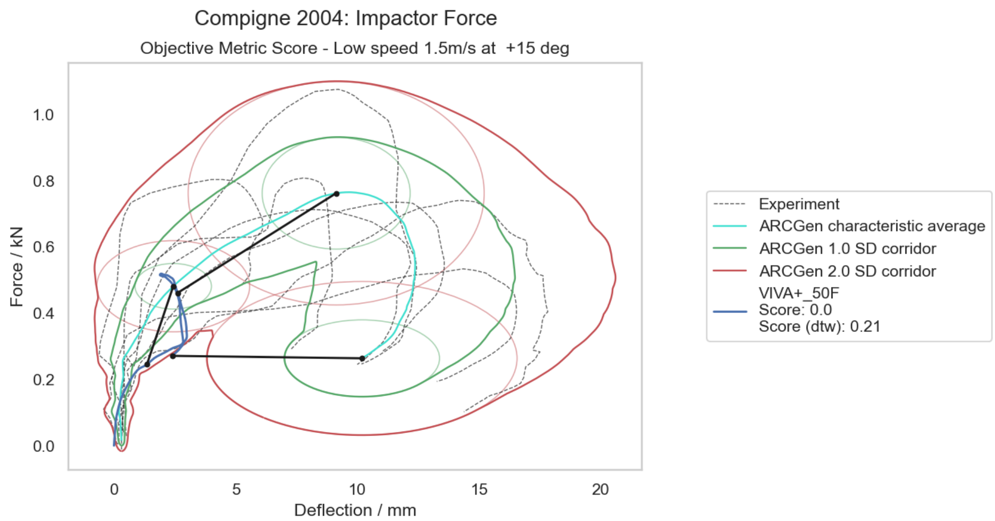

Figure 84 - Compigne loadcase - ARCGen corridor for right shoulder impact at 1.5 m/s and +15° angle.

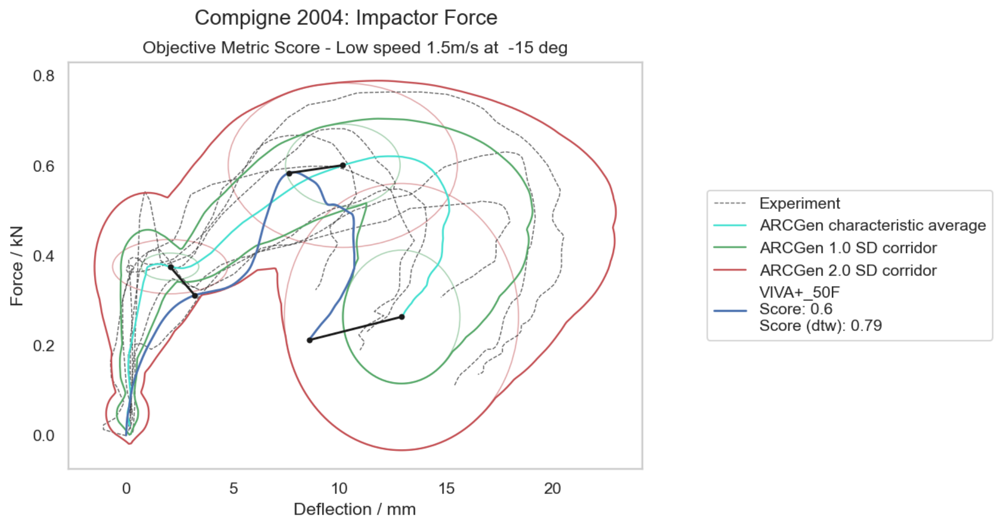

Figure 85 - Compigne loadcase - ARCGen corridor for right shoulder impact at 1.5 m/s and -15° angle.

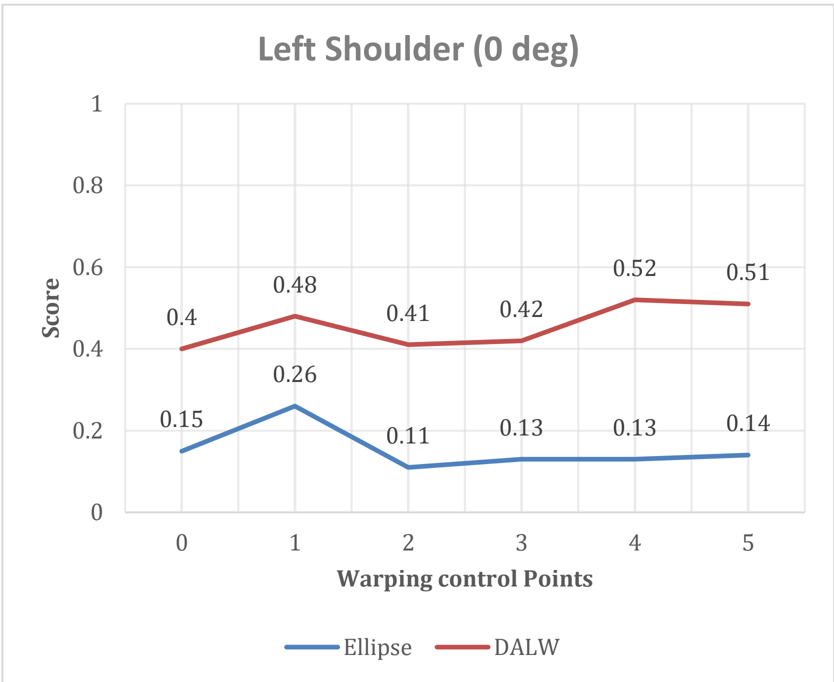

Figure 86 - Compigne loadcase - nWarpCtrlPts results on left shoulder impact at 4 m/s and 0° angle.

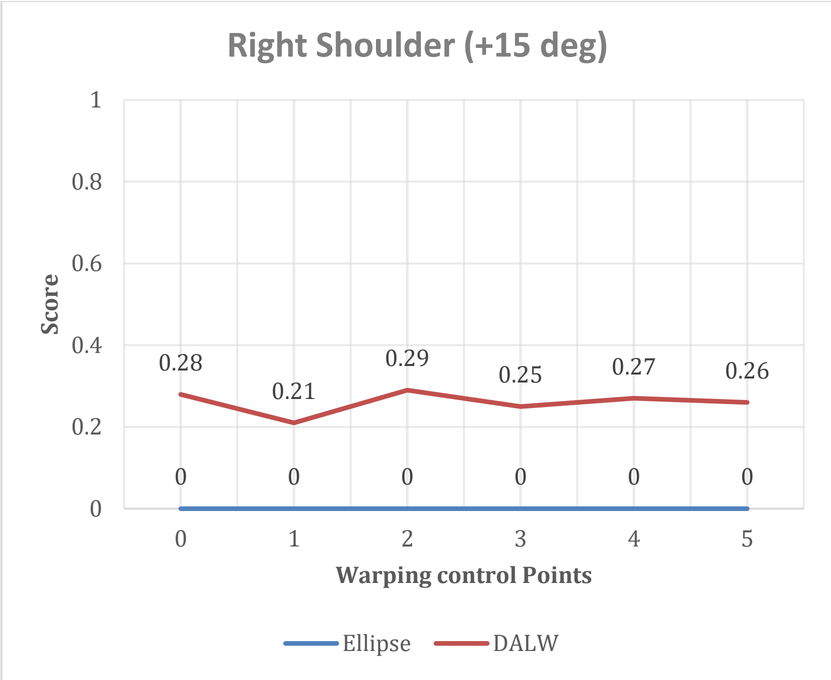

Figure 87 - Compigne loadcase - nWarpCtrlPts results on right shoulder impact at 1.5 m/s and +15° angle.

Figure 88 - Compigne loadcase - nWarpCtrlPts results on right shoulder impact at 1.5 m/s and 0° angle.

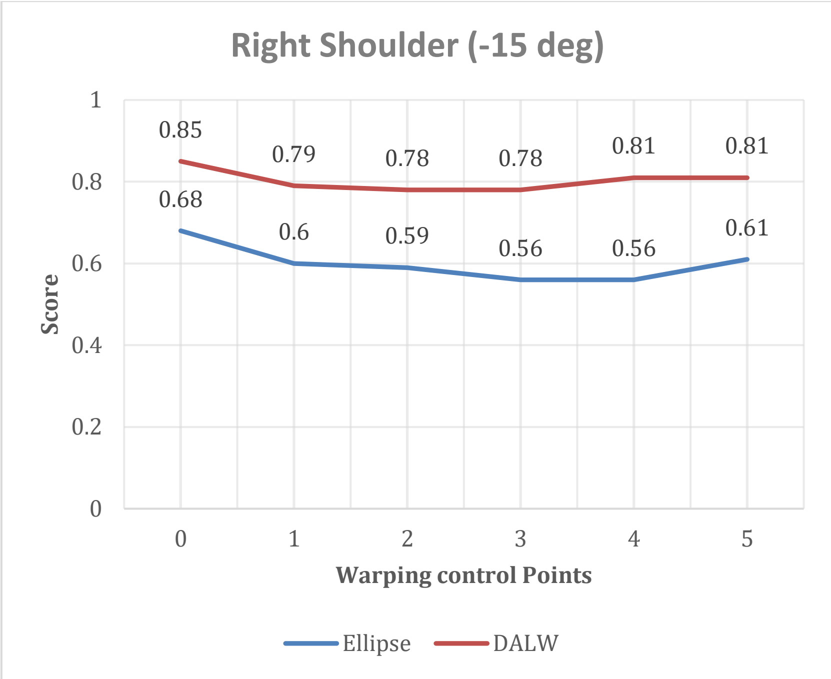

Figure 89 - Compigne loadcase - nWarpCtrlPts results on right shoulder impact 1.5 m/s and -15° angle.

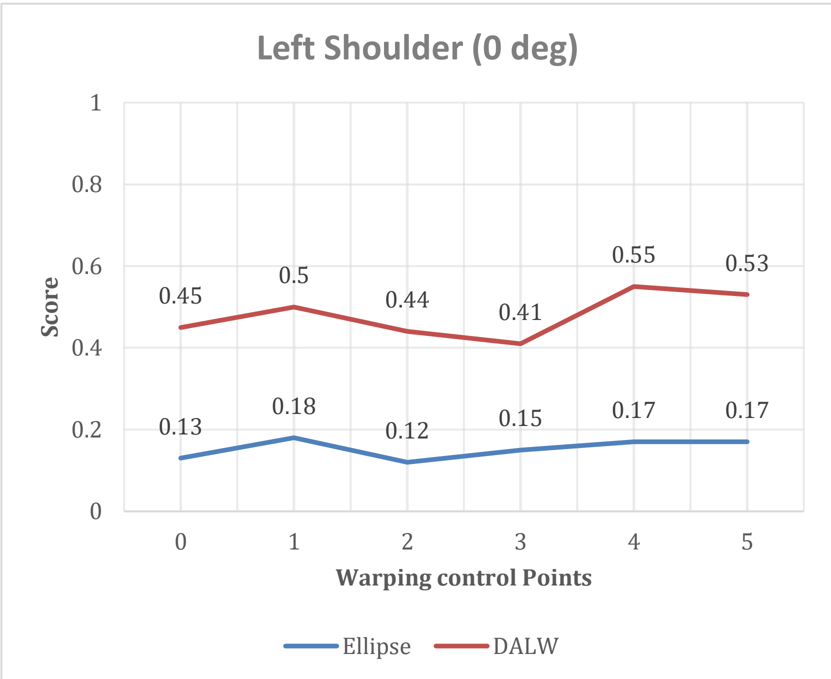

Figure 90 - Compigne loadcase - nWarpCtrlPts results on left shoulder impact at 4 m/s and 0° angle.

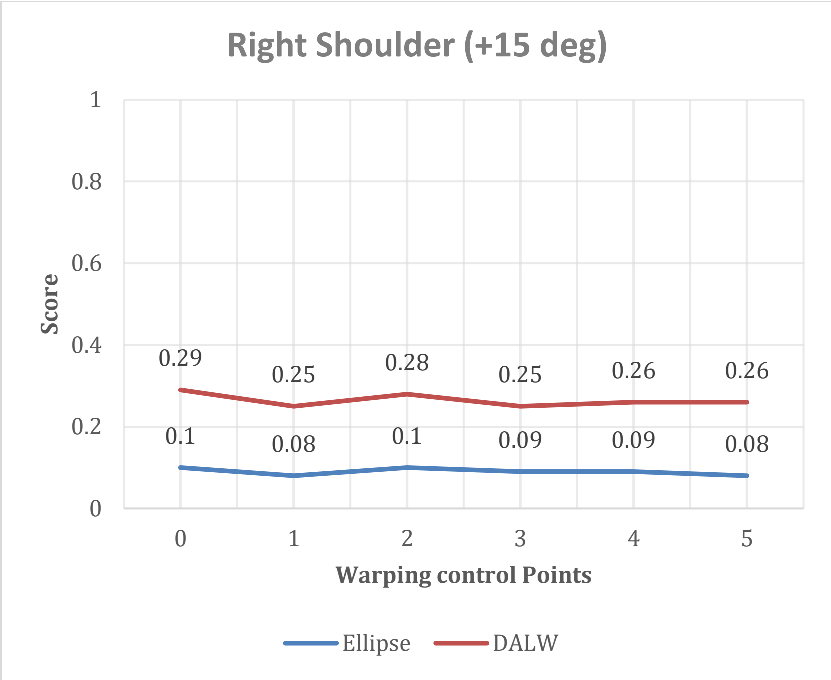

Figure 91 - Compigne loadcase - nWarpCtrlPts results on right shoulder impact at 1.5 m/s and +15° angle.

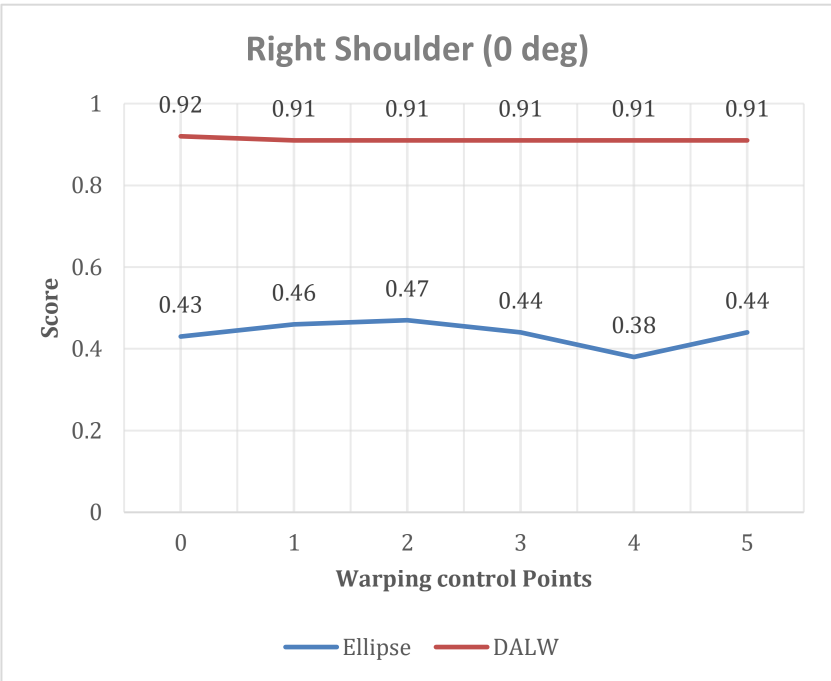

Figure 92 - Compigne loadcase - nWarpCtrlPts results on right shoulder impact at 1.5 m/s and 0° angle.

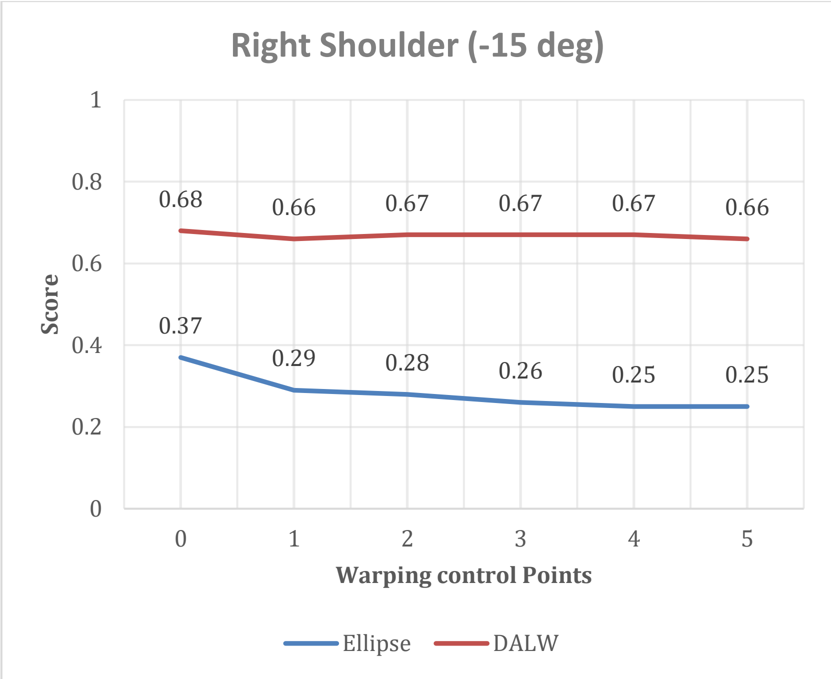

Figure 93 - Compigne loadcase - nWarpCtrlPts results on right shoulder impact at 1.5 m/s and -15° angle.

Appendix D

Table 28 - PMHS subject demographics and corridor inclusion matrix for Agnew and Shaw thoracic impact loadcases (Oblique 60° and Lateral 90°, Condition I).

Subject	Sex (M/F)	Age (years)	Height (in cm)	Weight (in kg)	50 F Corridor
Oblique (60°) - Condition I					
503	M	79	180	65.8	
504	M	80	165	80.7	
505	M	77	178	66.2	
506	M	87	175	65.7	
507	M	53	165	65.3	
601	M	63	186	93	
602	M	79	164	74.8	
A	F	53	170	48.5	
B	F	69	157	44.2	
C	F	63	170	51.3	
Average		70	171	65.5	
Lateral (90°) - Condition I					
503	M	79	180	65.8	
504	M	80	165	80.7	
505	M	77	178	66.2	
506	M	87	175	65.7	
507	M	53	165	65.3	
601	M	63	186	93	
602	M	79	164	74.8	
A	F	53	170	48.5	
C	F	63	170	51.3	
D	F	68	153	43.1	
Average		70	170.6	65.4	

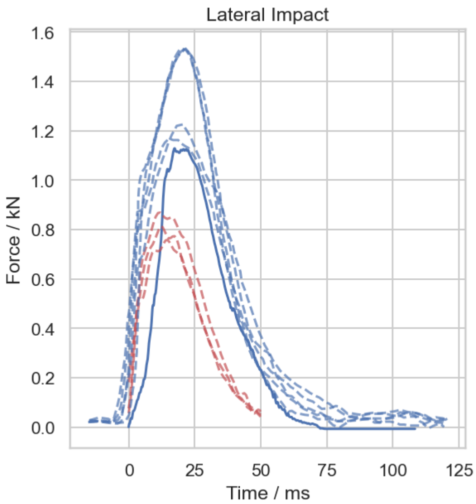

Figure 94 - Agnew loadcase - Lateral impact (force-time plot).

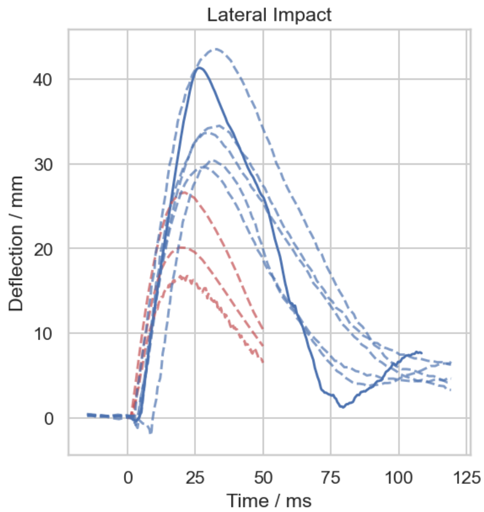

Figure 95 - Agnew loadcase – Lateral impact (deflection-time plot).

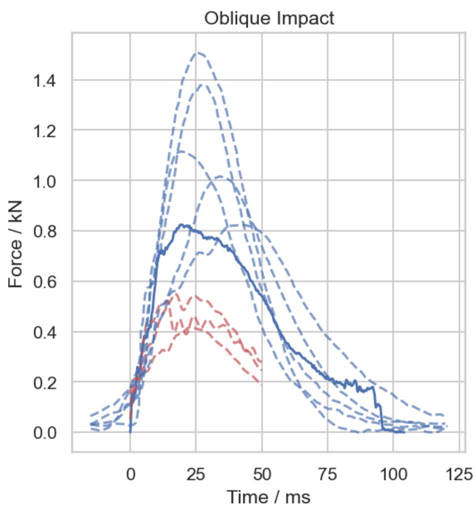

Figure 96 - Agnew loadcase - Oblique impact (force-time plot).

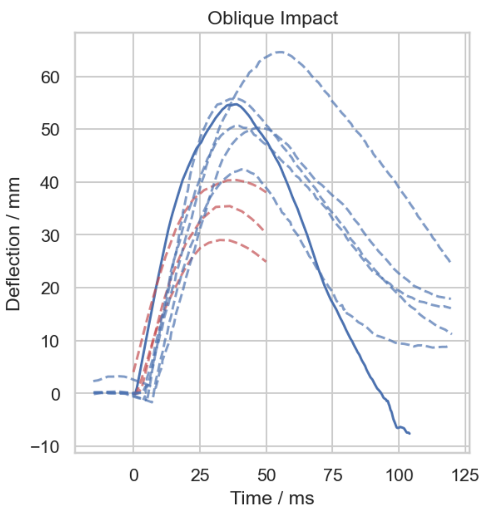

Figure 97 - Agnew loadcase – Oblique impact (deflection-time plot).

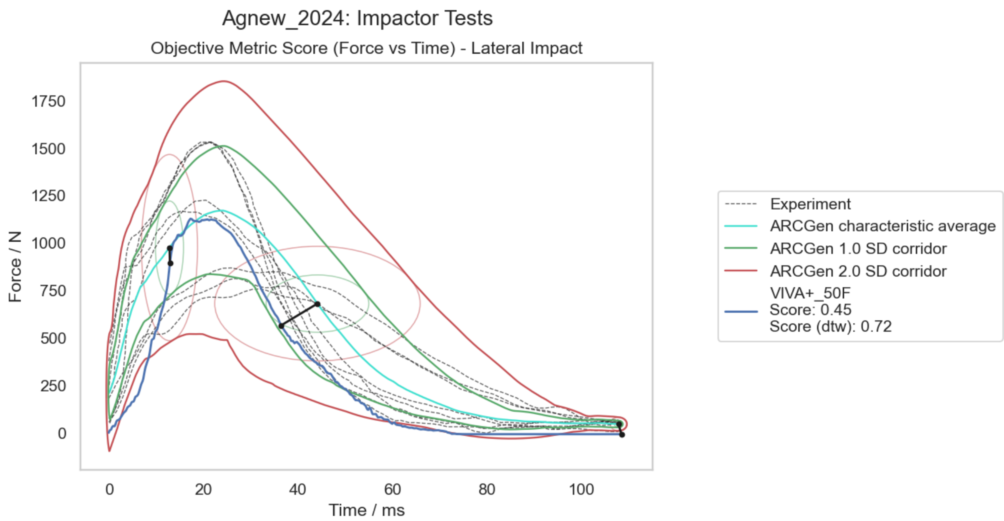

Figure 98- Agnew loadcase - ARCGen corridor for Lateral impact (force-time).

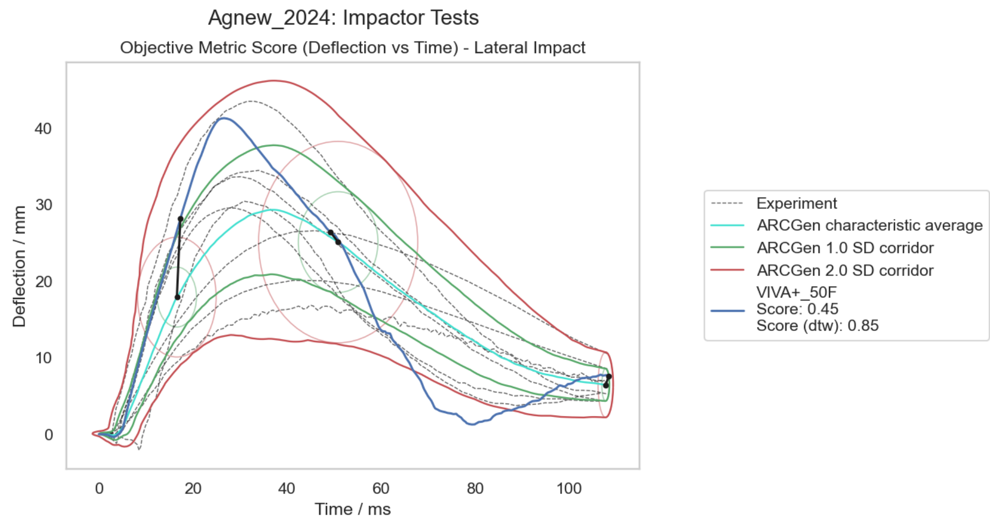

Figure 99 - Agnew loadcase - ARCGen corridor for Lateral impact (deflection-time).

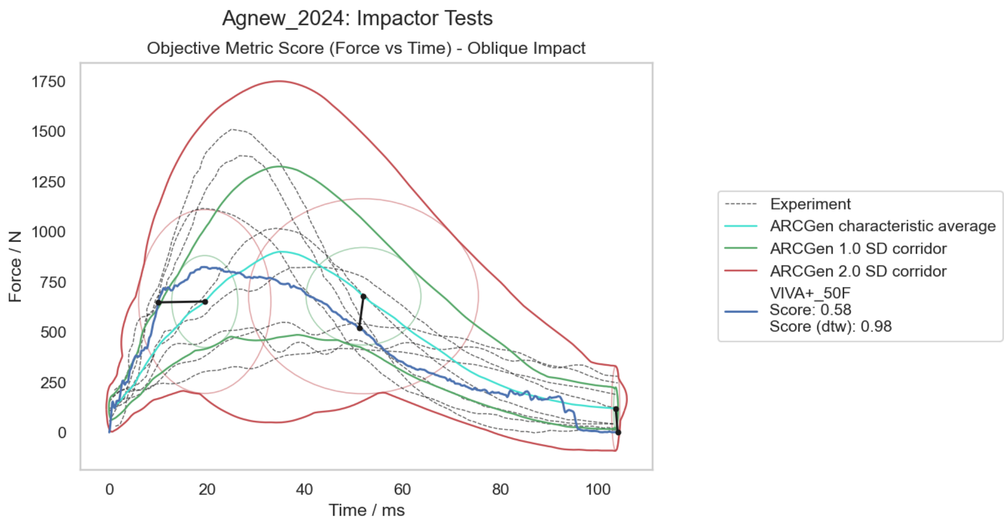

Figure 100 - Agnew loadcase - ARCGen corridor for Oblique impact (force-time).

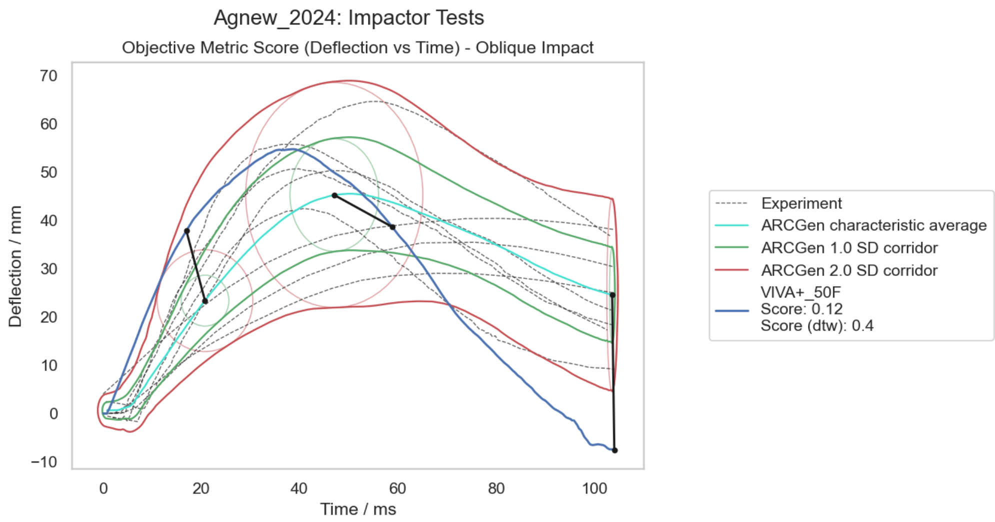

Figure 101 - Agnew loadcase - ARCGen corridor for Oblique impact (deflection -time).

Table 29 - Component-wise ISO 18571 scores for Agnew loadcase

Measure	Corridor	Phase	Magnitude	Slope	Overall
Oblique impact					
Force vs Time	0.191	0.664	0	0.501	0.309
Deflection vs Time	0.244	0.227	0.735	0.331	0.356
Lateral impact					
Force vs Time	0.415	0.859	0	0.501	0.438
Deflection vs Time	0.512	0.7	0.73	0.354	0.562

Table 30 - Individual ISO scores for each subject of Agnew loadcase (force-time)

Subject	Corridor	Phase	Magnitude	Slope	Overall
Oblique impact					
503	0.709	0.691	0.868	0.646	0.725
505	0.782	0.941	0.682	0.624	0.762
506	0.661	0.936	0.511	0.608	0.675
507	0.501	0.5	0.948	0.491	0.588
602	0.752	0.918	0.8	0.598	0.764
A	0.317	0.945	0.363	0.183	0.425
B	0.26	0.941	0	0	0.292
C	0.308	0.855	0.207	0.337	0.403
Lateral impact					

503	0.76	0.964	0.765	0.707	0.791
505	0.793	0.982	0.79	0.695	0.811
506	0.705	0.973	0.776	0.625	0.757
507	0.787	0.9	0.848	0.619	0.788
602	0.723	0.977	0.897	0.66	0.796
A	0.619	0.791	0.651	0.696	0.675
B	0.636	0.8	0.715	0.723	0.702
C	0.618	0.805	0.618	0.618	0.655

Table 31 - Individual ISO scores for each subject of Agnew loadcase (deflection-time)

Subject	Corridor	Phase	Magnitude	Slope	Overall
Oblique impact					
503	0.307	0.332	0.824	0.652	0.484
505	0.537	0.655	0.817	0.741	0.657
506	0.393	0.695	0.709	0.695	0.577
507	0.324	0.127	0.524	0.693	0.399
602	0.477	0.605	0.794	0.647	0.6
A	0.169	0.505	0.278	0	0.224
B	0.133	0.536	0.032	0	0.167
C	0.322	0.336	0.388	0	0.273
Lateral impact					
503	0.256	0.209	0.316	0.578	0.323
505	0.331	0.568	0.293	0.653	0.435
506	0.468	0.582	0.812	0.64	0.594
507	0.304	0	0	0.535	0.229
602	0.359	0.505	0.348	0.581	0.43
A	0.39	0.464	0.285	0	0.306
B	0.293	0.509	0.241	0	0.267
C	0.278	0.286	0.114	0	0.191